

Aus dem Institut für Experimentelle Schmerzforschung  
der Medizinischen Fakultät Mannheim  
(Direktor: Prof. Dr. med. Martin Schmelz.)

Assessment of GABA<sub>A</sub> mediated changes in excitability in mouse  
somatosensory neurons

Inaugural dissertation  
For obtaining the Doctor scientiarum humanarum (Dr. sc. hum.)  
of the  
Medical Faculty Mannheim  
of the  
Ruprecht-Karls-University  
Heidelberg

Presented by  
MSc Kyra Sohns

Born in: Ludwigsburg

2024

Dekan: Prof. Dr. med. Sergij Goerd  
Referent: Prof. Dr. med. Martin Schmelz

# Contents

Abbreviations.....	viii
1 Introduction .....	1
1.1 Neuronal excitability and information processing.....	2
1.1.1 Cellular determinants of neuronal excitability.....	2
1.1.2 Activity-dependent changes of neuronal excitability .....	4
1.2 Modulation of excitability by GABA.....	5
1.3 Chloride gradients .....	6
1.4 Afferent nerve fibre classes .....	9
1.5 Sensitization and GABA effects on activity-dependent excitability changes .....	10
1.6 Assessment of excitability.....	11
1.6.1 Compound Action Potential Recordings.....	11
1.6.2 Calcium imaging.....	12
1.7 Aims & Hypotheses.....	14
2 Methods.....	16
2.1 Ethical approval for animal experiments .....	17
2.2 Animals, anaesthesia and housing.....	17
2.2.1 Transgenic mouse lines.....	17
2.2.2 Floxed reporter lines.....	20
2.3 Extracellular recording of Compound Action Potentials.....	21
2.3.1 Sural nerve preparation.....	21
2.3.2 C-CAP recording setup.....	22
2.3.3 Principle of axonal threshold tracking .....	24
2.3.4 Optogenetic stimulation .....	26
2.4 Isolation and cell culture of DRG neurons .....	26
2.5 Calcium imaging.....	27
2.6 Solutions .....	28
2.6.1 Calcium imaging solutions .....	28
2.6.2 C-CAP recording solutions .....	28
2.6.3 Pharmacological agents.....	28
2.7 Data Analysis.....	29
2.7.1 C-CAP .....	29
2.7.2 Analysis of Fluorescence Images .....	29
2.7.3 Statistics.....	30

3	Results.....	31
3.1	Chapter 1: Axonal threshold tracking investigation of GABAAR-mediated chloride currents in unmyelinated sensory afferents .....	32
3.1.1	Depolarising GABA effects in the sural nerve are mediated by GABA <sub>A</sub> R .....	32
3.1.2	Required interval for stable GABA excitability responses upon repetitive application.....	33
3.1.3	Modulation of GABA effects by intermittent electrical stimulation .....	36
3.1.4	Depolarizing GABA responses are not blocked by NKCC1 antagonism with bumetanide .....	37
3.1.5	Interaction between intermittent electrical stimulation bouts and NKCC1-mediated inward chloride transport.....	39
3.1.6	Depletion of the chloride gradient with brief exposure to GABA.....	40
3.1.7	NKCC1 is responsible for maintaining the intra-axonal chloride gradient....	41
3.1.8	No major role of depletion of the chloride gradient for repetitive GABA at 2 min intervals.....	42
3.1.9	Optogenetically induced depolarisation in Trpv1-positive fibres of the sural nerve	43
3.1.10	Chloride manipulation in sensory axons using yellow light stimulation ...	44
3.2	Chapter 2: Calcium imaging to evaluate GABA effects in DRG neurons .....	46
3.2.1	GABA evoked calcium transients in DRG neurons .....	46
3.2.2	Classification of GABA-responsive cells .....	47
3.2.3	Extracellular calcium influx mediates the GABA transient.....	49
3.2.4	Calcium responses to repeated GABA application .....	53
3.2.5	Effect of prolonged firing on calcium responses to GABA .....	54
3.2.6	Effect of reduced extracellular chloride on GABA-evoked calcium response amplitude .....	55
3.2.7	Bumetanide inhibits NKCC1-associated chloride loading in DRG somata ....	59
4	Discussion.....	61
4.1	Axonal threshold tracking in C-fibre axons .....	62
4.1.1	Unusual role of GABA in modulating nociceptor excitability.....	62
4.1.2	Pharmacological characterization of GABA mediated chloride currents.....	63
4.1.3	Activity-dependent modulation of GABA responses .....	63
4.1.4	Repetitive GABA responses .....	64
4.1.5	Limitations of electrically-induced CAP for excitability testing.....	67
4.2	Calcium imaging to evaluate GABA effects in DRG neurons.....	69
4.2.1	Mechanisms of GABA-induced calcium transients .....	69
4.2.2	Cell-specific GABA responses.....	70
4.2.3	Repetitive GABA application and chloride loading in naïve sensory somata	72

4.2.4	Modulation of chloride gradients .....	73
4.2.5	Comparison of excitability parameters assessed by CAP recordings and calcium imaging.....	75
4.2.6	Conclusions.....	77
5	Summary.....	78
6	References .....	80
7	Curriculum vitae .....	96
8	Acknowledgements.....	97

## TABLE OF FIGURES

Figure 1 Schematic for the role of GABA-mediated depolarisations on excitability in the central and peripheral nervous systems.....	7
Figure 2 Measurement of conduction velocity in nerve fibre classes.....	9
Figure 3 A schematic to depict an action potential (AP) and the sodium channels contributing to the rising phase as well as the calcium channels activated during the repriming phase in addition to the chloride conductance associated with a GABA-mediated depolarisation. ....	14
Figure 4 Schematic for PCR primer strategy .....	20
Figure 5 Comparison of ChR2 and NpHR excitation spectra and functionality.....	21
Figure 6 Preparation of mouse sural nerve .....	22
Figure 7 Schematic of transverse section through peripheral nerve.....	23
Figure 8 Compound action potential recording equipment and principle of propagation of stimuli .....	23
Figure 9 Implementation of axonal threshold tracking in QTRAC.....	24
Figure 10 Schematic depicting calcium imaging setup .....	27
Figure 11 GABA depolarises sensory axons .....	32
Figure 12 GABA responses in C-fibre axons are mediated by GABA <sub>A</sub> R.....	33
Figure 13 GABA responses diminish at intervals shorter than 5 minutes.....	34
Figure 14 Repetitive GABA responses elicited at different intervals .....	35
Figure 15 Excitability responses to repeated GABA application at ten minute intervals.....	35
Figure 16 Intermittent bouts of electrical stimulation in between GABA applications increase the subsequent GABA response .....	37
Figure 17 Axonal GABA responses before and after intervention with bumetanide are not significantly influenced by NKCC1 blockade .....	38
Figure 18 Bumetanide does not act as a GABA <sub>A</sub> R antagonist.....	39
Figure 19 Intermittent high frequency stimulation during bumetanide exposure did not inhibit enhanced excitability increases in response to GABA .....	40
Figure 20 Shorter application times suggest less likelihood of GABA <sub>A</sub> R desensitisation .....	41
Figure 21 Repetitive GABA application in Bumetanide progressively reduces the excitability response to GABA.....	42
Figure 22 GABA <sub>A</sub> R desensitise at shorter intervals, but NKCC1 begins to take effect after approximately 10 minutes .....	43
Figure 23 Example of experimental approach for activation of Trpv1;ChR2 positive axons in threshold tracking experiments.....	44
Figure 24 Example of experimental approach to activation of Trpv1;eNpHR3.0 positive fibres in threshold tracking experiments.....	45
Figure 25 GABA produced calcium transients in isolated dorsal root ganglion neurons with a GABA <sub>A</sub> -receptor pharmacology .....	47
Figure 26 Calcium responses to electrical stimulation can be split into TTX-r and TTX-s.....	48
Figure 27 Effect of TTX on GABA-evoked calcium responses .....	49
Figure 28 Extracellular calcium influx mediates GABA induced calcium transients.....	50
Figure 29 Voltage-gated calcium channels responsible for calcium influx in response to GABA application .....	51
Figure 30 Calcium responses to repeat GABA application.....	53
Figure 31 An intervening bout of action potential activity reduces the calcium response amplitude to GABA .....	54

Figure 32 A longer recovery between electrical stimulus and GABA response shows no evidence of action potential dependent increase .....	54
Figure 33 Repetitive GABA applications at ten minute intervals, followed by a burst of high frequency firing reveals a reduction in amplitude of subsequent calcium transient in response to GABA .....	55
Figure 34 No significant change in response size from normal GABA to GABA in low chloride .....	56
Figure 35 Replacing chloride in the extracellular solution reduced the GABA-induced calcium transient significantly.....	56
Figure 36 Testing the depletion of the chloride gradient in a reduced extracellular chloride solution.....	57
Figure 37 Recovery of the chloride-depleted GABA transients .....	58
Figure 38 GABA-evoked calcium transients are reduced by bumetanide after long exposure	59
Figure 39 NKCC1 blockade with bumetanide progressively reduces the GABA-evoked calcium transients.....	60

## ABBREVIATIONS

### ***Abbreviation***

<i>ADS</i>	Activity-dependent slowing
<i>AP</i>	Action potential
<i>ATP</i>	Adenosine 5'-triphosphate
<i>CAP</i>	Compound Action Potential
<i>CaV</i>	Calcium channel
<i>C-CAP</i>	C-fibre Compound Action Potential
<i>ChR2</i>	Channelrhodopsin 2
<i>CNS</i>	Central nervous system
<i>CRAC (Orai1)</i>	Calcium-release activated calcium channel
<i>DHP</i>	Dihydropyridine
<i>DMEM</i>	Dulbecco's Modified Eagle's Medium
<i>DMSO</i>	Di-Methyl-Sulfoxid
<i>DNA</i>	Deoxyribonucleic acid
<i>dNTPs</i>	Deoxynucleotide Triphosphates
<i>DRG</i>	Dorsal root ganglion
<i>EDTA</i>	Ethylenediaminetetraacetic acid
<i>eg</i>	For example
<i>eNpHR</i>	enhanced Natronobacterium pharaonic halorhodopsin
<i>ER</i>	Endoplasmic reticulum
<i>E<sub>x</sub></i>	Equilibrium potential
<i>EYFP</i>	Enhanced yellow fluorescent protein
<i>FBS</i>	Fetal bovine serum
<i>GABA</i>	Gamma-aminobutyric acid
<i>GABA<sub>A</sub>R</i>	GABA-A-Receptor
<i>GABA-T</i>	GABA-Transaminase
<i>GAD</i>	Glutamic acid decarboxylase
<i>GAT-1</i>	GABA Transporter 1
<i>GDNF</i>	Glial derived neurotrophic factor
<i>GECI</i>	Genetically-encoded calcium indicator
<i>GPCR</i>	G-protein coupled receptor
<i>HBSS</i>	Hank's balanced salt solution
<i>HCN</i>	Hyperpolarisation-activated cyclic nucleotide
<i>HEPES</i>	N-2-Hydroxyethylpiperazine-N-2-Ethane Sulfonic Acid
<i>HT</i>	High-threshold
<i>HVA</i>	High-voltage activated
<i>Hz</i>	Hertz
<i>IB4</i>	Isolectin-B4
<i>I<sub>h</sub></i>	Hyperpolarisation-activated currents
<i>KCC2</i>	Potassium-chloride cotransporter 2
<i>KI</i>	Knock-in
<i>LT</i>	Low-threshold
<i>LVA</i>	Low-voltage activated
<i>MgSO<sub>4</sub></i>	Magnesium sulfate

<i>MR</i>	Mechanoreceptors
<i>mRNA</i>	Messenger ribonucleic acid
<i>Na<sup>+</sup>/K<sup>+</sup>-ATPase</i>	Sodium-potassium ATPase pump
<i>NaV</i>	Sodium channel
<i>NDAE</i>	Sodium dependent anion exchanger
<i>NGF</i>	Nerve growth factor
<i>NpHR</i>	Natronobacterium pharaonic halorhodopsin
<i>NKCC</i>	Sodium-potassium-chloride cotransporter
<i>NKCC1</i>	Sodium-potassium-chloride cotransporter 1
<i>PBS</i>	Phosphate buffered saline
<i>PCR</i>	Polymerase chain reaction
<i>PNS</i>	Peripheral nervous system
<i>RMP</i>	Resting membrane potential
<i>ROI</i>	Region of interest
<i>rmp</i>	Rounds per minute
<i>RT</i>	Room temperature
<i>SDH</i>	Spinal dorsal horn
<i>SERCA</i>	Ca <sup>2+</sup> -ATPase of the sarco-/endoplasmic reticulum
<i>SOCE</i>	Store-operated calcium entry
<i>STIM1</i>	Stromal interaction molecule 1
<i>TAE</i>	Buffer solution containing Tris base, acetic acid & EDTA
<i>TTA-A2</i>	(2-(4-cyclopropylphenyl)-N-((1R)-1-(5-((2,2,2-trifluoroethyl)oxo)-pyridin-2-yl)ethyl)acetamide)
<i>TTA-P2</i>	3,5-dichloro-N-[1-(2,2-dimethyl-tetrahydro-pyran-4-ylmethyl)-4-fluoro-piperidin-4-ylmethyl]-benzamide
<i>TTX</i>	Tetrodotoxin
<i>TRPV1</i>	Transient receptor potential vanilloid 1
<i>VGCC</i>	Voltage-gated calcium channel(s)
<i>V<sub>m</sub></i>	Membrane potential
<i>WT</i>	Wild-type

1 INTRODUCTION

## 1.1 Neuronal excitability and information processing

Neuronal excitability is the fundamental component of how information is processed in the peripheral and central nervous systems. It determines the generation and transmission of action potentials as the basis for neuronal communication on all levels: encoding of sensory input, synaptic transmission, plasticity, learning and neuronal network dynamics. Therefore, two basic perspectives emerge when modulation of neuronal excitability is discussed: which are the mechanisms that determine neuronal excitability and what are the consequences of a change in basal excitability. This thesis focuses on GABA (gamma-aminobutyric acid) effects influencing excitability of nociceptors, particularly on those changes that modulate nociceptive activity patterns. It is inferred that such changes in nociception will modify the input to the central nervous system (CNS) and should therefore have consequences for the sensation of pain. However, pain as defined by the IASP (Raja et al., 2020) is a highly complex sensation that is best understood in a bio-psycho-social model. The experience of pain involves several intricate relationships between the brain and the spinal cord and while there is evidence for a major role of input from primary afferent nociceptors in chronic pain, it is by far not sufficient to explain the level of suffering in individual patients. Influences from the environment and not to mention internal psychological aspects also play a tremendous role. Therefore, this thesis does not set out to study mechanism of pain, but rather it sets out to clarify how neuronal excitability is modulated in primary afferent neurons, when they are persistently active, thereby improving our knowledge in basic nociception.

### 1.1.1 Cellular determinants of neuronal excitability

Of the four basic tissues (connective, epithelial, muscle and nervous), nerve and muscle are both excitable, that is, they are able to generate and propagate action potentials (AP). The conduction of an action potential serves to transfer information, typically from its receptive field, either a dendrite for neurons in the central nervous system, or its axonal terminal endings in the peripheral nervous system (PNS). Electrical signals as potential differences are transferred along the axon culminating in presynaptic release of a chemical transmitter. The action potential represents a transient change in the cell's membrane potential. The membrane potential ( $V_m$ ) is the difference in voltage across the membrane:

$$V_m = V_{in} - V_{out}$$

Equation 1 Membrane potential ( $V_m$ ) calculation

and can be approximated using the permeability (P) of the membrane to each ion and the intracellular and extra-cellular concentration of each ion, according to the Goldman-Hodgkin-Katz equation:

$$V_m = \frac{RT}{F} \ln \left\{ \frac{P_{Na}[Na^+]_e + P_K[K^+]_e + P_{Cl}[Cl^-]_i}{P_{Na}[Na^+]_i + P_K[K^+]_i + P_{Cl}[Cl^-]_e} \right\}$$

Equation 2 Goldman-Hodgkin-Katz Equation including ion gradients for sodium, potassium and chloride

Where  $R$  is the gas constant,  $T$  is the temperature (in Kelvin,  $K$ ),  $F$  is the Faraday constant,  $P$  is the permeability and  $[X]_e$  and  $[X]_i$  are the relative extracellular and intracellular concentrations. Under physiological conditions the distribution of concentration for each ion is shown in Table 1 below.

<i>Ion</i>	Intracellular concentration (range in mM)	Extracellular concentration (range in mM)	Nernst/reversal/equilibrium potential ( $E_x$ ) (mV)
$Na^+$	5 - 20	130 - 160	+55
$K^+$	130 - 160	4 - 8	-80 - -90
$Ca^{2+}$	50-1000(nM)	1.2 - 4	+50 - 70
$Cl^-$	1 - 60	100 - 140	-65
$HCO_3^-$	1 - 3	20 - 30	-10 - -20

Table 1 Distribution of ions in intracellular vs extracellular space and resultant Nernst potentials

These chemical ionic gradients are maintained by activity of the  $Na^+/K^+$ -ATPase pump (sodium-potassium ATPase pump) that extrudes 3  $Na^+$  and imports 2  $K^+$  ions with each catalytic ATP split (Sen and Post, 1964). The  $Na^+/K^+$ -ATPase is a P-type pump comprising three protein subunits, a single alpha, a single beta and FXYD subunits (Benarroch, 2011) and must undergo conformational changes to allow ions to pass (active transport), when working against an electrical or chemical gradient. This active transport requires ATP. The  $Na^+/K^+$ -ATPase pump is electrogenic; the transported ions are charged and their movement influences the membrane potential. Neuronal activity causes transient changes in the flow of ions and thereby the gradients across a membrane and the pump works to restore resting membrane potential (RMP) and prevent intracellular accumulation of sodium (Benarroch, 2011).

The direction of current flow is defined by the net movement of positive ions. The current flow through a channel in response to the electrochemical driving force (defined by the concentration gradient of the ion and the electrical potential difference across the membrane) defines the current-voltage relationship. This means that a change in ionic concentration gradient will change the overall net driving force for this ion. Maintenance of ion gradients and the resting membrane potential (see Tab.1 for details) is controlled by the driving force of ions, their equilibrium potentials ( $E_x$ ), and the opening probabilities of ion channels or transporters. Opening probabilities refers to the time that the channel is open spontaneously or in response to a stimulus compared to the time being closed. Ion channels are not constitutively open, they are "gated," which means the opening probability of ion channels is increased by the stimuli they are responsive to. For example, by physical stimuli (such as heat- or mechanically-gated channels), by mediator binding ("ligand-gated" channels) or by changes in membrane potential ("voltage-gated" channels). In sensory neurons the interaction of stimuli with heat-, mechanical- or ligand-gated ion channels underlies the transduction of such stimuli into a generator potential, which induces action potentials via the activation of axonal voltage-gated sodium channels ( $Na_v$ ; so-called spike initiation). These channels are also crucial for the conduction of action potentials along the axon to the first synapse in the dorsal horn of the spinal cord. While these mechanisms are straight forward and appear to allow precise predictions, it is important to note that there are numerous consequences of action potentials

that modulate neuronal excitability, thereby resulting in several feedback loops that also determine activity-dependent changes in neuronal excitability.

### 1.1.2 Activity-dependent changes of neuronal excitability

There are several steps to an action potential of which the timing and relation to one another is understandable and trackable. After opening during the upstroke of an action potential (see Figure 3), voltage-gated sodium channels enter an inactivated state during the absolute refractory phase, in which no additional action potential may be generated (Hodgkin and Huxley, 1952). This is followed by conformational changes back to the closed-state, where the generation of action potentials is again possible, albeit at higher thresholds (relative refractory period; (Hodgkin and Huxley, 1952)). In this way, action potentials are self-regenerative.

Nonetheless, perhaps more complex are the several mechanisms that can modify short-term neuronal excitability following a single action potential: after-hyperpolarisation will decrease excitability, while after-depolarisation can increase excitability. Mechanisms for after-hyperpolarisation include prolonged opening of voltage-gated (M-current, Kv7.1–Kv7.5) and calcium-activated potassium channels ( $K_{Ca}$ ; sK1-4) which reduce firing activity to prevent neurotoxicity as a consequence of excessive firing (Dwivedi and Bhalla, 2021). In contrast, after-depolarisations have been linked to hyperpolarisation-activated cyclic nucleotide (HCN) channels responsible for hyperpolarisation-activated currents ( $I_h$ ) (Moalem-Taylor et al., 2007), which aim to limit hyperpolarisation (Mazo et al., 2013).

Still more complex, is the struggle to determine how not one, but all of these factors interact in phases of high frequency firing. Cumulatively, frequent action potentials increase the intracellular sodium concentration, activating the  $Na^+/K^+$ -ATPase, which in turn hyperpolarises the membrane potential and counteracts inactivation of sodium channels. The dynamics of ion channels and previous firing activity, shape future bursting activity (Kueh et al., 2016). In some cases, the combination of these processes leads to a pronounced activity-dependent slowing (ADS). In nociceptive C-fibres, this is particularly prominent and reduces their conduction velocity, but also limits their ability for high frequency firing and often leads to conduction failures (Thalhammer et al., 1994; Tigerholm et al., 2014). Prolonged hyperpolarisations are common after bursting activity (Rang and Ritchie, 1968) and  $I_h$  currents have been linked to slowing in C-fibres, which is in turn reduced after upregulation of HCN channels following nerve damage (Mazo et al., 2013).

Further, a direct correlation between ADS, conduction velocity and neuronal excitability has been shown (De Col et al., 2012; Tigerholm et al., 2014). Activity-dependent slowing reduces nociceptor excitability upon repetitive discharge based on changes in membrane potential (eg. hyperpolarisation) (Bostock et al., 2003), increase in intracellular sodium or inactivation of sodium channels (De Col et al., 2008; Zhang et al., 2017) and the activity of the  $Na^+/K^+$ -ATPase pump working to restore RMP (Mazo et al., 2013). Interestingly, the  $Na^+/K^+$ -ATPase pump is partially responsible for a lasting hyperpolarisation (Baylor and Nicholls, 1969; Rang and Ritchie, 1968) and will remain active for a prolonged time (Sharples et al., 2021), thereby over-compensating the action potential mediated accumulation of intracellular sodium. However,

inflammatory states reduce the magnitude of ADS in rat C-fibres (Dickie et al., 2017) and in human fibres (Obreja et al., 2018) and thereby maintain high frequency firing.

There are only few mechanisms that counteract activity-dependent reduction of neuronal hyperexcitability, one of which is the hyperpolarisation-activated current (Mazo et al., 2013) that has already been mentioned. Interestingly, there is also evidence, that GABA-mediated chloride currents can reduce activity-dependent hypo-excitability (Bonalue et al., 2021; Carr et al., 2010).

## 1.2 Modulation of excitability by GABA

The ability for an excitable cell to become active, generating and propagating action potentials, is counterbalanced with the inhibitory mechanisms inherent to the nervous system. Synaptic inhibition thus serves as the opposing force to excitation and is inextricably linked with the excitability of a cell.

Fast synaptic inhibition is mediated by GABA and glycine, the two main inhibitory neurotransmitters of the CNS. GABA, first characterised by Roberts and Frankel (1950) and the main focus here, is synthesized by GAD (glutamic acid decarboxylase), which is located only in cells that use GABA as a neurotransmitter (Bowery and Smart, 2006; Ghit et al., 2021; Roberts and Frankel, 1950). The enzyme exists in two isoforms, GAD65 and GAD67, which differ in cellular localization (Rowley et al., 2012). Both forms catalyse the conversion of glutamate to GABA. This is followed by transport and/or storage of GABA in synaptic vesicles for release of GABA usually at the synaptic cleft. A depolarisation of the presynaptic membrane, mediating the influx of calcium, stimulates release of GABA into the cleft via calcium-dependent exocytosis, allowing binding with one of two receptors: GABA<sub>A</sub>R or GABA<sub>B</sub>R. If there is no binding, GABA reuptake may occur by GAT-1 (GABA transporter 1) in neurons (Bowery and Smart, 2006). Two forms of reuptake are known: reuptake by terminals, allowing recycling of GABA, or reuptake by astrocytes which commences degradation by GABA transaminase (GABA-T) (Bowery and Smart, 2006).

Historically, there are three types of GABA receptors with which GABA may bind; GABA<sub>A</sub>, GABA<sub>B</sub>, and GABA<sub>C</sub>, determined by the subunit composition. GABA<sub>C</sub> receptors are now considered isoforms of GABA<sub>A</sub>R as they are composed of only rho subunits, which may pair with other GABA<sub>A</sub> subunits, and are similar in ion channel structure and function (Olsen and Sieghart, 2008). GABA<sub>A</sub> and GABA<sub>B</sub> receptors are structurally and pharmacologically separate and while both are generally inhibitory, they act in distinct ways.

GABA<sub>B</sub> receptors are metabotropic, G-protein coupled receptors (GPCR) (Terunuma, 2018). Upon binding of GABA with a postsynaptic GABA<sub>B</sub>R, these trigger the opening of K<sup>+</sup> channels via G<sub>αi</sub> and G<sub>αo</sub>-type G-proteins, resulting in a hyperpolarisation (Terunuma, 2018). On the other hand, GABA<sub>A</sub>R, which will be the focus in this thesis, belong to the cys-loop ligand-gated ion channel superfamilies, of which further examples are the TRP (transient receptor potential) channels or ATP-gated (adenosine 5'-triphosphate) channels. The cys-loop superfamily in which GABA<sub>A</sub>R is an anionic channel, also includes glycinergic and nicotinic receptors. Each receptor is pentameric (comprising five subunits), with an N-terminal domain containing the signature cys-loop, plus four transmembrane domains (Connolly and Wafford, 2004). The pore created in the middle constitutes the channel; the gating mechanism requires binding of an agonist

(GABA, muscimol) to open the channel by re-configuration and allow conductance of ions (chloride and to a lesser extent bicarbonate).

The pentameric formation of the GABA<sub>A</sub>R means that, with 19 subunits to choose from, each permutation will change the functional and pharmacological properties of the receptor (Sallard et al., 2021). Altogether, there are 6 alpha, 3 gamma, 3 beta, 3 rho, and 1 each of respective epsilon, delta, pi and theta subunits (Ghit et al., 2021). Post-synaptically localised receptors almost always include a specific combination of subunits: 2 alpha (1-3), 2 beta (1-3) and a gamma and these are different from those composing extra-synaptic receptors (delta, 2 alpha (4-6) and 2 beta (2 or 3)) (Ghit et al., 2021).

The GABA subunit composition determines the electrophysiological parameters, such as kinetics (eg. (de-)activation time, desensitization) and functionality (eg. EC50). Desensitization of the channel may occur with repetitive high-frequency opening, or with a long exposure. Channels composed of specific subunit variants may desensitize faster than others, and this influences the time course of an inhibitory post-synaptic current and therefore the effect on neuronal inhibition (Sallard et al., 2021).

GABA binding with GABA<sub>A</sub>R can generate two forms of inhibitory currents: phasic and tonic. Phasic inhibition describes the transient vesicular release from the pre-synapse and binding of GABA on the post-synaptic membrane to open GABA<sub>A</sub>R-mediated chloride channels allowing relatively fast ion conductance and thereby inhibition, occurring at the synapse (Sallard et al., 2021). A use-dependent rundown (Cifelli et al., 2013) that is accompanied by a slow deactivation and therefore creates smaller responses with consecutive applications (Reichling et al., 1994), enables the protection of neurons against pathologically extreme inhibition and is also seen in temporal lobe epilepsy (Cifelli et al., 2013). Tonic inhibition, on the other hand, whereby GABA escapes re-uptake (Conti et al., 2004; O'Neill and Sylantsev, 2019; Palma et al., 2007), usually occurs at extra-synaptic receptors and can be random and temporally dispersed (Farrant and Nusser, 2005). It creates slow neuronal inhibitory currents (Palma et al., 2007) which have also been linked to mechanisms contributing to chronic pain (Delgado-Lezama et al., 2021).

### 1.3 Chloride gradients

Since GABA<sub>A</sub>R are chloride-permeable channels, the impact of inhibitory signals via GABA<sub>A</sub>R is determined by the transmembrane chloride gradient and a change in regulation of this gradient will modify excitability (Chen et al., 2014; Zhu et al., 2014). Chloride concentrations are dynamically regulated by neuronal development and activity in the adult nervous system (Raimondo et al., 2017). Therefore, the relationship between chloride and excitability is of particular interest for the maintenance of neuronal inhibition and normal excitable states.

NKCC1 (sodium-potassium-chloride cotransporter 1) is responsible for transporting chloride into the cell, while KCC2 (potassium-chloride cotransporter 2) transports chloride out (Yamada et al., 2004). Prenatally, upregulated NKCC1 expression maintains a high intracellular chloride concentration, rendering the equilibrium potential for chloride ( $E_{Cl}$ ) more depolarized than the RMP (Ben-Ari, 2002, 2007). Therefore, the driving force for chloride is directed outward, and upon opening of GABA<sub>A</sub>R, chloride flows out, pushing the membrane potential towards  $E_{Cl}$  and

depolarizing the neuron. This depolarisation may even exceed the threshold for action potential initiation (Ben-Ari, 2002, 2007; Pressey et al., 2023). With maturation, the upregulation of KCC2 and downregulation of NKCC1 results in a reduction of the intracellular Cl<sup>-</sup> concentration (around 5-10mM). A negative shift in the reversal potential of GABA ( $E_{GABA}$ ) to very close to RMP (approx. -70mV) accompanies the increase in KCC2 expression (Ben-Ari, 2002; Prescott, 2015). Under these conditions, the opening of a chloride channel hyperpolarises the neuron and is inhibitory. The relative chloride concentrations in a central neuron intra- and extra-cellularly are reiterated here, but can be found in Tab. 1. (approx. 5mM and 110mM, respectively (Schulte et al., 2018)).

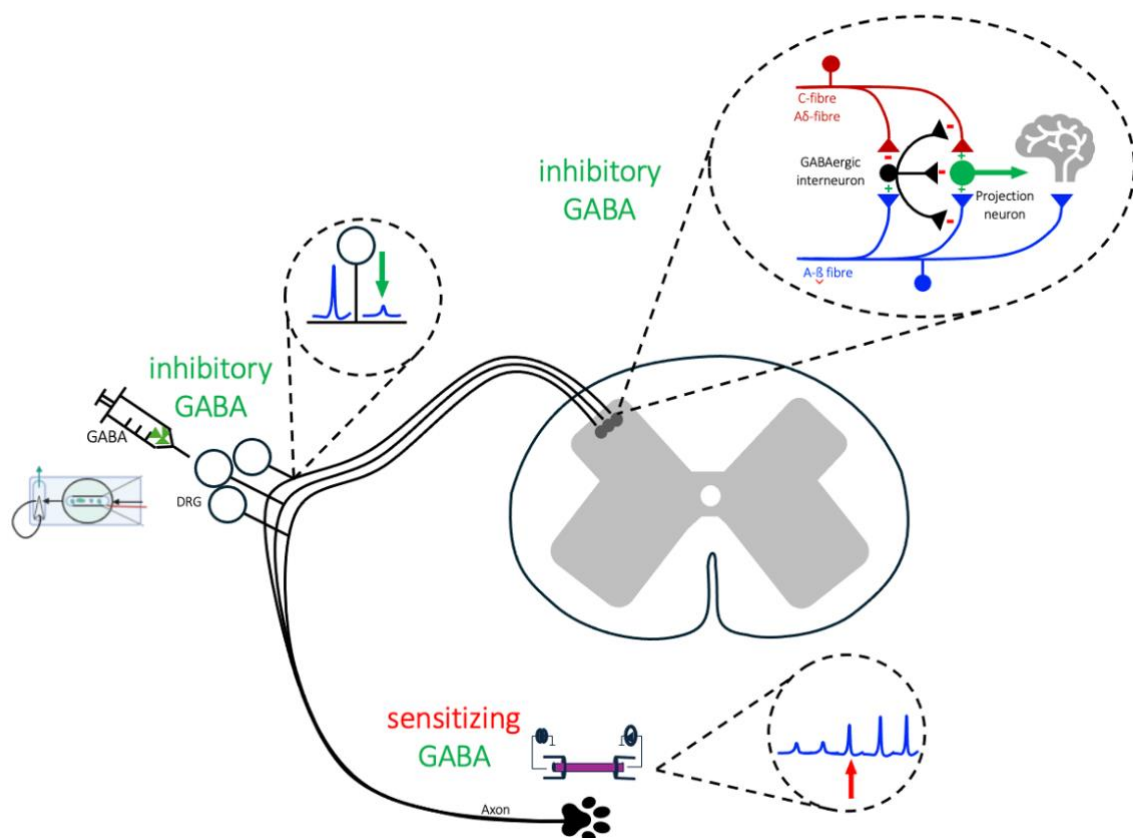


**Figure 1 Schematic for the role of GABA-mediated depolarisations on excitability in the central and peripheral nervous systems.** In the spinal dorsal horn, GABAergic interneurons mediate primary afferent depolarisation (PAD), which results in presynaptic inhibition caused by shunting mechanisms or inactivation of voltage-gated sodium channels. In the T-junction, the axonal bifurcation, GABA is equally inhibitory, resulting a reduced reliability of action potentials to be conveyed to the first synapse in the dorsal horn of the spinal cord. This functional consequence is said to resemble that of presynaptic inhibition. In this study, calcium imaging was used to investigate the effect of GABA on the excitability of cultured DRG neurons. In contrast, GABA in the axon of the peripheral afferent may have an opposite sensitizing effect, in which it can promote ongoing firing of action potentials. Here axonal threshold tracking was used to investigate the role of GABA-mediated chloride currents on excitability of the sural nerve. Adapted from (Du et al., 2017)

In contrast, primary afferent dorsal root ganglion (DRG) neurons (Wilke et al., 2020), which relay information from the periphery to the CNS where they synapse initially in the spinal dorsal horn (see Figure 1), as well as olfactory sensory neurons (Restrepo, 2005) and trigeminal ganglion neurons (Schöbel et al., 2012), the intracellular chloride concentration is maintained elevated even throughout maturation. This is based on the presence of NKCC1 and lack of KCC2 expression, that would transport Cl<sup>-</sup> out of the cell (Wilke et al., 2020). Subsequently, the  $E_{Cl}$

(now around  $-27\text{mV}$ , (Rocha-Gonzalez et al., 2008)) is more positive than RMP of the cell, although it should be mentioned that this is very variable (approx.  $-16\text{mV} - -46\text{mV}$ ) (Alvarez-Leefmans et al., 1988; Rocha-Gonzalez et al., 2008). When  $\text{GABA}_A\text{R}$  are activated under these conditions, chloride will exit the cell and cause a depolarisation. Importantly, the functional net effect of this depolarisation on neuronal excitability may vary depending on the location of the neuron (see Figure 1).

In the spinal dorsal horn, the depolarisation is inhibitory, causing a reduced spike propagation (Prescott, 2015) and reduction in excitability. There are several proposed methods of this: the opening of the chloride channel as a result of an invading action potential may cause inactivation of voltage-gated sodium channels causing a reduction in excitability (Wilke et al., 2020), or reduce the amplitude of a depolarisation caused by excitatory input (shunting inhibition; (Price et al., 2009)). This describes the counteracting of the chloride outflow through GABA channels by the inflow of current through glutamate receptors (Doyon et al., 2016). The effect of this is a quenching of release of excitatory neurotransmitters at the synapse.

This concept is at the heart of the Gate Control Theory of pain, proposed by Melzack and Wall (1965), stating that inhibitory interneurons in the spinal dorsal horn (SDH), gate nociceptive information coming from the periphery. Painful stimuli are conveyed when the gate is open, whereas non-painful signals close the gate. In their model, small diameter fibres (C- and A-delta fibres) synapse on and excite nociceptive projection neurons, which carry their information further in the brain, while also synapsing on and inhibiting inhibitory interneurons. Low threshold large diameter fibres ( $\text{A}\beta$ ) on the other hand, activate these inhibitory interneurons, whereas under normal conditions, their synapses on nociceptive projection neurons are subthreshold (see Figure 1). Thus, this theory comprises the concept of primary afferent depolarisation (PAD) which relies on the presynaptic inhibition by GABAergic interneurons (Eccles, 1961). Presynaptic inhibition constitutes the method of communication by which primary afferents in the spinal dorsal horn interact and under normal circumstances, PAD and presynaptic inhibition work to reduce pain (Prescott, 2015).

Since there are few synapses at which the neurotransmitter may act, the role of  $\text{GABA}_A\text{R}$  in the neuronal sensory soma or peripheral axons remains unclear. Only recently has a fully functional GABAergic system been characterized in the dorsal root ganglia of the mouse, showing that GABA can be produced and released by DRG neurons and taken up by satellite glial cells (Du et al., 2017). The authors suggest that the GABA release from somata of DRG neurons reduces pain behaviours in vivo, by reducing the reliability of action potential conduction via the axonal T-junction in the DRG (Du et al., 2017) (see Figure 1). The functional consequences of the depolarizing effect of GABA directly at the T-junction thus resemble spinal presynaptic inhibition and thus, the authors suggest a gate control mechanism of pain within the local environment of peripheral afferent somata (Du et al., 2017; Fuller et al., 2023).

In light of the above findings from (Du et al., 2017), it seems obvious that for example, changes in the chloride gradient in spinal cord neurons or along the primary afferents, or in the DRG, can actually switch normal GABA-mediated inhibition to the opposite excitatory effect, which has been hypothesised as important mechanism to explain hyperexcitability in chronic pain (Price et al., 2009; Wu and Wang, 2023). In fact, in the spinal cord KCC2 downregulation contributes to neuropathic pain (Coull et al., 2003). Increasing GABAergic inhibition reduces

changes in  $E_{\text{anion}}$  but is only effective to a certain value of  $E_{\text{anion}}$  around  $-60\text{mV}$ , after which the effect becomes excitatory (Prescott et al., 2006; Price et al., 2009). Additionally, sensitization of nociceptors from injury may alter the regular functioning in these afferents and cause hyperexcitability (Gwak and Hulsebosch, 2011).

#### 1.4 Afferent nerve fibre classes

The sensation of pain subserves an appropriate protective response and is therefore crucial for survival. Specialized A- and C-fibres are responsible for transmitting such nociceptive information. There are three types of A-fibres each with different defining characteristics of modality and responsivity. A- $\alpha$  (A-alpha) and A- $\beta$  (A-beta) fibres are large in diameter, myelinated and fast-conducting. These fibres are mechanoreceptors (MR) and can respond to relatively weak stimuli, for example, innocuous light touch. In contrast, A- $\delta$  (A-delta) nociceptors are thinly myelinated, of a medium diameter, and contain two subtypes: high threshold mechanonociceptors (HT) and low threshold mechanoreceptors (LT). HT fibres can respond to both mechanical and chemical stimuli, but their threshold for noxious heat is approximately  $45^{\circ}\text{C}$ . They produce sharp, short-latency pain. C-fibres are unmyelinated and slowly conducting small diameter axons, which are also polymodal, ie. can encode a variety of stimuli (see Figure 2). It should be mentioned, that action potentials are conducted along myelinated axons in a saltatory fashion, which increases the speed of propagation.

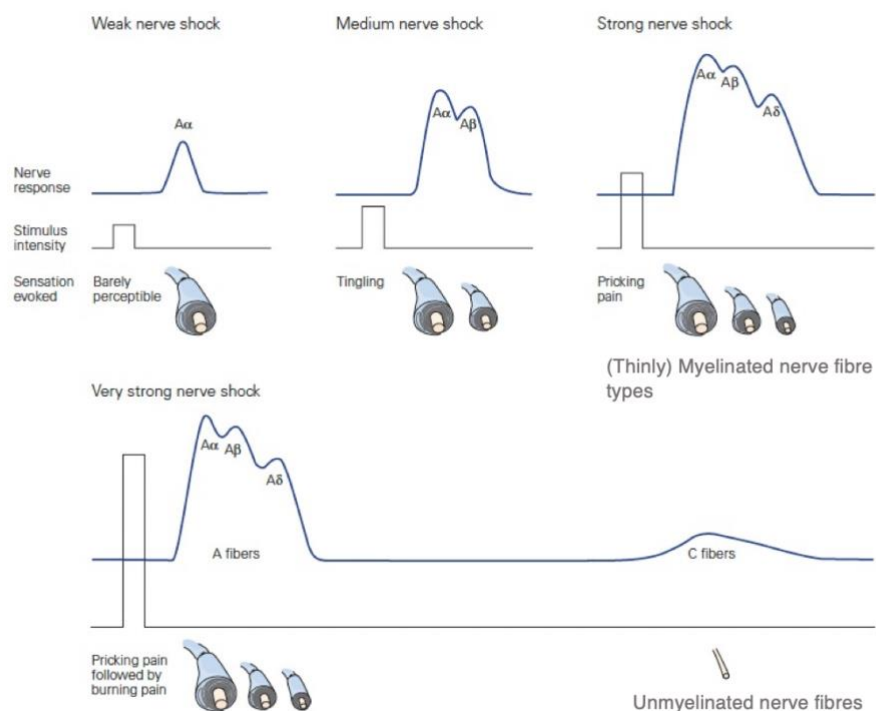


**Figure 2 Measurement of conduction velocity in nerve fibre classes.**

An increasing stimulus intensity of nerve shock recruits more fibre types. C-fibres are shown as the slowest responding type. Adapted from (Kandel et al., 2021).

In mice, C-fibres can be broadly discriminated into two groups; those that release neuropeptides (peptidergic) such as CGRP or substance P and respond to nerve growth factor (NGF), and those that are IB4 positive (non-peptidergic) and respond to the neurotrophic factor GDNF (glial derived neurotrophic factor) (Basbaum et al., 2009). Laminae I & II are referred to as the superficial dorsal horn of the spinal cord and are the main targets for nociceptive primary afferents. Specifically, peptidergic C-fibres project to lamina I, while non-peptidergic C-fibres usually project to lamina II. Lamina II is also known as substantia gelatinosa because of the lack of myelinated fibres.

TRPV1 (transient receptor potential vanilloid-1) is expressed in a majority of nociceptive peptidergic C-fibres (Brandt et al., 2012;Guo et al., 1999). The expression of TRPV1 allows C-fibres to be activated by hot temperatures above 45°C and a low pH. The channel is activated by the chemical capsaicin, the compound found in chili's that makes them spicy. The responses to capsaicin are often used to distinguish C-fibre nociceptors and implicates these neurons in involvement in mechanisms underlying neurogenic inflammation (Immke and Gavva, 2006).

In general, recent studies using single cell expression data of murine dorsal root ganglia neurons have confirmed the general separation into peptidergic and non-peptidergic nociceptors, but have also identified several additional subpopulations (Sharma et al., 2020). The translation of the murine classification of nociceptors has proven problematic and new nomenclatures have been proposed for human nociceptors (Tavares-Ferreira et al., 2022).

### 1.5 Sensitization and GABA effects on activity-dependent excitability changes

Inflammatory mediators may sensitize nociceptors, which can change their firing patterns and can explain inflammation-related pain and hypersensitivity. Sensitization is described as a reduction in the threshold to stimuli that may be nociceptive, in addition to an increase in the magnitude of the response (Gold and Gebhart, 2010). Classically, it involves facilitated transduction of nociceptive stimuli by sensitizing transduction molecules such as TRPV1, resulting in a reduced heat activation threshold for TRPV1 channels and thermal hyperalgesia (Caterina and Julius, 2001). Nociceptive input into the dorsal horn may also sensitize nociceptive processing in the spinal cord leading to central sensitization, that is classically found in the non-injured surroundings of a peripheral injury. This could also be due to a mechanism of disinhibition (Prescott, 2015) and may occur in the absence of an insult, caused by changes in membrane properties, thereby creating hypersensitivity (Latremliere and Woolf, 2009). In addition to the peripheral sensitisation of sensory transduction via injury, and central sensitisation in the spinal cord, inflammatory mediators can also increase axonal excitability (Rukwied et al., 2013) and facilitate high frequency discharge in nociceptors (Werland et al., 2021). A higher frequency discharge scales with the magnitude of the perceived pain, i.e. increased action potential frequency, gives rise to more pain.

Interestingly, GABA has been shown to increase the excitability of C-fibres during high-frequency firing, reducing ADS (Bonalume et al., 2021;Carr et al., 2010). This is important as it would suggest GABA-mediated chloride currents can have opposite effects on nociceptor excitability depending on the effector site along the neuron. In contrast to the inhibitory effects at the DRG and pre-synaptically (see Figure 1), there may be a facilitation of higher discharge

activity along the axon. Moreover, as has been mentioned GABA and chloride are dynamically regulated throughout maturation and inhibitory GABAergic synapses themselves exhibit synaptic plasticity that is regulated by activity (Bannai et al., 2009). Furthermore, an activity-dependent upregulation of NKCC1 activity has also been shown in unmyelinated C-fibre axons from the mouse, indicating a further mechanism of action of NKCC1-mediated chloride transport in regulating excitability (Bonalume et al., 2021). Thus, GABA-mediated chloride currents in nociceptive afferents are optimally positioned to limit activity-dependent reduction of excitability.

## 1.6 Assessment of excitability

Electrophysiological recordings study the electrical properties of tissues and cells, in particular action potential generation and propagation. In essence, electrophysiology studies the excitability of a neuronal cell, using manipulations of voltage or current or even electrical stimulation, on a whole system, single cell or ion channel level. The studies can be done using intra- or extra-cellular recording systems, such as patch clamp of a single neuron, or the use of extracellular multi-electrode arrays, respectively, as well as the use of optical imaging technologies with fluorescent indicators (Spira and Hai, 2013). This study focused on the use of electrophysiological recordings for excitability of C-fibres.

### 1.6.1 Compound Action Potential Recordings

Unfortunately, the direct investigation of unmyelinated fibre types via intracellular recordings is rather difficult owing to their relatively small size. As mentioned, an electrophysiological assessment of nerve fibres exploits the ability of nerves to generate and relay electrical signals. Compound action potential (CAP) recording techniques, in varying forms, have been previously used to assess the excitability of the phrenic nerve (Erlanger and Gasser, 1924), the vagal nerve (Ordelman et al., 2010), the optic nerve (Hopper et al., 2023), human C-fibres (Carr et al., 2010) and mouse C-fibres (Bonalume et al., 2021). While conventional nerve recording techniques often focus on the number of fibres activated and their conduction velocity, the CAP recording technique, used also in the present study, adds information about the stimulus intensity required to activate a certain percentage of axons, thereby providing indirect evidence for membrane potential changes. Electrical stimulation of a peripheral nerve will generate an action potential in some or all of the axons within the nerve. The combination of these electrically-evoked action potentials in multiple axons can be recorded extracellularly as a compound action potential. The CAP represents the summation of individual action potential signals from axons in the nerve in a synchronous fashion. Thus, an increase in the amplitude of the CAP represents an increase in the number of axons activated by a given stimulus intensity, up to a maximum at which all axons are activated. This means, in comparison to a cellular action potential which occurs in an all-or-none fashion, the CAP is a graded phenomenon. This also explains why the CAP shape does not reflect that of an actual action potential.

Key parameters in determining excitability from CAP recordings are: the stimulus intensity required to evoke a CAP of a certain percentage (usually 40%) of its maximum size (suprathreshold stimulation) and, the intensity required for the same 40% amplitude, 30 ms after a conditioning suprathreshold stimulus. Together, they allow indirect assessment of changes in membrane potential (Bonalume et al., 2021; Bostock et al., 2003; Moalem-Taylor et al., 2007). The stimulation intensities required are monitored during the experiments (“threshold tracking”) and effects following interventions (eg. pharmacological) are assessed. As has been mentioned, the action potential relies on the influx of sodium causing a depolarisation of the membrane. Therefore, compound action potential recordings mainly rely on sodium channel kinetics, their availability and the actual membrane potential (see Figure 3). As eluded to, modulation of the membrane by prior activity may change the ability of an axon to propagate numbers of action potentials.

### 1.6.2 Calcium imaging

Calcium channels, just like sodium, potassium and chloride ion channels are key players in altering the membrane potential based on the positive charge entering the cell. Beyond this generic role of their charge, calcium ions have a complex role in intracellular signalling of cells in general, and in particular in neurons, where they are at the forefront of several transduction pathways. Indeed, the action potential-mediated depolarisation opens calcium channels, culminating in the influx of calcium into a cell, that stimulates the release of synaptic vesicles containing neurotransmitters. Often a characteristic of the action potential is also the ‘hump’ on the repolarising phase. This is due to incomplete inactivation of voltage-gated sodium channel 1.8 (NaV1.8) and calcium currents via high-voltage activated (HVA) calcium channels (Blair and Bean, 2002). The inward calcium current accompanying the action potential can trigger, for example, gene transcription or neurotransmitter release, but can also be used for live cell imaging (see below).

To maintain the steep transmembrane calcium gradient (see Table 1), many ion channels, transporters and pumps are involved. This is particularly important for the complex intracellular signalling functions of intracellular calcium and neurotoxicity related to extreme intracellular calcium levels. There are two main entryways for calcium into the cell: store-operated calcium entry (SOCE) and voltage-gated calcium channels (VGCCs). The smooth endoplasmic reticulum in the nerve cell body and axon acts as an internal calcium store. Influx from the extracellular space occurs when calcium has been depleted from internal stores (eg. endoplasmic reticulum). Orai1 (also known as calcium release-activated calcium channels) and STIM1 (stromal interaction molecule) plasma membrane channels are activated that allow influx of extracellular calcium which is then used to replenish the intracellular stores (Arjun McKinney et al., 2022; Brini et al., 2014)

Influx of calcium through VGCCs occurs via the coupling of electrical activity at the membrane (changes in membrane potential, ie. depolarisation) to biological processes. Voltage-gated calcium channels are divided broadly into two categories and most cells express at least four of these high-voltage activated or low-voltage activated (LVA) channels. High voltage-activated calcium channels activate with voltages positive between -40mV to -20mV, whereas low

voltage-activated channels only need mild depolarisations of the membrane potential, as low as -60 to -40mV, for activation (see Figure 3 for depiction).

One of the HVA channels is the CaV1 family encoding L-type channels. L-type channels are characteristically sensitive to inhibition by dihydropyridines (DHP) such as nimodipine or nifedipine and exhibit relatively slow voltage-dependent gating characteristics (Simms and Zamponi, 2014), including also relatively slow inactivation time constants (Catterall, 2011). DHP-type antagonists are known to bind in the active formation of the channel to optimise their inhibitory actions, which is often equal to a depolarised state (Rane et al., 1987). P-/Q-type, N-type and R-type calcium channels constitute the other HVA VGCC's. These calcium channel types often contribute to vesicular neurotransmitter release. P-/Q-type is inhibited by the  $\omega$ -Agatoxin (Nimmrich and Gross, 2012), and the N-type calcium channel is inhibited by the  $\omega$ -conotoxins isolated from the venomous marine snail (Olivera et al., 1994). CaV2.3 refers to the R-type calcium channel subfamily and, interestingly, can be inhibited by the GABA<sub>B</sub>R agonist baclofen (Wormuth et al., 2016), as well as organic trace meta cations, such as Zinc and Copper (Schneider et al., 2020).

<i>Channel</i>	Ca <sup>2+</sup> type channel	Tissue	Blocker	Voltage-dependence
<i>CaV1.1-1.4</i>	L	Muscle, neurons	Dihydropyridines	HVA
<i>CaV2.1</i>	P/Q	Neurons	$\omega$ -Agatoxin	HVA
<i>CaV2.2</i>	N	Neurons	$\omega$ -conotoxin	HVA
<i>CaV2.3</i>	R	Neurons	Zinc, Copper, baclofen	HVA
<i>CaV3.1-3.3</i>	T	Muscle, neurons	Nickel, TTA-P2	LVA

Table 2 Calcium channel subtypes and their functional specifications

The LVA channels, triggered by milder depolarisation, include CaV3 calcium subtypes forming T-type calcium channels. The blockers TTA-A2 and TTA-P2 that have shown efficacy in blocking T-type calcium channels are state-dependent, preferring the inactivated state, but have been shown to be effective for analgesia in rodent models of pain (Choe et al., 2011; Sandrini et al., 2011). See Table 2 for summary of VGCC types.

In addition to calcium influx from the interstitial space via voltage-gated calcium channels there are also delicately regulated intracellular calcium stores that contribute to the complex neuronal calcium signalling (Brini et al., 2014). The key intracellular compartments for calcium homeostasis are the endoplasmic reticulum (ER) and mitochondria. Loading of the ER and concomitant reduction of intracellular calcium levels is a function of SERCA (Ca<sup>2+</sup>-ATPase of the sarco-/endoplasmic reticulum) pumps (Brini et al., 2014). Conversely, calcium release from the ER is primarily controlled by inositol 1,4,5-triphosphate and ryanodine receptors (Smith et al., 2023). The role of mitochondria for calcium homeostasis has recently gained major interest in the context of neurodegeneration (Baev et al., 2022; Brini et al., 2014). Calcium-dependent long-term regulation and modulation via intracellular stores were of limited interest for our study as mainly acute changes of excitability were studied using live cell imaging.

Calcium imaging exploits intracellular calcium dynamics with the use of a membrane permeant fluorescent dye accumulating in the cytosol, because the lipophilic part of the molecule is cleaved by intracellular esterases preventing the dye from leaving the cell (Cameron et al., 2016). The dye increases fluorescence intensity upon binding of calcium and thus is a sensitive probe for assessing intracellular calcium transients and is used for live cell imaging. In vitro calcium imaging is advantageous to determine direct and sensitising effects of pharmacological agents, for example. The technique has also been used in combination with electrical field stimulation to determine the excitability of DRG neurons (Koopmeiners et al., 2013). Therefore, the use of calcium imaging provides insights into the excitability of individual neurons, with moderately high temporal resolution at a high throughput due to the fact that many neurons can be imaged at once.

### 1.7 Aims & Hypotheses

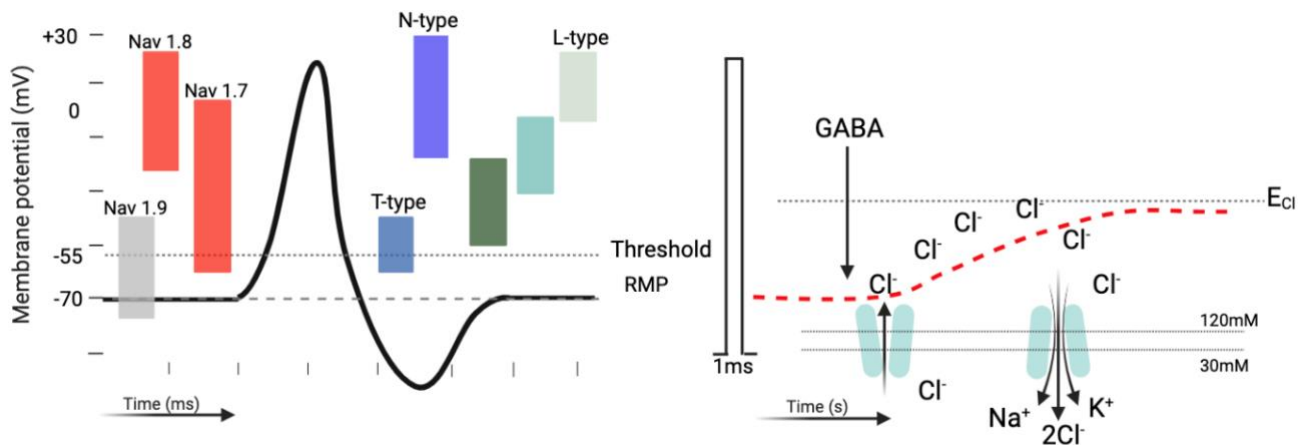


**Figure 3** A schematic to depict an action potential (AP) and the sodium channels contributing to the rising phase as well as the calcium channels activated during the repriming phase in addition to the chloride conductance associated with a GABA-mediated depolarisation.

Left, the coloured panels depict the membrane potentials (mV) during which the channel is open and allows ion flux. The action potential occurs over a timescale of milliseconds (ms). The dotted line at -55mV represents the threshold for AP initiation, while the dashed line depicts the resting membrane potential (RMP) voltage (mV). The 1ms pulse depicts the trigger for the action potential. Right, the chloride potentials are shown, where GABA is given, resulting in a chloride efflux, while the membrane potential slowly depolarises over a timescale of seconds, to reach the chloride equilibrium potential ( $E_{Cl}$ ). The inside of the cell has a high intracellular chloride concentration (30mM) while the extracellular chloride concentration is around 120mM. The NKCC1 pump works to restore the intracellular chloride concentration, by transporting 1 Na<sup>+</sup>, 1 K<sup>+</sup> and 2 Cl<sup>-</sup> ions back into the cell. The nature of the slow depolarisation will influence the ability to initiate an AP, in that it will inactivate sodium channels, while potentially still activating calcium channels. Made using BioRender.com.

Here, it was of particular interest to study the role of GABA-mediated chloride currents in limiting activity-dependent inhibition in peripheral primary afferents. In the CNS, GABAergic interneurons inhibit relay of nociceptive signals via primary afferent depolarisation and presynaptic inhibition. Yet, reversal of the chloride gradient in spinal cord neurons can switch a normal GABA-mediated inhibition to the opposite excitatory effect which has been hypothesized as important mechanism to explain hyperexcitability in chronic pain (Price et al., 2009; Wu and Wang, 2023). Traditionally, mechanisms inducing hyperexcitability are at the

forefront when considering concepts for chronic pain, for example, gain of function mutations of voltage-gated sodium channels (Alsaloum et al., 2021;Dib-Hajj et al., 2005).

In this work, we follow up on an alternative concept based on inhibition. The presence of GABA during high-frequency firing actually reduces C-fibre ADS (Carr et al., 2010), thereby limiting hypo-excitability and maintaining firing rates. What's more, GABA-mediated chloride currents are facilitated by hyperpolarisation (Bonalume et al., 2021;Carr et al., 2010). In axons from peripheral nerves, GABA can increase excitability, suggesting a depolarising mechanism (Carr et al., 2010) similar to the actions in DRG neurons, where it causes a depolarisation and an increase in intracellular calcium as measured by calcium imaging (Reichling et al., 1994).

In terms of the mechanism regulating intracellular chloride and consequently its driving force, an activity-dependent upregulation of NKCC1 activity has also been shown in unmyelinated C-fibre axons from the mouse (Bonalume et al., 2021) after high frequency firing. Thus, GABA-mediated chloride currents may actually be optimally positioned to limit activity-dependent reduction of excitability in C-fibres and thereby reduce conduction failure. This work focused on axonal GABA effects that might contribute to chronic pain via reduced activity-dependent neuronal inhibition combining a direct electrophysiologic approach and live cell imaging. Specifically, we studied temporal profiles of GABA effects and the impact of modulating the neuronal chloride gradient.

## 2 METHODS

## 2.1 Ethical approval for animal experiments

Ethical approval for the use of tissue from mice was obtained from the standing committee on ethical use of animals at the Medical Faculty Mannheim, Heidelberg University (approval numbers I-21/05 and I-21/15) and in compliance with guidelines for the welfare of experimental animals as stipulated by the Federal Republic of Germany.

## 2.2 Animals, anaesthesia and housing

Experiments were performed on adult (from 7 weeks of age) male and female C57BL/6N wild-type and transgenic mice (see *Transgenic mouse lines* below). Mice were kept in a housing facility with a controlled environment comprising a 12h light-dark cycle and tempered at 20°C with access to food and water *ad libitum*.

For tissue preparation, mice were anaesthetised with volatile anaesthesia (Isoflurane, CP Pharma, Burgdorf, Germany). Adequate depth of anaesthesia was determined with suppression of the hind paw withdrawal reflex, checked using a toe pinch on either side to avoid reflex adaptation. For experiments involving removal of the sural nerve, mice were killed by cervical dislocation. For experiments involving removal of spinal dorsal root ganglia (DRG; calcium imaging and patch clamp recordings, see *Isolation and cell culture of DRG neurons*), mice were killed by decapitation, minimizing damage to the cervical ganglia.

### 2.2.1 Transgenic mouse lines

Conditional transgenic mice were generated using the Cre-LoxP system that enables tissue-specific gene expression. Three mouse lines were maintained, one expressing heterozygotic Cre-recombinase and two carrying homozygotic loxP sites flanking a stop codon upstream of a reporter. The transgenic Cre-line used here had Cre-recombinase inserted downstream of the promoter for TRPV1 (transient receptor potential vanilloid-1) and mice are referred to here as Trpv1-Cre mice. Two loxP reporter mouse lines were also used. In the first line, the loxP stop sequence was used to regulate ChR2-EYFP (channelrhodopsin-enhanced yellow fluorescent fusion protein) expression from the Rosa26 locus. This line was generated by the Allen Institute for Brain Science and designated by them as Ai32 according to their transgenic nomenclature (see Tab. 3). The second reporter line had a loxP stop sequence upstream of the fusion protein Halorhodopsin-EYFP (eNpHR 3.0/EYFP) and was also generated by Allen Institute for Brain Science and designated Ai39 ((Madisen et al., 2012); see Tab. 3).

Abbreviation	Fluorescent reporter	Jax Stock No.	Mouse strain specification	Allen Brain Institute nomenclature
<i>ChR2</i>	Channelrhodopsin, EYFP	024109	B6.Cg-Gt(ROSA)26Sor <sup>tm32</sup> (CAG-COP4*H134R/EYFP) <sup>Hze</sup> /J	Ai32
<i>eNpHR 3.0</i>	Halorhodopsin, EYFP	014539	B6;129S-Gt(ROSA)26Sor <sup>tm39</sup> (CAG-hop/EYFP) <sup>Hze</sup> /J	Ai39

**Table 3** Abbreviation and genetic strain of transgenic mice carrying fluorescent reporter proteins

To generate experimental mice in which reporter expression was restricted conditionally to cells expressing Cre-recombinase, the breeding strategy encompassed mating homozygote mice, ie. a male Trpv1-Cre homozygote mouse was crossed with a female homozygote Ai32 mouse. The resulting mice were heterozygotic for both alleles, leading to the conditional expression of Cre and thus expression of Chr2-EYFP in TRPV1+ cells (see Tab. 4 for possible pairing outcomes). The expression of the fluorescent protein was verified in cells upon inspection with a fluorescent microscope.

Similarly, mice expressing the fusion protein Halorhodopsin-EYFP (eNpHR 3.0/EYFP) in TRPV1+ cells were generated by crossing female homozygotic Ai39 (eNpHR 3.0-EYFP) mice with a homozygotic male Trpv1-Cre mouse above (eNpHR 3.0;TRPV1), generating heterozygotic mice. The Cre line was maintained by crossing homozygotic animals with each other. Nonetheless, occasionally it was not possible to cross only homozygote mice, thus the Punnett square in Table 4 indicates the outcome of various pairings.

	Homozygote Trpv1-Cre	Heterozygote Trpv1-Cre
Homozygote Rosa26 either Ai32/Ai39	100% Ai32/Ai39 KI/WT; Trpv1-Cre KI/WT	100% Ai32/Ai39 KI/WT 50% Trpv1-Cre KI/WT 50% Trpv1-Cre WT/WT
Heterozygote Rosa26 either Ai32/Ai39	100% Trpv1-Cre KI/WT 50% Ai32/Ai39 KI/WT 50% Ai32/Ai39 WT/WT	25% Ai32/Ai39 KI/WT;Trpv1-Cre KI/WI 25% Ai32/Ai39 WT/WT; Trpv1-Cre WT/WT 25% Trpv1-Cre KI/WT; Ai32/Ai39 WT/WT 25% Ai32/Ai39 KI/WT; Trpv1-Cre WT/WT

**Table 4 Example Punnett square for genetic crosses between Trpv1-Cre mice and Ai32 or Ai39 mice**

Tissue from ear punches, collected as part of the identification procedure for mice and taken at approximately four weeks of age as the animals were weaned, was used for genotyping by PCR (polymerase chain reaction). PCR is used to amplify DNA by ‘unzipping’ the double-stranded DNA into a single strand. Oligonucleotides of approx. 20-mer served as primers for DNA polymerase when/if they anneal to their target strands, for DNA polymerase to add base pairs on the 3’ end (Chuang et al., 2013).

Ear punches were placed in 100µl lysis buffer (25mM NaOH, 0.2mM EDTA) overnight at 55°C. The following morning 100µl neutralization buffer (40mM Tris, pH 5) was added and the mixture was vortexed, spun for 3 minutes at 13000rpm and 0.5µl of the resulting supernatant was used for the PCR genotyping reaction.

PCR primers were purchased from Eurofins Genomics (Ebersberg, Germany). Oligomer sequences for Cre forward and Cre-reverse and TRPV1-forward and TRPV1-reverse, listed in Table 5, were used for genotyping for the TRPV1-Cre insert in a 50µM primer mix (see Tab. 6 for Master mix composition). For the Rosa locus, primers to amplify product from Rosa-WT (wild-type) and Rosa-KI (Knock-in) alleles were used and comprised respectively a Rosa common and Rosa WT reverse pair and Rosa common and CMV-CAG reverse pair for the KI sequence. A common 33.3µM primer mix was made for these reactions (see Tab. 6).

Standard PCR techniques were used and each primer pair was implemented in the master mix recipe in Table 6. Amplification was performed using a thermocycler (Biometra T-Personal Thermocycler 48, Analytik Jena, Jena, Germany) with an annealing temperature of 59°C for ROSA and 61°C for TRPV1-Cre primers. PCR products were loaded into a 2% agarose (Merck, Darmstadt) gel (composition: 120ml TAE with 2.4g agarose) and run at 150V for 40 minutes. The Cre and TRPV1-WT product had a predicted length of 500bp and 495bp respectively. These

were loaded into separate reactions because of their similarity in length. ROSA-KI and ROSA-WT products were expected to be 471bp and 264bp in length, respectively. The 3 primer strategy used to genotype ROSA-WT or KI inserts utilizes two reverse primers against a common forward primer (see Fig 4B. for primer strategy).

Insert	Primer	Oligomer sequence
Cre	Forward sequence	GGTGCAAGTTGAATAACCGG
	Reverse sequence	CAGAGACGGAAATCCATCGC
TRPV1-WT	Forward sequence	GTTTCAGGGGAGAACTGGAAGAACT
	Reverse sequence	TAGTCCAGCCATCCAAAAGTC
ROSA	ROSA common forward	GCTCAGTTGGGCTGTTTTGG
	ROSA WT reverse	AGACTCCCGCCCATCTTCTA
	KI: CMV-CAG reverse	TAGGGGGCGTACTTGGCATA

**Table 5 Oligomer sequences for PCR primers**

	Volume for 1 run ( $\mu$ l)	10X Master mix ( $\mu$ l)	Use	Source
10X ThermoPol Buffer (2mM Mg <sup>2+</sup> final)	2	20	Increases enzyme stability	New England Biolabs (NEB), MA, USA
10mM dNTP's (200 $\mu$ M final)	0.4	4	Provides nucleotides for the unzipped DNA strand using the template of a single side	Invitrogen, Waltham, MA, USA
50 $\mu$ M Primer mix (0.5 $\mu$ M final)/ 33.3 $\mu$ M for ROSA-KI	0.16 (0.24 for ROSA)	1.6 (2.4 for ROSA)	Short DNA sequences corresponding to the DNA region of interest	Eurofins Genomics, Ebersberg, Germany
100mM MgSO <sub>4</sub> (+1mM Mg <sup>2+</sup> final)	0.2	2	Catalyzes the phosphodiester bond between the primer and a dNTP	NEB
Taq DNA polymerase (0.5U final)	0.1	1	Polymerizes the new DNA strand	NEB
ddH <sub>2</sub> O	To total: 20	To total: 200	Helps extraction of material into solution	n/a

**Table 6 Master mix for PCR genotyping reactions**

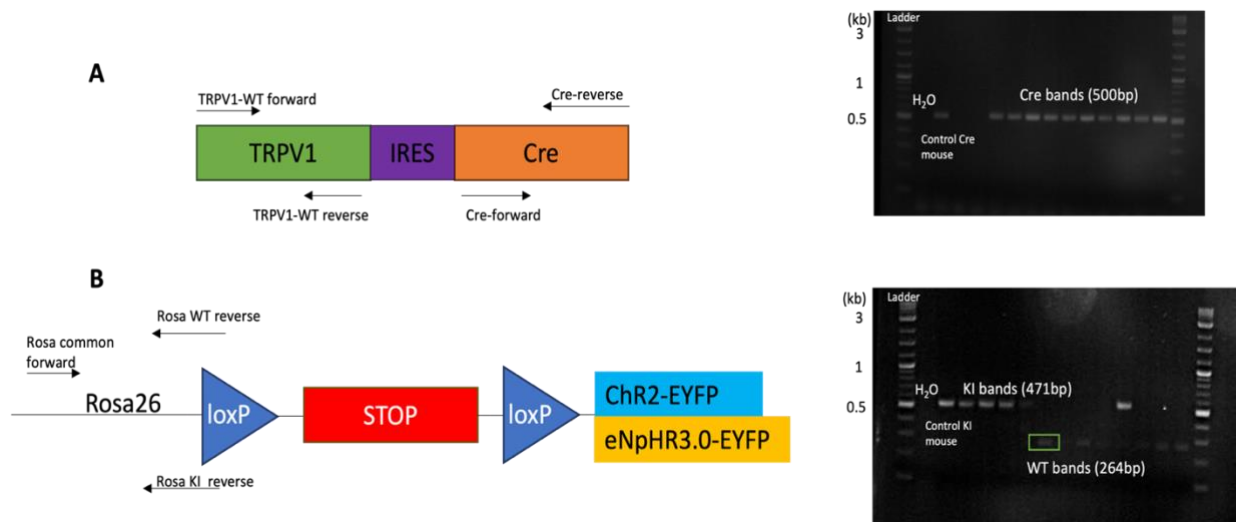


**Figure 4 Schematic for PCR primer strategy**

A) the TRPV1 promoter (green), with an IRES (internal ribosomal entry site, purple) and Cre insert (orange) with arrows indicating the location and direction of PCR primers. The right panel is an example gel of PCR products. B) The Rosa26 ubiquitous promoter is upstream of the loxP-Stop-loxP sequence that is later removed by Cre-recombinase to allow expression of the reporter proteins ChR2-EYFP (blue) or eNpHR3.0-EYFP (yellow). Primer locations and directions are indicated by arrows. Panel on the right show an example gel with a green box surrounding WT bands.

### 2.2.2 Floxed reporter lines

Two transgenic reporter lines, Ai32 and Ai39 were used in which reporter expression was regulated by removal of a floxed stop sequence. Ai32 is a reporter line for channelrhodopsin. Channelrhodopsin-2 is a light activated ion channel, originating from green algae (*Chlamydomonas reinhardtii*), that enables algae to migrate to ambient light conditions best suited for photosynthesis (Deisseroth and Hegemann, 2017). Engineered channelrhodopsin 2 (ChR2) with a point mutation at H134R, increases the conductance of the non-selective cation channel that opens in response to blue light with a peak sensitivity at approximately 450nm (see Fig. 5A). In response to illumination, ChR2 undergoes a conformational change, opening the channel to allow potassium, calcium and sodium ion flux resulting in a net inward current (Nagel et al., 2003) and depolarisation (Fig. 5B). ChR2 provides a means of changing membrane potential without disturbing surrounding cells (Espinosa-Juarez et al., 2023). ChR2 is desensitized by prolonged illumination, with a time constant of approx. 20ms (Nagel et al., 2003; Zamani et al., 2017) and the extent of desensitization is dependent upon the light power density (Yawo et al., 2013), pH and membrane potential (Nagel et al., 2003). Recovery from desensitization has a time course of approximately 10 seconds and this is enhanced by hyperpolarized potentials and lower extracellular pH (Nagel et al., 2003).

A halorhodopsin reporter mouse was also used to influence intracellular chloride. Halorhodopsins are light-activated microbial opsins that pump chloride ions into the cell and respond maximally to light at approximately 580nm (Schobert and Lanyi, 1982) (see Fig. 5A). Halorhodopsins were first isolated from prokaryotic haloarchaea and the inward chloride transporter NpHR derives from *Natronobacterium pharaonis* (*Natronomas pharaonis*). In their natural environment which is usually high in chloride, they can pump chloride intracellularly even against an existing concentration gradient (Han and Boyden, 2007; Schobert and Lanyi,

1982). The engineered variant eNpHR3.0 hyperpolarizes cells and typically inhibits neuronal firing (Zhang et al., 2007) (see Fig. 5B).

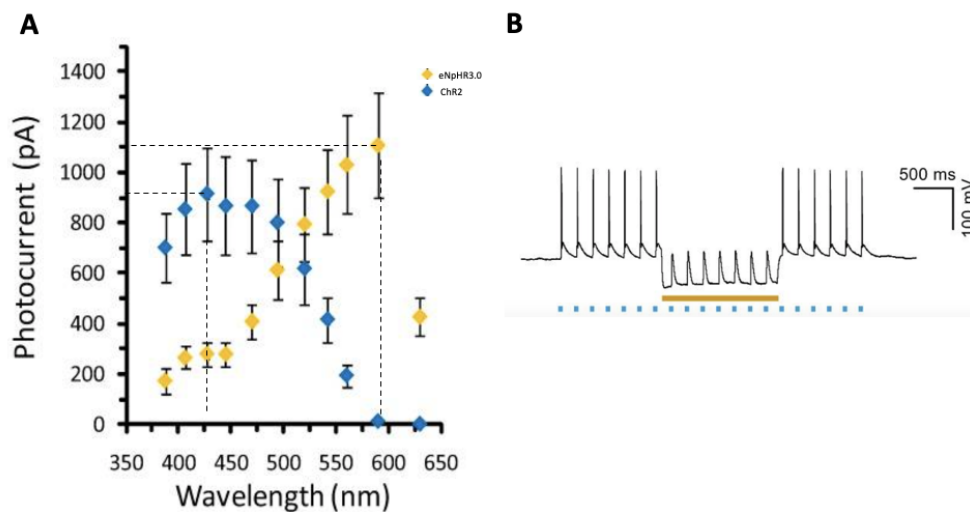


**Figure 5 Comparison of ChR2 and NpHR excitation spectra and functionality**

A) Excitation spectra for ChR2 (blue) and NpHR (yellow). Dashed vertical lines indicate excitation maxima at 460nm (ChR2) and 590nm (eNpHR 3.0) respectively. B) blue light to activate ChR2, results in depolarisation strong enough to elicit an action potential, and exposure to yellow light (NpHR) inhibits spike initiation. Adapted from (Gradinaru et al., 2010).

Halorhodopsins desensitize slower than ChR2 with a time course of seconds and in response to prolonged light exposure there is a decay of effective inhibition with a time course of about 16.8s (Han and Boyden, 2007). Halorhodopsins recover from a desensitized state with a time course of approximately five minutes (Madisen et al., 2012).

NpHR and ChR2 can be combined, using transgenic lines expressing both fluorescent proteins under separate promoters. In neurons from these mice exposing them to yellow light whilst giving brief pulses (15ms) of blue light can be used to achieve opposing effects on modulation of membrane potential (Zhang et al., 2007) (see Fig. 5B).

## 2.3 Extracellular recording of Compound Action Potentials

### 2.3.1 Sural nerve preparation

The sciatic nerve is the longest peripheral nerve in mammals. It trifurcates in the popliteal fossa into the common peroneal, tibial and sural nerves. The sural nerve is located superficially in the distal hind limb and is generally considered to be a purely sensory nerve, containing both myelinated A-fibres and unmyelinated C-fibres (Schmalbruch, 1986), rendering it appropriate for sensory threshold tracking experiments. In humans, the sural nerve has been reported to carry a relatively small and variable number of motor axons (Amoiridis et al., 1997).

To isolate the sural nerve in mice, the hind legs were shaved and disinfected with 70% ethanol. A small incision was made in the skin at the area of the tibialis anterior/tibial bone and this was extended medially and proximally to the popliteal fossa and further proximal to the hip forming a triangle (Fig. 6A). The skin was separated from underlying tissue by blunt dissection and reflected. Biceps femoris posterior was cut at its insertion and reflected medially to expose the popliteal fossa and the trifurcation of the sciatic nerve. From this branching point the sural nerve travels inferiorly between the lateral and medial heads of the gastrocnemius muscle to

the Achilles tendon. The origin of the sciatic nerve at the hip was identified and the nerve cut as close to its exit point from the spinal column as possible (see Fig. 6A). The isolated sciatic-sural nerve section was pinned gently to the base of a tissue bath to form a T-shape. The bath was filled with HEPES-buffered physiological solution and the silicone base of the bath was black to enable better visual contrast (Fig. 6B). The epineurium of the nerve was removed carefully by de-sheathing reducing the diffusion barrier to enable better permeation of drugs (see Fig. 7 for schematic of peripheral nerve). The sural nerve was then separated from the sciatic trunk before being mounted in an organ bath (see Fig. 8).

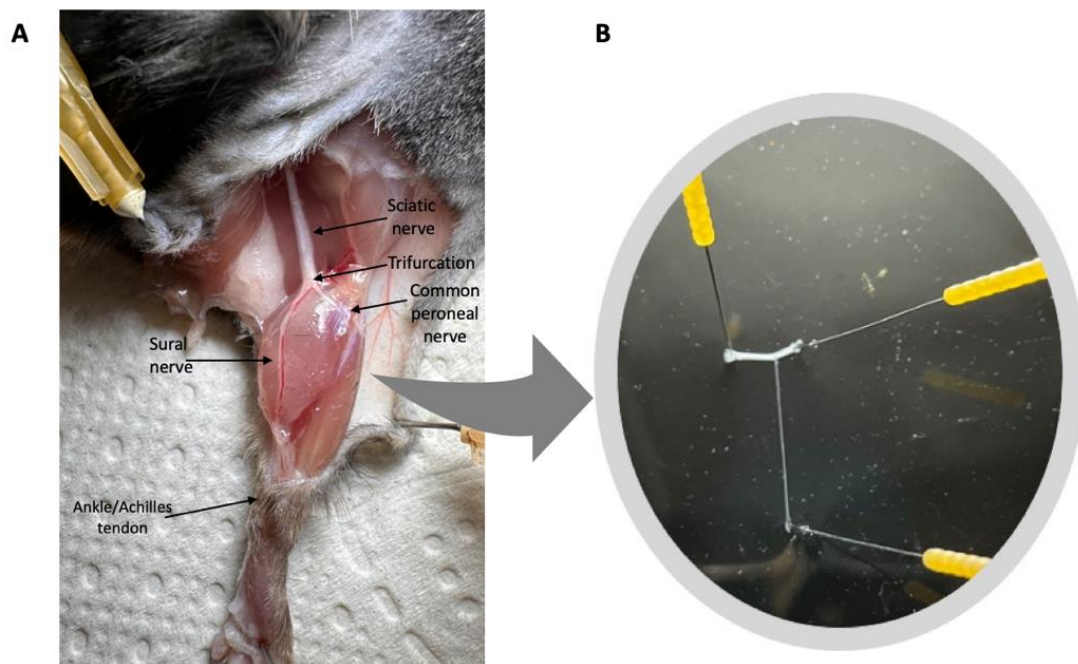


**Figure 6 Preparation of mouse sural nerve**

A) the exposed sciatic nerve and its trifurcation into sural, common peroneal and tibial (not shown here) nerves exposed following a skin incision from the iliac crest to the ankle, near the Achilles tendon. B) the T-shaped sciatic-sural nerve section pinned to the base of a tissue bath in preparation of 'desheathing'.

### 2.3.2 C-CAP recording setup

The de-sheathed sural nerve was mounted between recording electrodes in a custom made organ bath with a nominal volume of 750 $\mu$ l (Fig 8B). The nerve was suspended between two glass pipettes each containing a small silicone diaphragm. The silicone rubber diaphragms were made from a mixture of silicone and catalyst in a 1:1 ratio. Each end of the nerve was carefully drawn through a small opening in the silicone membrane using a thin fluid-filled polyurethane tube to affix the nerve with negative pressure. The opening in the silicone is self-sealing. This provides mechanical stability and serves as a high resistance electrical seal between that portion of nerve within the organ bath and that inside the glass pipette. Over this sealing resistance, current to stimulate was delivered to one end of the nerve and extracellular current was recorded over the silicon seal resistance at the other end of the nerve. Pairs of chlorided silver wire electrodes were used to stimulate and record. For each electrode pair, one electrode was inside the glass pipette and the other electrode inside the bath. For recording, the electrode within the glass pipette was connected to the non-inverting input of the amplifier. For stimulation, the electrode in the organ bath was the cathode and the anode was inside the glass pipette. Constant current electrical stimulation was delivered using an A395 (World

Precision Instruments, FL, USA). To generate a compound action potential with a C-fibre component, 1ms rectangular pulses at intensities of up to 50 $\mu$ A were used.

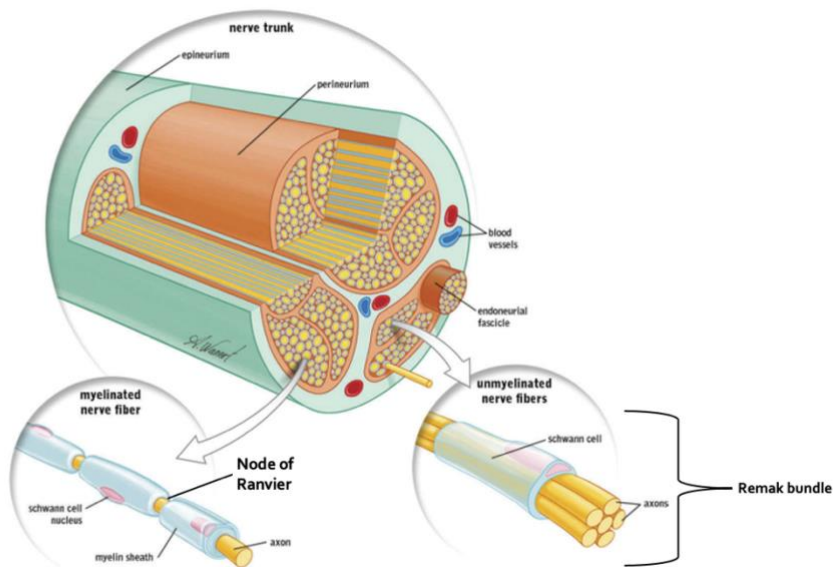


**Figure 7 Schematic of transverse section through peripheral nerve**

showing macroscopic structure including the epineurium, perineurium, endoneurium, individual nerve bundles and their myelinated (left) and unmyelinated (right) axons, including the structure of a Remak bundle, a bundle of unmyelinated C-fibre axons surrounded by a non-myelinating Schwann cell. Adapted from (Ilfeld et al., 2016).

Since action potentials initiate at the cathode (see Fig. 8 A&C) the conduction distance along the nerve was measured for each experiment as the distance between the ends of the two glass pipettes. Conduction distances varied between 3-8 mm. The bath was perfused continuously by a peristaltic pump (Watson-Marlow 502S, GEMINI, Germany) at a flow rate of 6-8 ml/min with HEPES-buffered physiological solution (see *Solutions*) bubbled with 100% O<sub>2</sub>.

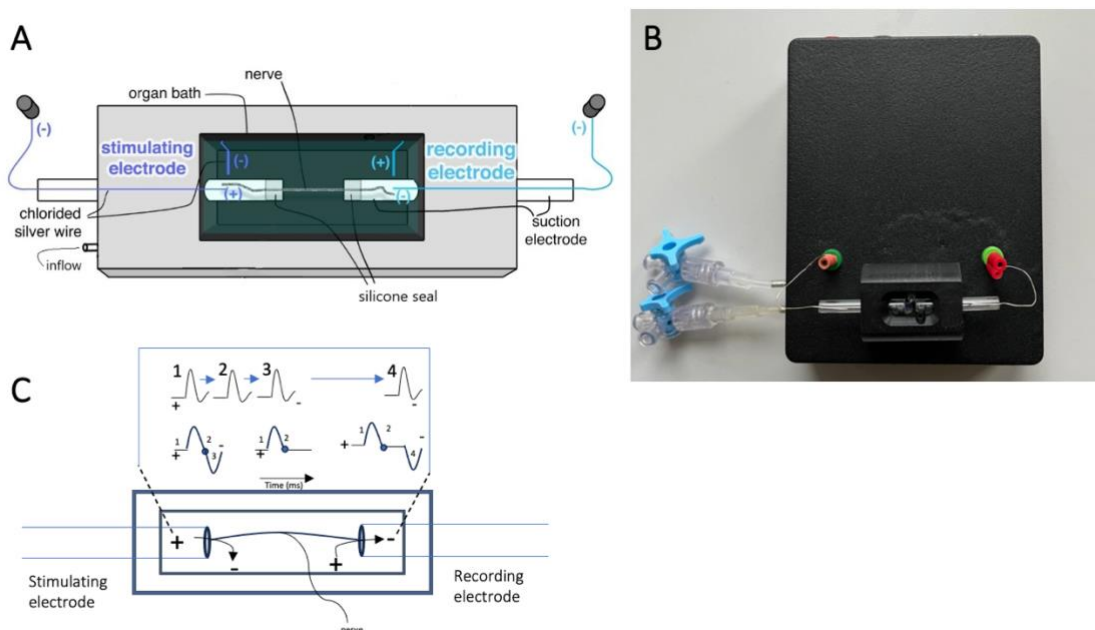


**Figure 8 Compound action potential recording equipment and principle of propagation of stimuli**

A) A schematic of the organ bath depicted in B) labelled with the stimulation and recording electrodes, where the nerve is placed in between the two silicone seals. C) An action potential (AP) generated at the tip of the left electrode (stimulating electrode) propagates to the recording electrodes on the right. As the AP passes the positive recording electrode, it results in an upward deflection of the voltage recording (positive, 1). Propagation to a point between the two electrodes results in no difference between '-' and '+' and thus a zero crossing of the voltage signal (2) and subsequently as the AP passes the -

electrode a downward (negative) voltage deflection is recorded (3; depending on how long the propagation is, 4). A) Adapted from (Bonaiuto et al., 2021).

A Windkessel on the input and output sides of the bath served to minimise pulsatile flow and to isolate the organ bath electrically. Pharmacological substances were added to the perfusing solution by changing the source of solution from one cylinder to another containing the substance diluted to the appropriate concentration. The approximate amount of time required for the substance to reach the bath was 35-40 seconds. The temperature of the solution in the bath was measured by a thermistor placed in the bath and maintained, typically between 28-31°C, with an inline Peltier device.

### 2.3.3 Principle of axonal threshold tracking

Extracellular signals were recorded from isolated segments of mouse sural nerve using a pair of platinum wire electrodes in a custom made organ bath (See Fig. 8B). Signals were amplified (N104 Neurolog, Digitimer, Hertfordshire, United Kingdom), filtered (HumBug, Digitimer) and digitised (NI-600, National Instruments, Austin, TX, USA) and then processed using QTRAC software (Hugh Bostock, Digitimer). QTRAC is a stimulus-response data programme with online capacity to acquire data and track electrical thresholds or latencies. In this study, QTRAC was used to track the electrical activation threshold of axons in mouse sural nerve.

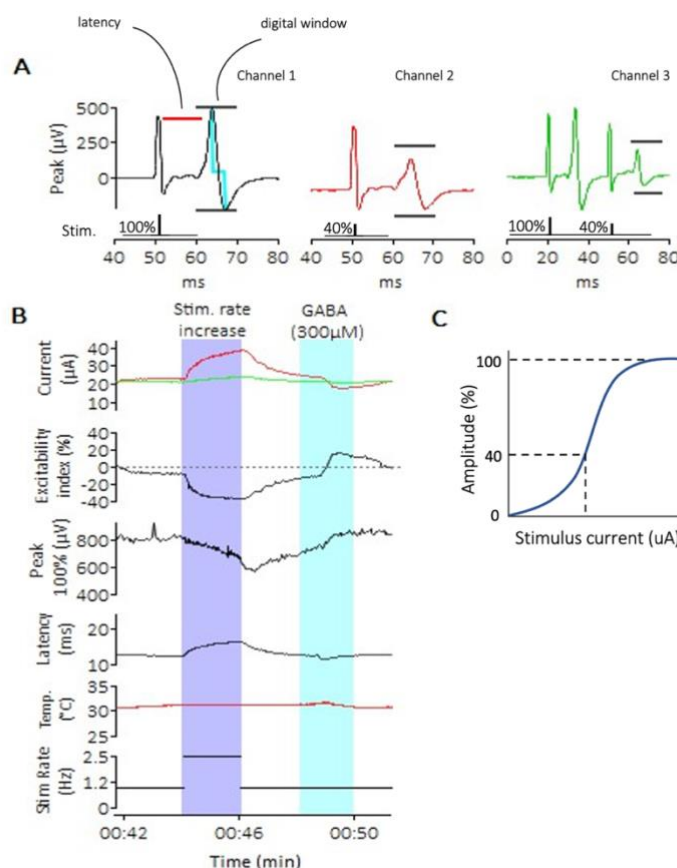


#### Figure 9 Implementation of axonal threshold tracking in QTRAC

A) Axonal excitability is assessed in sets of three. The first stimulus channel is set at a supra-maximal current to evoke a 100% C-CAP response (ie. all axons assumed to respond, black trace); the second stimulus channel (red trace) is adjusted to evoke a C-CAP at an amplitude of 40% of the 100% C-CAP evoked by preceding Channel 1 stimulus.

The third channel is adjusted to maintain a C-CAP at an amplitude of 40% of the 100% response, but 30 ms after a supramaximal conditioning stimulus (green trace). The latency indicated in the 100% stimulus trace represents the delay to 50% of the C-CAP positive peak. The digital window is set to restrict the domain of assessment to a time window encompassing the C-CAP without the stimulus artefact of A-CAP. B) Current required to evoke a C-CAP of 40% amplitude (red) and a conditioned C-CAP of 40% amplitude (green). The excitability index is determined from the ratio of red and green traces in the upper panel. The peak and latency traces reflect parameters determined for each 100% C-CAP. The stimulus rate, i.e. the reciprocal of the interval between each channel is shown in the bottom trace in A. Purple shading indicates an increase in the stimulus rate and the light blue shading indicates application of GABA (300µM). C) The recruitment curve showing C-CAP amplitude as a function of stimulus current is sigmoid in form and is steepest at a C-CAP of approximately 40%

shading indicates an increase in the stimulus rate and the light blue shading indicates application of GABA (300µM). C) The recruitment curve showing C-CAP amplitude as a function of stimulus current is sigmoid in form and is steepest at a C-CAP of approximately 40%

Electrical stimulation of a peripheral nerve will generate an action potential in some or all of the axons within the nerve. The combination of these electrically-evoked action potentials in multiple axons can be recorded extracellularly as a compound action potential (CAP). The CAP represents the summation of individual action potential signals from axons in the nerve. Thus, an increase in the amplitude of the CAP represents an increase in the number of axons activated by a given stimulus intensity, up to a maximum at which all axons are activated. This means, in comparison to a cellular action potential, which occurs in an all-or-none fashion, the CAP is a graded phenomenon. The relationship between the amplitude of the CAP and the stimulus current required to evoke each CAP amplitude is sigmoid in form (See Fig. 9C). The principle of threshold tracking as implemented by QTRAC, is to adjust the amplitude of a fixed width (1ms) electrical current pulse, such that the amplitude of the resulting CAP remains constant. The target size of the CAP is typically chosen to be 40% of the maximum CAP amplitude. A value of 40% is chosen because it represents the steepest portion of the sigmoidal relationship between stimulus current and CAP amplitude (Fig. 9C).

To evaluate excitability in C-fibre axons, the C-fibre compound action potential (C-CAP) is used. The C-CAP signal can be tracked in isolation using a time window, i.e. a window positioned at a set time after the electrical stimulus, within which only the C-CAP is evoked (see Table 7 for QTRAC commands and Fig. 9A&B for implementation). QTRAC monitors several parameters of both the stimulus and the resulting C-CAP. Specifically, for the C-CAP, the peak-peak amplitude and the latency of the response after the stimulus (determined as the delay to 50% of the C-CAP positive peak). QTRAC also records the stimulus width (typically 1ms), stimulus current amplitude and the temperature of the bath at the time of each electrical stimulus.

To examine the effect of GABA on C-fibre axons, the electrical excitability of C-fibres was monitored over time using QTRAC (Figure 9). QTRAC generates a set of three stimuli in a repeating sequence, with a variable interval between each stimulus (adjustable per protocol) but typically set to 2 seconds. Within the QTRAC program each stimulus in the set of 3 is designated a channel. The first channel used a supramaximal stimulus current, i.e. a stimulus current adequate to evoke a maximal (100%) C-CAP (black, Fig. 9A). For this C-CAP evoked by a supra-maximal stimulus, all axons (i.e. 100%) are assumed to respond. The stimulus current required to ensure a 100% C-CAP was established at the beginning of each experiment and subsequently held constant throughout. The second stimulus channel (red, Fig. 9A) was adjusted each time to evoke and maintain a C-CAP at an amplitude of 40% of the 100% C-CAP response evoked by the preceding stimulus channel 1. The third stimulus channel (green, Fig. 9A) was also adjusted to maintain a C-CAP at an amplitude of 40% of the 100% response, but in this case a 100% supramaximal conditioning stimulus was delivered 30ms prior to the stimulus adjusted to evoke the 40% C-CAP response. Channel 2 is thus referred to as an unconditioned tracking stimulus while channel three is a conditioned tracking stimulus. Both channels strive to evoke a 40% C-CAP. The use of the conditioned stimulus channel 30ms prior to the test stimulus was to normalise threshold changes for fluctuations in the absolute threshold of axons. Previous reports using single C-fibre axons have shown that a time point 30ms after an action potential, C-fibre axons are in a consistent and stable excitability state (Bostock et al., 2003). Normalisation of the unconditioned threshold (channel 2) to the conditioned threshold (channel 3) was calculated using Equation 3 to derive an excitability index. QTRAC continuously adjusts the current required to evoke a target 40% C-CAP response and adjusts the amplitude of the test stimulus iteratively to achieve this.

The calculation of an excitability index, allows visualization of an increase or decrease in excitability of axons in response to interventions (eg. pharmacological, high frequency stimuli). Changes in excitability index reflect changes in membrane potential (Bonalume et al., 2021; Moalem-Taylor et al., 2007). Excitability index is the ratio of the difference between the

conditioned and unconditioned stimulus currents relative to the current intensity for the unconditioned response expressed as a percentage (see Equation 3). As an example, negative values of excitability index indicate that more current is required to evoke an unconditioned 40% response (Carr et al., 2010).

$$\text{Excitability index (\%)} = 100 * \frac{(40\% \text{ conditioned current} - 40\% \text{ current})}{40\% \text{ current}}$$

Equation 3 Formula for calculation of excitability index

QTRAC command	Meaning	Function
WW	Windows width	width of the window
WS	Windows start	where the window for response tracking should start
ML800		Low pass filter 800Hz
GS	Grab traces/stop grabbing traces	Grab traces for shapes of the response to save and use later in analysis
DX/DY	Display X, Display Y	Adjusting scaling of X & Y
DC	Display channel	Which channels to show
TW	Test width	Width of the test stimulus
TH	Test height	Amplitude of test stimulus
SC	Select channel	Selecting channels to use
SS	Stimulus start/stop	Start or stop stimulation
FC/FS	File close/File save	File close/file save

**Table 7 QTRAC commands and their functions**

#### 2.3.4 Optogenetic stimulation

Photo-stimulation allows high spatiotemporal resolution (Beaudry et al., 2017) and was used here to activate selectively Trpv1;Chr2 expressing axons in the sural nerve and cultured DRG neurons. An LED light source (LEDD1B T-cube LED Driver, ThorLabs, Newton, NJ, USA) was coupled to a fibre optic with a fine canula (400µm core, 20mW, 470nm wavelength) to deliver amplitude and time modulated light pulses. To stimulate Trpv1;eNpHR3.0 axons, a wavelength of 595nm was used. The light guide was positioned above the recording bath (Fig 8B) so that light was focused on a small segment of nerve.

#### 2.4 Isolation and cell culture of DRG neurons

Adult C57BL/6N mice were anesthetized with isoflurane and killed by decapitation. Dorsal root ganglia (DRG) were isolated from cervical, thoracic and lumbar segments. Cervical dislocation was avoided when removing DRG neurons as it mechanically disrupts the cervical ganglia. The mouse was placed in a ventral position and the tail removed at the lumbosacral joint. Scissors were used to cut longitudinally along the left and right sides of the vertebral column, in a cranio-sacral plain, through the muscles and ribs. A slight arch was made around the ribs for orientation of the thoracic portion of the vertebral column. Scissors were used to cut beneath the vertebra, exposing the lungs and inner organs and finally to excise the column from the rest of the body. Once removed, the spine was cleaned of excess tissue.

Dorsal root ganglia are located in each intravertebral foramen adjacent to the spinal cord. A pair of forceps was used to pinch the first cervical vertebrae and then a second pair was used to pull the bone apart exposing the spinal canal containing the cord. Forceps were used to carefully push the cord matter to one side and expose the dorsal root ganglion. There are 31 pairs of spinal nerves and thus 62 dorsal root ganglia. Once a ganglion had been exposed, forceps were used to clasp the root and gently pull. The same was done on the opposite side and this method of dissection was continued down to the lumbar segments to extract as many individual DRG as possible.

DRG were collected and placed in chilled sterile HBSS ( $\text{Ca}^{2+}/\text{Mg}^{2+}$  added; Thermo Fischer, Karlsruhe, Germany) before being cleaned of excess tissue (eg. roots) and digested in HBSS with liberase (1.8U/ml, Roche, Mannheim, Germany) for 40 minutes at 37°C. Digested ganglia were triturated and transferred to DMEM with added 10% FBS and 1X penicillin-streptomycin (Thermo Fischer). Cells were centrifuged for 2 minutes at 1200 rpm, triturated, resuspended and centrifuged a second time before being plated and allowed to adhere.

In preparation of plating, 25mm coverslips in 35mm petri dishes were coated with a drop of poly-L-lysine/laminin (1:100, both from Sigma Aldrich, St. Louis, MO, USA) and placed in the incubator for 30-90 minutes. After removal, cover slips were rinsed with ddH<sub>2</sub>O and a 10µl drop of laminin/ddH<sub>2</sub>O (1:10), placed centrally on the cover slip, was left to dry until plating. Cells were plated in a volume of 40µl and allowed to adhere for 1-2 hours before 2ml medium was added. Dishes were left overnight in a humidified incubator at 37°C and 5% CO<sub>2</sub>.

## 2.5 Calcium imaging

Fluorescence calcium imaging was always performed within 36 hours of neuronal plating. Cells were loaded with the intensity based calcium indicator Fluo8-AM (AAT Bioquest, Sunnyvale, CA, USA) by incubation in DMEM medium containing Fluo8 (3µM) for 20-30 minutes in the dark and at room temperature. After incubation, cells were rinsed twice with imaging solution (see *Solutions*) before the coverslip on which the cells were plated was

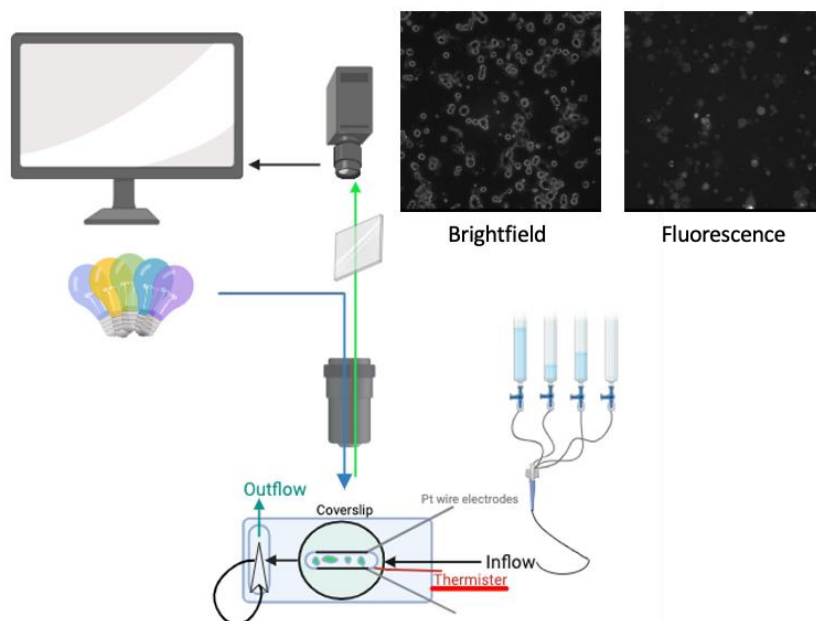


**Figure 10 Schematic depicting calcium imaging setup** with example brightfield and fluorescent images labelled. Created with BioRender.com

transferred to a stage-mounted slotted bath (RC-21 BRFs, Warner Instruments, Holliston, MA, USA). Coverslips were sealed to form the base of the slotted bath with an annulus of silicone grease that was pressed to the

chamber to create a water tight seal. The bath allowed uni-directional flow of the perfusing solution. Inflow was regulated by a gravity driven system through a manifold to exchange different solutions. The outflow was regulated by a small reservoir emptied continuously with a vacuum pump. Chemical stimulation was delivered by hand-switching between reservoirs in the manifold tap system. The nominal bath volume was 263 $\mu$ l. The slotted bath was equipped with a pair of platinum wire electrodes for electrical field stimulation (see Figure 10).

Images were acquired using a back-illuminated 512 x 512 pixel cooled EMCCD camera (Evolve 512, Photometrics, Tucson, AZ, USA) connected to the side port of an Axiovert 200 microscope (Zeiss, Jena, Germany). Cells were imaged with a 10x objective (NA 0.25, PH1, Neofluar) and a filter set comprising excitation BP 450–490 nm, dichroic 510 nm and emission LP 515 nm (Chroma Technologies, Bellows Falls, VT, USA). Brightfield illumination was provided by the microscope's halogen lamp. An initial brightfield image and a stationary fluorescent image were captured to monitor any subsequent movement and to demarcate cells. During recordings, fluorescence images were acquired at 0.5 Hz or every 2 seconds using a 10ms exposure to 465nm LED (Prior Scientific Instruments, Cambridge, UK). Images were acquired initially over 3 minutes to establish baseline. The relative timing of camera frame grabs, LED exposure and electrical stimulation were controlled by  $\mu$ Manager software synchronised with custom scripts via an Arduino Duemilanove. Constant current electrical field stimulation was delivered as 1ms rectangular pulses at 10Hz (DS7A, Digitimer).

## 2.6 Solutions

### 2.6.1 Calcium imaging solutions

The standard solution for calcium imaging comprised (in mM): 140 NaCl, 5 KCl, 10 D-glucose, 2 CaCl<sub>2</sub>, 1 MgCl<sub>2</sub>, 10 HEPES and pH was adjusted to 7.44 with NaOH. This imaging solution was used to dilute stock solutions to their final concentration for use on the day of each experiment. For solutions containing nominally zero extracellular calcium, CaCl<sub>2</sub> was replaced with an equimolar amount of MgCl<sub>2</sub>. Solutions in which the concentration of chloride was reduced comprised (in mM) 140 Na-gluconate, 5 K-gluconate, 10 D-glucose, 2 CaCl<sub>2</sub>, 1 MgCl<sub>2</sub>, 10 HEPES and pH was adjusted to 7.44 with NaOH. Osmolarity was measured using a vapour pressure osmometer (Model 5600, Wescor, South Logan, UT, USA) to ensure it was similar to the standard physiological solution (around 310-315 mOsm). A 45 mM potassium solution applied as a depolarising stimulus at the end of experiments was prepared by replacing 40 mM NaCl with an equimolar amount of KCl in the physiological solution.

### 2.6.2 C-CAP recording solutions

HEPES buffered physiological solution (referred to as 'HEPES' throughout) comprised (in mM) 118 NaCl, 3.2 KCl, 20 Na-gluconate, 6 HEPES, 1.5 CaCl<sub>2</sub>, 1 MgCl<sub>2</sub> and 10 D-Glucose. Osmolarity was measured and adjusted to around 310 mOsm, similar to the regular HEPES solution.

### 2.6.3 Pharmacological agents

Stock solutions of Fluo8-AM (1mM, AAT Bioquest, Pleasanton, CA, USA), capsaicin (50mM, Sigma Aldrich), picrotoxin (10mM, Sigma Aldrich), Bumetanide (100mM, ChemCruz, SantaCruz

Biotechnology, Dallas, TX, USA), Nifedipine (200mM, Merck, Darmstadt Germany), Nimodipine (10mM, Cayman Chemical, Ann Arbor, MI, USA) and TTA-P2 (10mM, Alomone Labs, Jerusalem, Israel) were dissolved in DMSO. Stock solutions for tetrodotoxin (TTX, 1mM, Sigma Aldrich), muscimol (100mM, Sigma Aldrich),  $\beta$ -alanine (100mM, Sigma Aldrich),  $\omega$ -conotoxin MVIIC (1mM, Alomone Labs) and Lanthanum (100mM, Sigma Aldrich) were made up in PBS. 100mM stocks of Bicuculline (Tocris Bioscience, Bristol, UK) and baclofen (Sigma Aldrich) were made by dissolving in chloroform and HCl, respectively.  $\text{NiCl}_2$  (1M, Sigma Aldrich) was held as a stock solution in distilled water.

GABA degrades rapidly in solution and thus stock solutions of GABA (100mM, Sigma Aldrich) were made up fresh on the day of each experiment in DPBS.

The desired concentration of each substance was obtained by dilution in the respective bath/perfusion solution on the day of each experiment.

## 2.7 Data Analysis

### 2.7.1 C-CAP

Initial data analysis for compound action potential recordings was performed in IGOR Pro 8 (WaveMetrics, Lake Oswego, OR, USA) using custom scripts. The excitability index was calculated for all data points using a custom script and changes in excitability index were measured as an averaged peak, determined within a given time frame (eg. application of a substance) and calculated as a three point average centered on the peak value. Change in excitability index was calculated from control (average 35s prior to entry) to peak (3-point average centred to peak). Data, such as changes in excitability index and raw peak, latency, stimulus rate and temperature values were transferred to Excel to determine averages and GraphPad Prism (Dotmatics, Boston, MA, USA) for statistical analyses. N numbers reflect the number of nerves used in analysis.

### 2.7.2 Analysis of Fluorescence Images

Image analysis was performed using ImageJ (Schindelin et al., 2012). Regions of interest (ROI) corresponding to individual cells were established by manually positioning circular ROIs. Only those cells responding to 45mM potassium, applied at the end of each experiment were considered for analysis and individual ROIs (cells) were considered biological replicates (eg. n=8, means 8 cells).

Initially, five background ROIs that did not contain cells were demarcated. The mean gray scale value determined from these five background ROIs was calculated for each image in a sequence and this background fluorescence was subtracted from the fluorescence intensity values (F) of all cell based ROIs. For cell based ROIs, fluorescence values over time were low-pass filtered using a 5 point sliding box-car average with reflection padding to account for end effects. Fluorescence values for each cell based ROI were then normalised. Normalised fluorescence ( $F/F_0$ ) traces were calculated for each ROI by dividing the fluorescence value for each image (F) by the average fluorescence value in that ROI during the first 20 images ( $F_0$ ).

To determine whether a cell “responded” to a given stimulus two criteria need to be met. First, a cell-based ROI was considered to have responded to a stimulus if the mean  $F/F_0$  value during stimulation, averaged over 15 time points, was greater than a threshold value. The threshold value was determined for each cell and each stimulus as the average  $F/F_0$  value plus three standard deviations (SD) determined from the 10 images immediately preceding stimulation.

The second criterion for inclusion was that the fluorescence had to have returned to within 10% of the initial fluorescence, i.e. immediately preceding the last stimulus, usually no less than 3 mins apart, (but could vary depending on stimulus), for each ROI. As an example, in a blocking experiment with GABA and bicuculline, the fluorescence had to return to the initial fluorescence preceding the first GABA response, prior to the addition of bicuculline. Fluorescence signals were inspected individually before inclusion. Cells that exhibited calcium transients in the absence of a stimulus were excluded.

For concentration-response data compiled for GABA, calcium responses for each concentration were normalised to the response of the average of two responses to 200 $\mu$ M GABA applied sequentially.

The TTX-ratio of DRG neurons responding to 10Hz stimulation was calculated as a quotient of the calcium signal upon stimulation under control conditions and with TTX.

### 2.7.3 Statistics

Statistical comparisons were performed using GraphPad Prism 10 (Dotmatics, Boston, MA, USA). Parametric group comparisons were performed using ANOVA for multiple groups with Bonferroni corrected t-tests as post-hoc comparisons. Student's t-tests were implemented for pairwise comparisons. If group sizes were less than 10, group comparisons were made using non-parametric Friedman's or Wilcoxon signed-ranks tests and Dunn's post-hoc. Data are presented as mean  $\pm$  SD. P values <0.05 were considered statistically significant. Dark grey closed circles in normalised panels of figures indicate averages.

### 3 RESULTS

### 3.1 Chapter 1: Axonal threshold tracking investigation of GABA<sub>A</sub>R-mediated chloride currents in unmyelinated sensory afferents

#### 3.1.1 Depolarising GABA effects in the sural nerve are mediated by GABA<sub>A</sub>R

The threshold tracking technique allows for an assessment of electrical properties of unmyelinated axons and their pharmacological modulation by graded activation of axons resulting in a summed response of different fibre types in a nerve, a compound action potential (CAP). As mentioned in the Methods section, the principle of axonal threshold tracking relies on the ability to electrically-evolve an action potential in some or all of the axons within a nerve, at a given stimulus intensity. QTRAC enables tracking of the action potential initiation threshold by adjusting the stimulus intensity to activate a certain proportion of axons, for example to elicit a response in 100% (black trace, Methods Fig. 9A) or in 40% of the axons (red trace, Fig 9A; Methods Fig. 9A). The excitability index is used to track the increase or decrease in axonal excitability in response to certain interventions. An increase in the excitability is observed upon depolarisation of membrane potential (Moalem-Taylor et al., 2007).

The presence of GABA<sub>A</sub>R in unmyelinated peripheral sensory afferents has been functionally established in human (Carr et al., 2010) and in mouse sural nerve (Bonalume et al., 2021) using this technique, and its activation was found to increase excitability in both species. Here, the threshold tracking technique was used to assess the functional role of GABA<sub>A</sub>R mediated chloride currents on excitability of C-fibre axons within the sural nerve, which are primarily skin afferents.

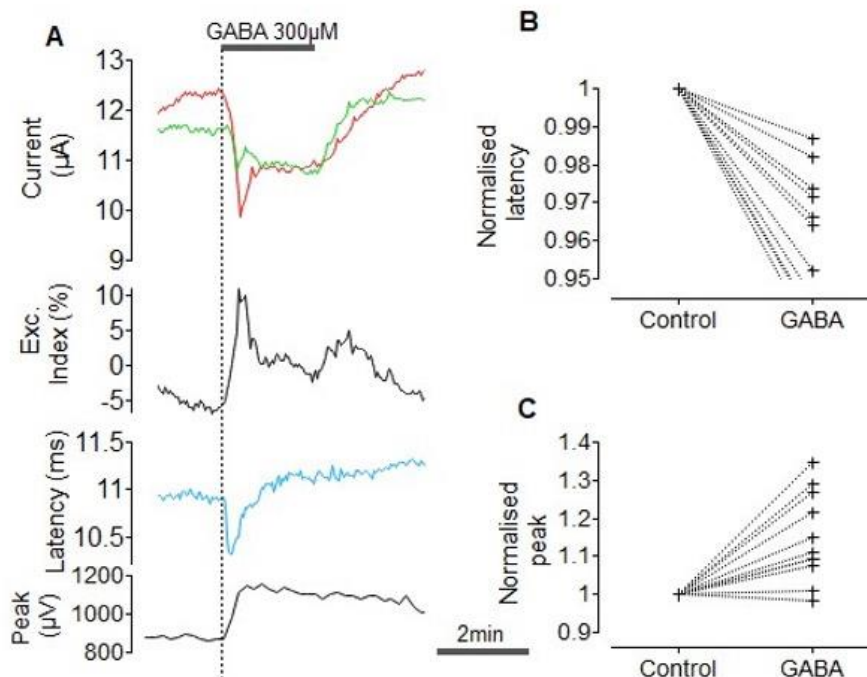


**Figure 11** GABA depolarises sensory axons reflected in an increase in the excitability index (black exc. Index (%) trace), a reduction in latency (A, blue latency trace & B,  $n=11$ ) and C) an increase in the peak ( $n=10$ , and A, peak trace).

In response to application of GABA ( $300\mu\text{M}$ ), there was a decrease in the threshold necessary to evoke a 40% (Fig. 12A, red trace) and 40% conditioned C-CAP (C-fibre CAP, Fig. 11A, green

trace), which is reflected in the increase in excitability index (Fig 11A, excitability index trace), indicating a membrane depolarisation as a result of GABA, in line with previous findings (Bonalume et al., 2021; Carr et al., 2010). The GABA-dependent increase in excitability occurred in a concentration-dependent manner with an  $EC_{50}$  of  $8.9\mu\text{M}$  ( $n=7$ , Fig 12 A&B). Although peak amplitude and latency varied, in most cases application of GABA caused a decrease in the latency, which is calculated as the delay to 50% of the C-CAP positive peak (paired t-test,  $t(10)=5.35$ ,  $p<0.001$ ,  $n=11$ ) (Fig. 11B) and an increase in peak-to-peak amplitude (Wilcoxon test,  $Z=21.0$ ,  $p=0.031$ ,  $n=10$ ) (Fig. 11C).

The GABA-induced increase of excitability was mediated by  $GABA_A$ R (Fig. 12 C&D). The mushroom alkaloid muscimol ( $100\mu\text{M}$ ,  $n=5$ , Fig 12C upper trace & 2D) and  $\beta$ -alanine ( $100\text{mM}$ ,  $n=12$ , Fig. 12C middle trace & 2D), a structural analogue of GABA activating  $GABA_A$ R (Wu et al., 1993), mimicked the effects of GABA ( $100\mu\text{M}$ ). The  $GABA_B$ R agonist, baclofen ( $100\mu\text{M}$ ) produced no detectable changes in excitability ( $n=9$ , Fig. 12C lower trace & D). Bicuculline ( $50\mu\text{M}$ ) reduced the GABA evoked increase in excitability index from  $17.1 \pm 8.06\%$  to  $4.92 \pm 2.26\%$  (paired t-test:  $t(3)=3.72$ ,  $p=0.034$ ,  $n=4$ ) (Fig. 12 E&F). The non-competitive allosteric modulator picrotoxin ( $50\mu\text{M}$ ) similarly reduced the increase in excitability from  $15.3 \pm 7.69\%$  to  $1.8 \pm 3.00\%$  (unpaired t-test,  $t(18)=5.16$ ,  $p<0.001$ ,  $n=10$ ) (Fig. 12 E&F).

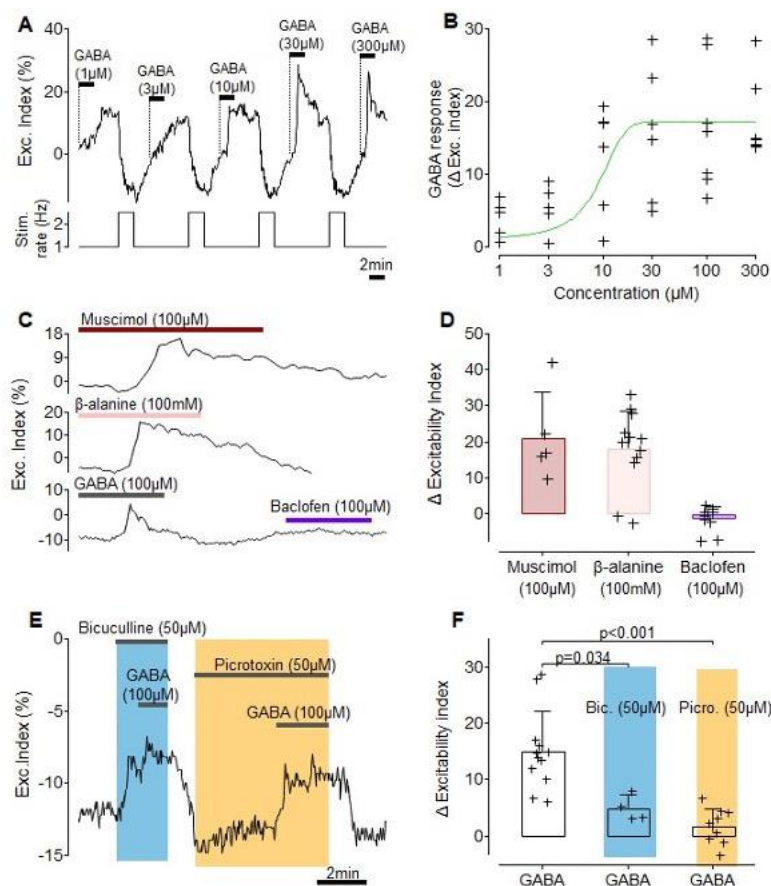


**Figure 12 GABA responses in C-fibre axons are mediated by  $GABA_A$ R**

A) Representative trace of excitability changes by increasing GABA concentrations  $1\mu\text{M}$ - $300\mu\text{M}$ . B) GABA increased the excitability index in a concentration-dependent manner with a calculated  $EC_{50}$  of  $8.9\mu\text{M}$ . C) Representative excitability traces of muscimol ( $100\mu\text{M}$ ),  $\beta$ -alanine ( $100\text{mM}$ ) and GABA and baclofen (both  $100\mu\text{M}$ ) each applied for two minutes, with pooled data in (D) showing responses to muscimol and  $\beta$ -alanine mimicking those of GABA, while baclofen has no effect. E) Bicuculline ( $50\mu\text{M}$ ) and picrotoxin ( $50\mu\text{M}$ ) in co-application with GABA ( $100\mu\text{M}$ ) reduce the excitability increase in response to GABA significantly (Bicuculline, paired t-test,  $p=0.034$ ; picrotoxin, unpaired t-test,  $p<0.001$ ).

### 3.1.2 Required interval for stable GABA excitability responses upon repetitive application

Neuronal chloride homeostasis is controlled by several chloride transporters, exchangers and channels. In DRG neurons, the intracellular chloride concentration is kept high due to a

predominance of NKCC1 expression and little to no KCC2 expression, which is responsible for chloride extrusion (Alvarez-Leefmans and Delpire, 2009; Kanaka et al., 2001). Consequently, GABA acts in a depolarising manner (Du et al., 2017; Zhang et al., 2015), triggering chloride efflux (an inward current) through the GABA<sub>A</sub>R. To investigate the kinetics of GABA-mediated chloride efflux in unmyelinated axons, repetitive GABA application at different intervals was tested.

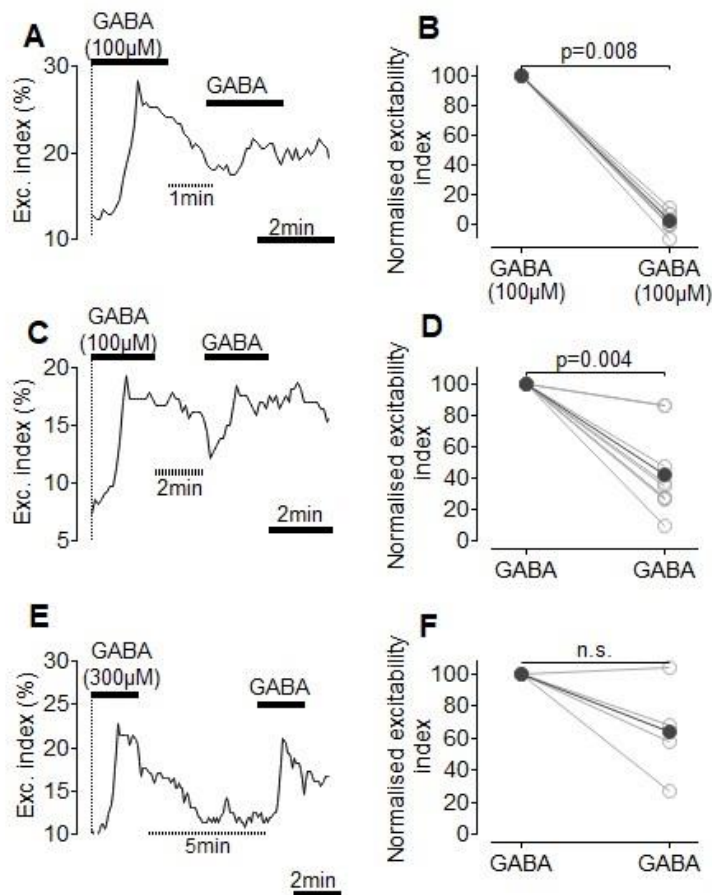


**Figure 13 GABA responses diminish at intervals shorter than 5 minutes**

A) Representative trace of two GABA responses each of 2 minutes duration, at an application interval of 1 minute B) Pooled data ( $n=8$ ) with control responses at 100% and second responses normalised to this (Wilcoxon,  $p=0.008$ ). C) Representative protocol depicting two GABA applications (2 min) given 3 min apart D) Pooled data ( $n=9$ ) revealing a reduction in response from 100% (control) to an average of 59% (black closed circles) (Wilcoxon,  $p=0.004$ ). E) Two GABA responses ( $n=4$ ) elicited in one recording, 5 minutes apart. F) Pooled normalised responses reflect a reduction from first response (normalised to 100%).

Applying a second GABA stimulus one minute after the first led to a significant reduction in response amplitude to an average of 3% of the control level with the GABA-induced increase of excitability index reducing from  $24.7 \pm 12.0\%$  to  $0.75 \pm 2.49\%$  (Wilcoxon test,  $Z=-36.0$ ,  $p=0.008$ ,  $n=8$ ) (Fig. 13 A&B). The GABA effect was also significantly reduced from  $11.3 \pm 4.51\%$  to  $4.21 \pm 2.30\%$  (42% of the control) at two minute intervals (Wilcoxon test,  $Z=-45.0$ ,  $p=0.004$ ,  $n=9$ ) (Fig. 13 C&D). A five-minute interval between GABA applications reduced the response to an average 64% of the control level (Wilcoxon test,  $Z=-8.00$ ,  $p=0.250$ ,  $n=4$ ) (Fig. 13 E&F). Thus, for shorter application intervals more pronounced tachyphylaxis is observed.

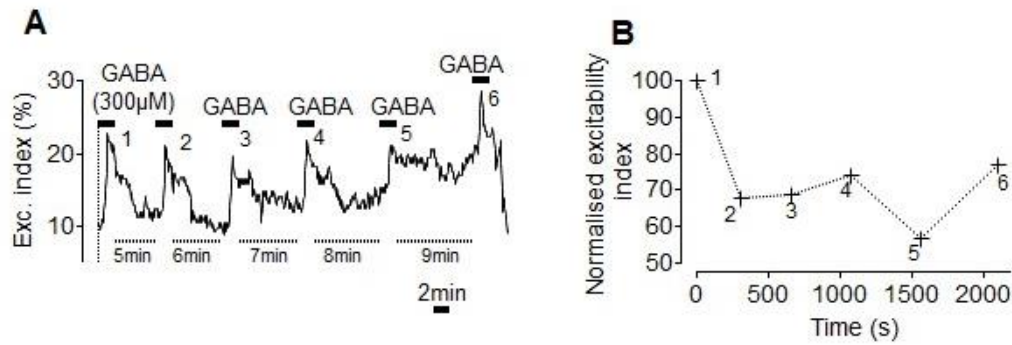


**Figure 14 Repetitive GABA responses elicited at different intervals**

A) Representative trace of responses elicited at intervals of 5, 6, 7, 8 and 9 minutes. B) Percent reductions from the first response (GABA 1 in A normalised to 100%) show a decline at five minutes then relatively steady maintenance from 6-8 minutes ( $n=1$ ).

Increasing the time between applications, in a pilot experiment, reveals that from 6 to 8 minutes there is a relatively stable excitability index change (Fig. 14 A&B, data in B represented as percentage of control GABA 1 in A,  $n=1$ ). Thus, an interval of 10 minutes was expected to yield stable GABA responses.

Indeed, GABA (300 μM) at ten minute intervals without intervention, even showed a minute increase in excitability from  $12.5 \pm 5.79\%$  to  $13.7 \pm 5.12\%$  (Wilcoxon test,  $W=21.0$ ,  $p=0.031$ ,  $n=6$ ) also represented in the normalised panel in Fig. 16C (Fig. 15 A-C).

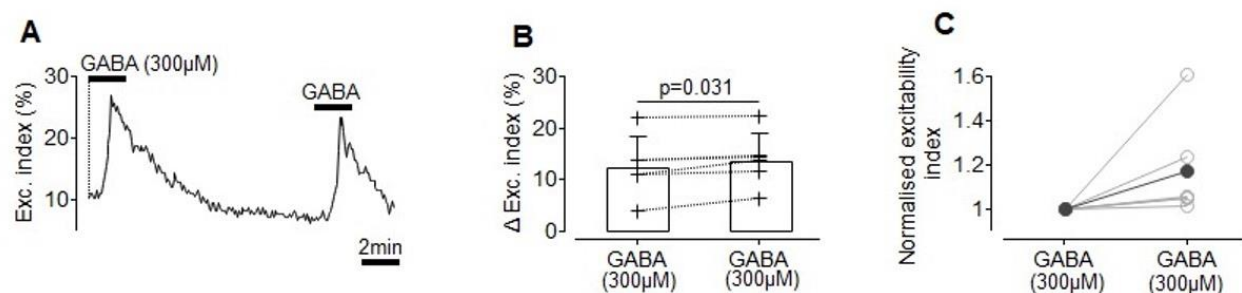


**Figure 15 Excitability responses to repeated GABA application at ten minute intervals**

A) Representative trace of experimental protocol of two GABA applications (2 minutes) with ten minutes in between B) Pooled data, showing even a minute increase in the GABA-induced increase in excitability index (Wilcoxon,  $p=0.031$ ). C) Normalised data from B, showing the same minute increase in average normalised excitability index.

GABA-mediated chloride efflux is sufficient to alter intracellular chloride concentrations in DRG neurons, which may well be exacerbated in smaller volume structures such as axons or CA1 neurons (Bonalue et al., 2021; Staley and Proctor, 1999). These findings indicate that the GABA-induced excitability increase requires an interval of longer than five minutes to retain a reproducible size, which is in line with previous findings suggesting the inflection point of recovery to control size is about five minutes (Bonalue et al., 2021). It was presumed that this kinetic was determined by NKCC1 activity re-establishing an intra-axonal chloride concentration within the given time frames, as there is ample evidence that NKCC1 is responsible for maintaining intracellular chloride concentrations in immature neurons (Gonzalez-Islas et al., 2009), dorsal root ganglion neurons (Alvarez-Leefmans et al., 1988) and their peripheral axons (Bonalue et al., 2021)

### 3.1.3 Modulation of GABA effects by intermittent electrical stimulation

The decline of GABA excitability responses at shorter application intervals was hypothesized to predicate on an imbalance between chloride outflow and insufficient inward transport of chloride via NKCC1. In short, a depletion of the chloride gradient could be responsible for the observed reduction of subsequent GABA responses.

In line with the idea that NKCC1 is responsible for re-establishing the chloride gradient, prior research has also posited a connection between increased action potential firing and activity of NKCC1 in CA1 neurons (Brumback and Staley, 2008) and sensory axons (Bonalume et al., 2021). Albeit reducing excitability of C-fibres (De Col et al., 2012), increased frequency of electrical stimulation has been shown to amplify the hyperexcitability by a subsequent GABA application (Carr et al., 2010).

Higher firing frequencies of C-fibres decreases their excitability via inactivation of NaV channels, increase of intracellular Na<sup>+</sup> concentration and hyperpolarisation based on increased Na<sup>+</sup>/K<sup>+</sup>-ATPase activity (Fig. 16 A&D, increased frequency causes reduction in excitability). Such hyperpolarisation increases the difference between the equilibrium potential for chloride ( $E_{Cl}$ ) and the actual membrane potential, thereby increasing the driving force for chloride and consequently, the GABA-induced excitability change. As NKCC1 is electroneutral the hyperpolarisation alone is not expected to interfere with its activity. However, as it utilizes the sodium gradient to transport two chloride, one potassium and one sodium molecule into the axon, one could assume that an activity-dependent intracellular increase of sodium concentration would reduce NKCC1 activity.

Therefore, the relationship between electrical activity, NKCC1 and GABA depolarisation was further investigated. A bout of increased electrical stimulation was applied intermittently between two GABA stimulations. Increasing the firing frequency from 0.6Hz (a stimulus interval of 1.6 seconds) to 2.5Hz (a stimulus every 0.4 seconds) for three minutes, between two GABA applications (12 minutes apart), had no significant effect on the peak amplitude of the subsequent GABA response (paired t-test:  $t(18)=0.557$ ,  $p=0.584$ ,  $n=19$ ) (Fig. 16 A-C), as also reflected in the normalised pooled data in C. In contrast, two successive periods of higher stimulation frequency, from a baseline of 0.5Hz (every 2 seconds) to 2.5Hz for two minutes each, between consecutive GABA applications, significantly increased the subsequent GABA-induced increase of excitability index from  $11.1 \pm 7.19\%$  to  $24.8 \pm 15.0\%$  (paired t-test,  $t(12)=3.86$ ,  $p=0.002$ ,  $n=13$ ) (Fig. 16 D-F). This constituted an average of an almost three-fold (2.7) increase in excitability when normalised to the first GABA response.

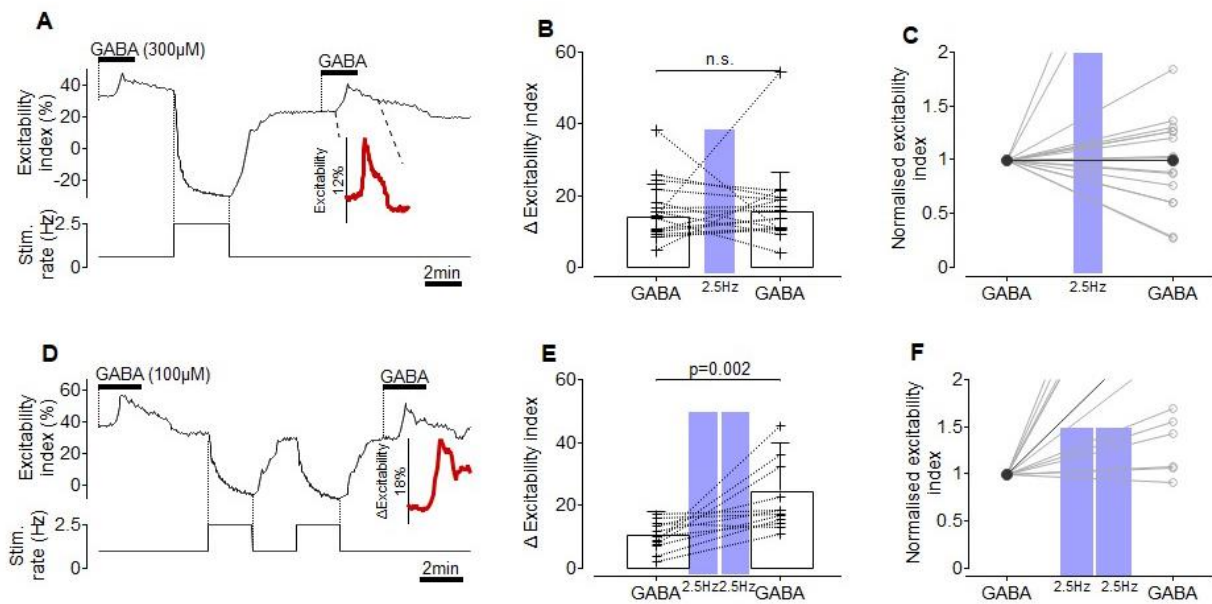


**Figure 16 Intermittent bouts of electrical stimulation in between GABA applications increase the subsequent GABA response**  
 A) Representative specimen including one increased frequency stimulus in between two GABA applications. B) There is no change of excitability index response to GABA after this single bout of high frequency firing (paired t-test, n.s.). C) Normalised responses from B show no change in average excitability increase. D). Representative trace of two bouts of intermittent high frequency stimulation between two GABA applications. E) These two bouts of high frequency firing significantly increase the GABA response amplitude (paired t-test,  $p=0.002$ ). F) Normalised responses show on average a three-fold increase of the second GABA stimulus after the intermittent electrical stimulation bouts.

### 3.1.4 Depolarizing GABA responses are not blocked by NKCC1 antagonism with bumetanide

Having established that intermittent bouts of action potential firing increases the subsequent GABA response, it was further investigated whether this is attributable to NKCC1 or other transporter proteins for example associated with sodium gradients, such as sodium dependent anion exchangers (NDAE) (Payne et al., 2003), using the NKCC1 blocker, Bumetanide. Bumetanide is a loop diuretic which acts as an NKCC transporter antagonist similar to furosemide, but relatively specific for NKCC1 (Russell, 2000), and has been used successfully to reduce intracellular chloride accumulation during prolonged seizure activity (Dzhalala et al., 2010). It was first attempted to interfere with the assumed re-establishing of the chloride gradient directly after a GABA application (Fig. 17A). Indeed, the amplitude of the GABA (300 $\mu$ M) responses following NKCC1 block by Bumetanide (50 $\mu$ M), briefly after a previous GABA application, were significantly reduced (Friedman test,  $\chi^2(8)=22.50$   $p=0.002$ , post hoc Wilcoxon with Dunn's correction GABA 2 - GABA 3,  $Z=3.031$ ,  $p=0.010$ ,  $n=4$ ) (Fig. 17 B&C).

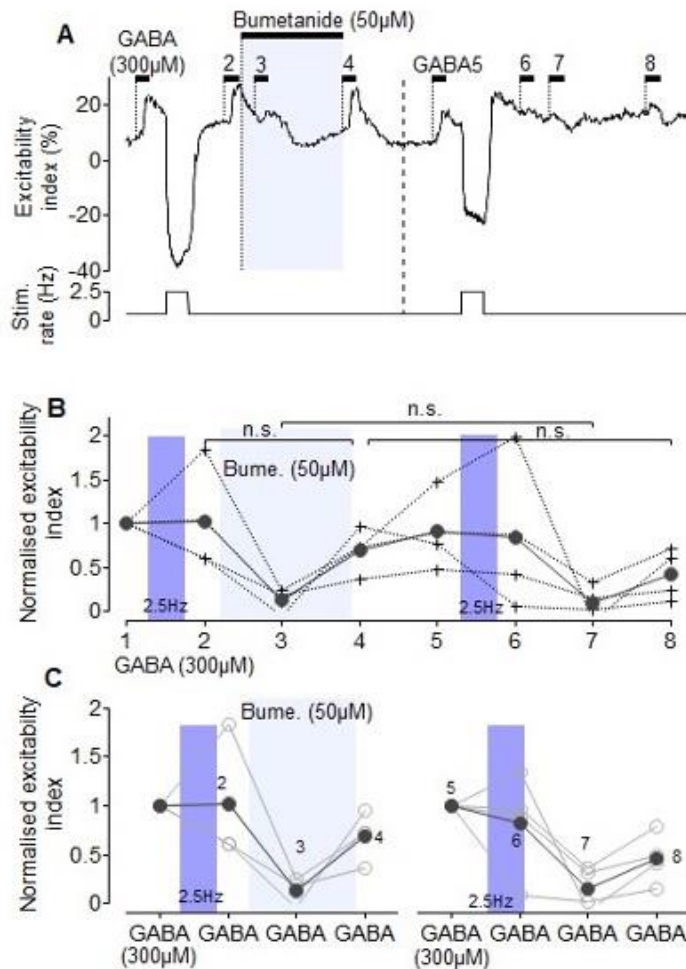


**Figure 17 Axonal GABA responses before and after intervention with bumetanide are not significantly influenced by NKCC1 blockade**

A) Representative trace of experimental protocol, depicting GABA (300µM) 1-4 with intervention of bumetanide (50µM) and GABA 5-8 the mirror without intervention for control purposes including trace depicting timing of increases in stimulation frequency (Hz). B) Pooled responses for all (n=4) normalised to GABA 1 in A, show there is no difference between GABA 2 and GABA 4 (post hoc Wilcoxon,  $p=0.993$ ), no difference between GABA 4 and GABA 8 (post hoc Wilcoxon, n.s.) and no significant change from GABA 3 to GABA 7 (post hoc Wilcoxon, n.s.) C) Left, pooled responses normalised to GABA 1 in A/B; right, pooled responses normalised to GABA 5 as control. Both show similar patterns of excitability increase and reduction. Light blue shading indicates application of bumetanide (50µM). Purple shading indicates high frequency stimulation.

However, despite prolonged bumetanide (50µM) application the subsequent GABA response was back to pre-bumetanide control levels (GABA 2 - GABA 4, post hoc Wilcoxon with Dunn's correction,  $Z=1.155$ ,  $p=0.993$ ). Importantly, the second part of the experimental protocol shown in Fig. 17A (after dotted line) reveals that even without intervention of bumetanide, there is a reduction in the GABA response (GABA 7) when the interval to the preceding GABA stimulation is short, followed again by an increase when this interval is longer. Indeed, there was no significant difference in the excitability response to GABA, between GABA 3 (bumetanide) and GABA 7 (control) (post hoc Wilcoxon,  $Z=0.000$ , n.s.) and no significant change between GABA 4 (recovery after bumetanide) and GABA 8 (control recovery) (post hoc Wilcoxon,  $Z=0.87$ , n.s.). At face value, this would imply that intervention with bumetanide did not significantly alter the GABA effects. The normalisation of the responses to the initial GABA response (GABA 1, Fig 17B) or additional normalisation of the final three GABA responses to their control GABA (GABA 5; Fig 17C) confirm the similar pattern of responses with and without bumetanide. A two-way ANOVA revealed no significant effects of bumetanide on the GABA responses (2-way RM ANOVA,  $N \times$  Bumetanide  $F(3,8)=1.635$ ,  $p=0.2568$ ).

In light of these results, it was sought to control for a possible antagonistic effect on GABA<sub>A</sub>R by bumetanide, as has been previously suggested (Sung et al., 2000), due to the observed reduction of the GABA response during co-application with bumetanide (GABA 3). A sufficiently long interval of 10-12 minutes was chosen to ensure the potential for full recovery of the

gradient. Nonetheless, the excitability index change in response to control GABA (300 $\mu$ M; 13.7  $\pm$  5.12%) was not significantly affected by incubation with Bumetanide (50 $\mu$ M) (14.8  $\pm$  3.5%; Wilcoxon test, Z=7.00, p=0.562, n=6) at these concentrations (Fig. 18 A-C).

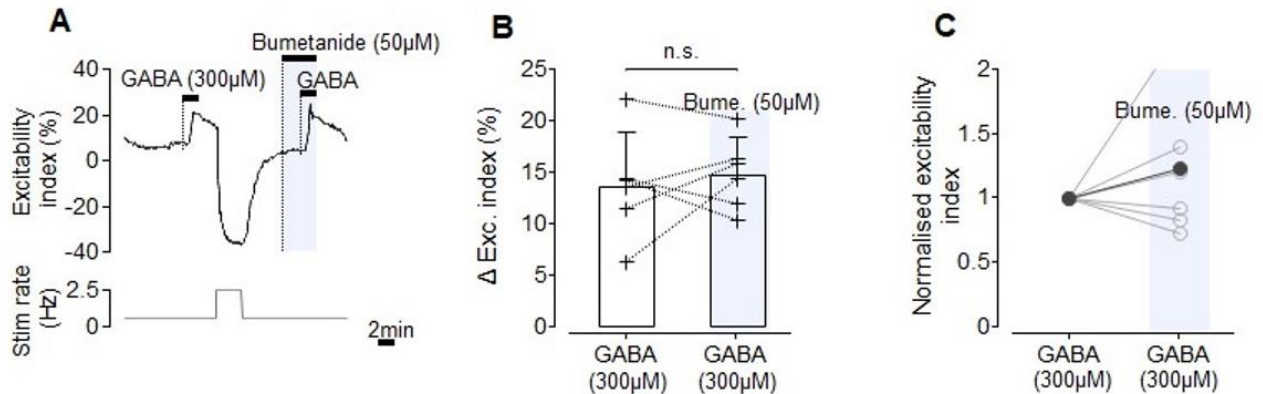


**Figure 18 Bumetanide does not act as a GABA<sub>A</sub>R antagonist**

A) Representative experimental trace depicting co-application of bumetanide (50 $\mu$ M) and GABA (300 $\mu$ M) B) There is no change in GABA response during co-application with Bumetanide (Wilcoxon, n.s, n=6.). C) Normalised values from B depicting a slight increase in average excitability index. Light blue shading indicates bumetanide (50 $\mu$ M) application.

### 3.1.5 Interaction between intermittent electrical stimulation bouts and NKCC1-mediated inward chloride transport

The efficacy of bumetanide increases with the amount of activity induced by a seizure (Dzhala et al., 2010), probably reflecting the activity-dependent shift in  $E_{Cl}$  via of upregulation of NKCC1 transport in response to changes in transmembrane ion gradients (Brumback and Staley, 2008). As has been stated, increased firing rates enhance excitability responses to GABA, possibly coupled to activity-dependent changes in NKCC1 (Bonalume et al., 2021; Carr et al., 2010). In an attempt to identify whether NKCC1 activity is increased by action potential firing in axons, bumetanide (20 $\mu$ M) was added during a period of high frequency stimulation, investigating whether the role of NKCC1 was critical during this intervention. Initially, two bouts of electrical stimulation were inserted between GABA (100 $\mu$ M) applications, but at lower firing frequencies than used previously (Figure 19).

While the significant reduction in excitability index in response to GABA 2 and GABA 3 (Fig 19A) from 13.02  $\pm$  5.67 to 3.01  $\pm$  3.79% (Friedman test,  $\chi^2= 9.960$ , p=0.009, post-hoc Wilcoxon with Dunn's correction, GABA 2- GABA 3, Z=2.45, p=0.043, n=5) is to be attributed to the short application interval, contrary to expectation, bumetanide exposure failed to inhibit the increase in excitability index in response to GABA 4. In fact, there was a significant increase in excitability from GABA 3 to GABA 4 (3.01  $\pm$  3.79% to 15.35  $\pm$  9.22%, post-hoc Wilcoxon, Z=2.94, p=0.010) and the post-bumetanide response (GABA 4) was similar to the control response before bumetanide (GABA 2) (post-hoc Wilcoxon, Z=0.49, n.s.) (Fig. 19B). This was not expected, considering GABA 3 was inserted to reduce the chloride gradient, which would then be prevented from re-establishing via incubation with bumetanide.

Considering the different numbers of stimulation periods, it could not be excluded that the lack of bumetanide effect is partially attributable to this. However, it was considered possible that at lower stimulation frequencies, the effect of multiple bouts is less pronounced. One could argue that only one bout of high frequency firing in bumetanide would have made it easier for bumetanide to influence the effects, however this was not the case.

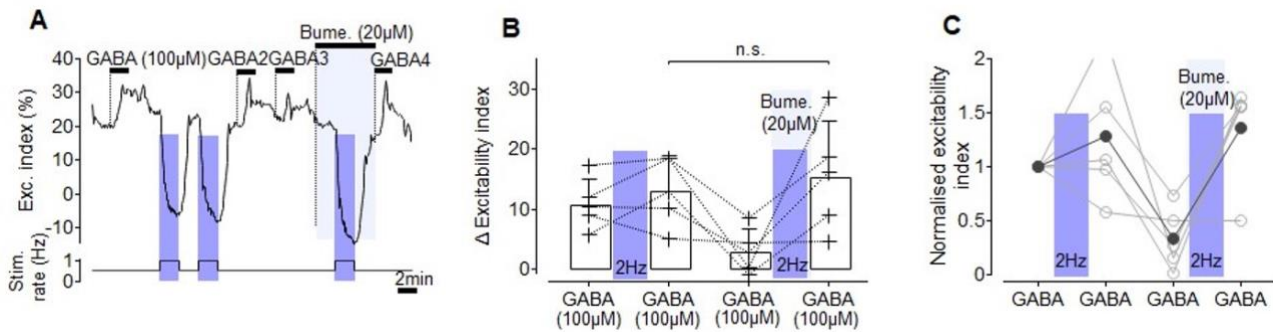


**Figure 19 Intermittent high frequency stimulation during bumetanide exposure did not inhibit enhanced excitability increases in response to GABA**

A) Representative trace depicting excitability responses and stimulation rate (Hz) over time. B) Change in excitability index from control to peak for GABA (100µM), GABA after charging, prior to entry into Bumetanide (20µM) and after washout of bumetanide (post hoc Wilcoxon, GABA 2- 4, n.s.). C) Normalised values from (B). Light blue shading indicates application of bumetanide. Purple shading indicates high frequency electrical stimulation.

Therefore, despite the limitations of the protocol in light of previous results suggesting the stimulation periods within bumetanide may not have been sufficient for a stimulus-induced increase in GABA excitability increase, there is no further evidence to suggest bumetanide affected the ability for NKCC1 to reload the intra-axonal chloride concentration during intermittent bouts of electrical stimulation. Having said that, it could also not be excluded that a residual chloride current existed during the recovery period prior to incubation with bumetanide (after GABA 3, Fig. 19A).

### 3.1.6 Depletion of the chloride gradient with brief exposure to GABA

The chloride gradient is expected to be reduced by GABA application and in particular prolonged or repetitive GABA application is expected to deplete this gradient. However, independent of the chloride gradient, prolonged or repetitive GABA application can also desensitize GABA<sub>A</sub>R and can produce rundown of the response, based on desensitization of the receptor and a reduced number available receptors (Sallard et al., 2021). Paradoxically, this desensitization would limit the effect of repetitive or prolonged GABA application on depletion of the chloride gradient. Therefore, protocols were designed that could differentiate between depletion of the chloride gradient and receptor desensitization. First, it was attempted to use several shorter GABA applications at shorter application intervals than used previously, to investigate whether this would alter the GABA response depletion. Using a shorter application time of one minute at two minute intervals, there was a gradual decrement in the response amplitude with subsequent applications (Fig. 20A).

Two-minute long applications at two-minute intervals as previously used but at a higher application frequency, the response was abolished after the third application and remained absent until a longer resting period was kept (Fig. 20B). Overall, after repetitive application, the GABA responses had virtually subsided (Friedmans test,  $\chi^2 = 21.05$ ,  $p = 0.033$ , post-hoc Wilcoxon GABA 1- GABA 11,  $Z = 2.831$ ,  $p = 0.009$ ,  $n = 3$ ). Blocking NKCC1 with bumetanide at this time, but allowing a longer resting period of the subsequent GABA stimulation to restore GABA-A function resulted in a recovery of the GABA response (GABA 1 - GABA 12, post hoc Wilcoxon,  $Z = 0.679$ ,  $p = 0.994$ ) (Fig. 20 A&B). Interestingly, with longer applications there was a quicker reduction in excitability increase with subsequent applications, but the excitability index increase after exposure to bumetanide was larger than that at shorter applications (10% vs 6%, respectively). This result indicates that receptor desensitization plays a significant role when repetitive GABA stimulations are given at short intervals. It is also interesting to note that for longer application periods of GABA peak effects on excitability are recorded during the application with normalisation starting already during the application time. Thus, one might conclude that some desensitization might occur already within the application time of GABA (see Fig. 20A, right close-up trace).

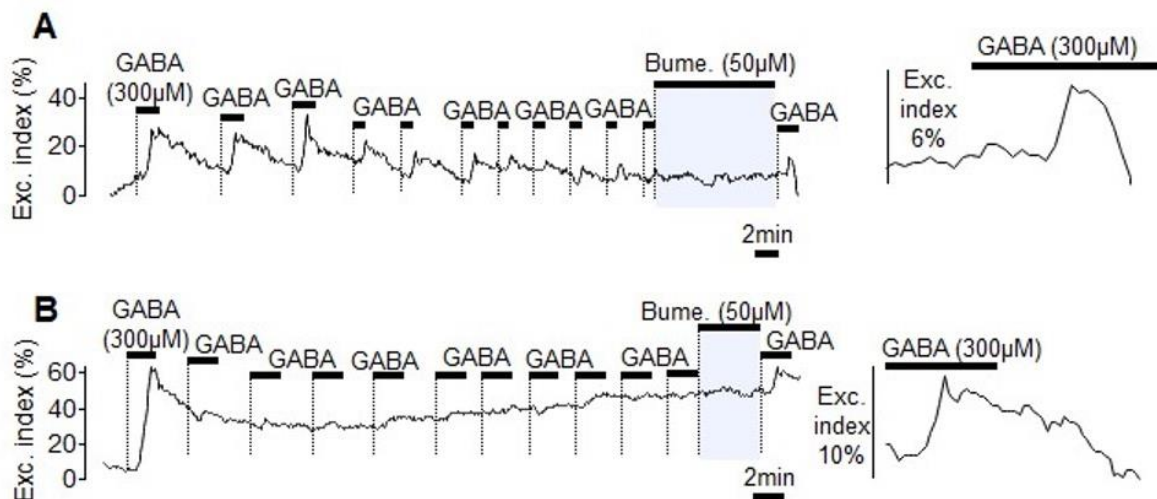


**Figure 20 Shorter application times suggest less likelihood of GABA<sub>A</sub>R desensitisation**

A) GABA applied initially for 2 minutes with varying intervals reveals a reduction in transient size; reducing the application time but retaining the interval shows further reduction, however bumetanide application does not seem to have an ostensible effect. The blown-up GABA response (right) reflects the response after Bumetanide incubation. B) Applications of 2 minutes at 2 minute intervals show an almost immediate reduction in GABA excitability response, however the increase after bumetanide is larger than in (A) suggesting receptor desensitisation. Right, the blown-up GABA response reflects the response after Bumetanide incubation. Light blue shading indicates bumetanide application.

### 3.1.7 NKCC1 is responsible for maintaining the intra-axonal chloride gradient

Considering the above results that rundown of the GABA receptor is likely for short repetition intervals, GABA (300µM) applications at ten minute intervals, which were shown to produce stable GABA effects (see Figure 15), were tested in combination with bumetanide (20µM) to conclusively establish an efficacy of the compound in inhibiting NKCC1 transport activity (Figure

21). In line with previous findings (Bonalume et al., 2021), the GABA response gradually declined with repetitive GABA applications (n=2) from  $14.43 \pm 0.6\%$  (GABA 1) to  $-1.34 \pm 0.72\%$  (GABA 5). This data confirms, that blocking NKCC1 by bumetanide reduces chloride transport into the cell and thereby leads to a depletion of the chloride gradient. When this block is applied for a sufficient time and GABA-induced chloride current are evoked repetitively, apparently a complete depletion of chloride gradient can result, which abolishes the GABA responses.

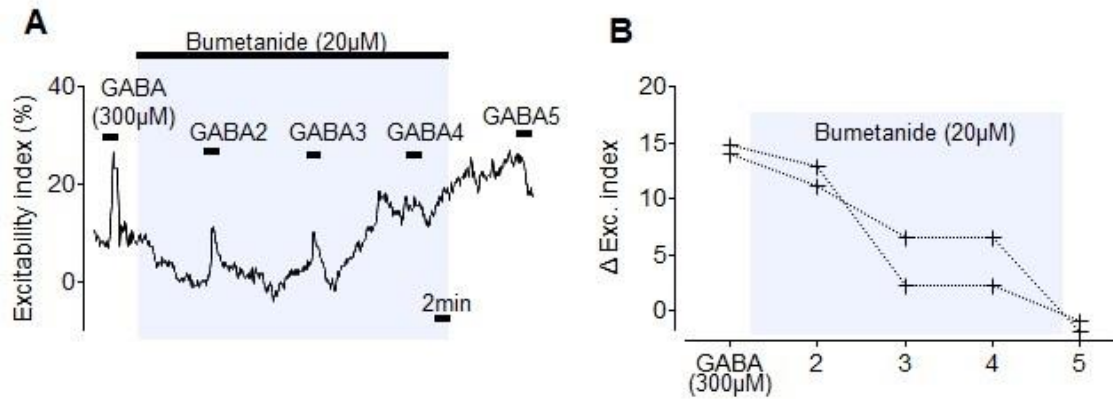


**Figure 21 Repetitive GABA application in Bumetanide progressively reduces the excitability response to GABA**

A) Exposing the nerve to Bumetanide ( $20\mu\text{M}$ ) during repetitive GABA ( $300\mu\text{M}$ ) application at ten-minute intervals, reduces the excitability increase in response to GABA. B) There is a significant reduction in excitability response amplitude with consecutive applications until a depleted response is seen (n=2). Light blue shading indicates bumetanide incubation.

### 3.1.8 No major role of depletion of the chloride gradient for repetitive GABA at 2 min intervals

To assess the potential effect of chloride gradient depletion at short repetition intervals of GABA, a twin stimulation with GABA ( $100\text{-}300\mu\text{M}$ ) at 2 min intervals was repeated after a pause of 10 minutes and an additional bumetanide ( $20\text{-}50\mu\text{M}$ ) block of NKCC1 was introduced to avoid restoration of the chloride gradient (Fig. 22A). The first and second GABA were applied to establish an initial response size and then to deplete this before directly entering bumetanide to prevent gradient re-establishment. In addition, an intermittent bout of electrical stimulation should ensure that the second GABA twin pulses were of comparable amplitude as under control conditions. GABA 3 was introduced in bumetanide to identify whether GABA 2 had produced rundown of the receptor or of the chloride gradient. GABA 2 and 3 were 10 minutes apart to avoid possible receptor desensitization.

Repetition of the GABA ( $100\text{-}300\mu\text{M}$ ) stimulation at a 2-minute interval led to a significant reduction (ordinary one way ANOVA,  $F(3, 37) = 9.735$ ,  $p < 0.001$ , post-hoc unpaired t-test with Bonferroni correction, GABA 1 - GABA 2,  $t(37) = 5.351$ ,  $p < 0.001$ , GABA 1 n=11) (Fig. 22B), as was expected from results of the desensitization protocol (see Fig. 10B). While GABA 3 (n=10) was not significantly reduced in comparison to GABA 1 control condition, GABA 4 showed some desensitization or depletion and was not significantly different from GABA 2 in control condition (post-hoc unpaired t-test with Bonferroni correction, GABA 2 (n=14) – GABA 4 (n=6),  $t = 1.368$ ,  $p = 0.448$ ). Rather than showing a more pronounced desensitization following bumetanide ( $20\text{-}50\mu\text{M}$ ), the reduction of second response (GABA 4) was rather less obvious. In



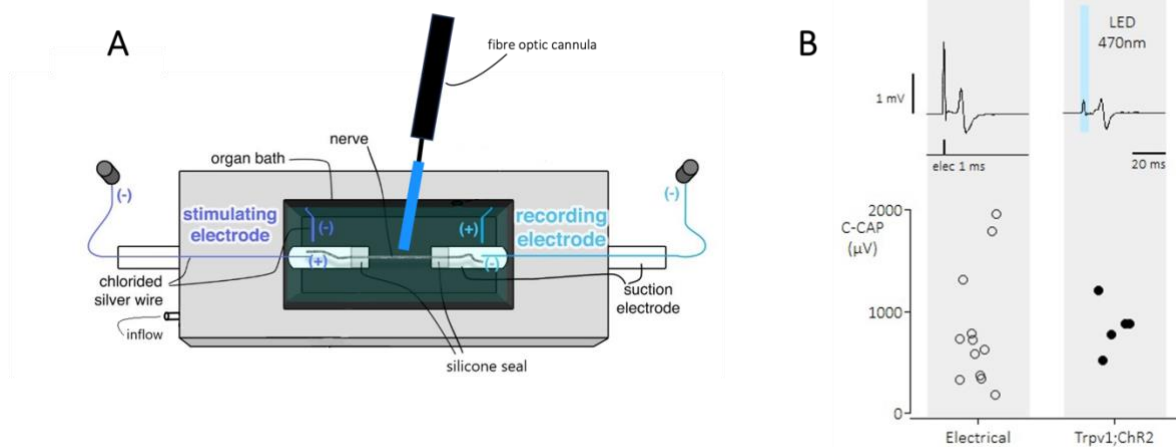


**Figure 23 Example of experimental approach for activation of *Trpv1;ChR2* positive axons in threshold tracking experiments**

A) A Schematic of the organ bath labelled with the stimulation and recording electrodes, where the nerve is placed in between the two silicone seals and the fibre optic cannula emitting blue light at a wavelength of 470nm above B) Left above, an electrically-evoked compound action potential with (below) data depicting peak-to-peak ( $\mu\text{V}$ ) values (black open circles). Right above, an optogenetically-evoked action potential (blue shading marks blue light) and the corresponding peak values beneath (black closed circles).

Initial experiments to approach this subject were conducted, attempting to initiate an action potential using blue light in the same setup used for threshold tracking experiments (Fig 23A). Using blue light pulses (470nm) of 2ms width, it was possible to evoke an action potential (Fig 23B) with an average peak of  $852\mu\text{V}$  (compared to  $810\mu\text{V}$  as evoked by 1ms electrical pulses). In some pilot experiments, it was also possible to use the threshold tracking technique to interpret threshold of an AP as elicited by optogenetic stimulation, and allow the stimulus-response system to adjust this accordingly. Further to this, GABA ( $300\mu\text{M}$ ) was applied in some experiments to see the potential to track the reduction in threshold to elicit a 40% and 40% conditioned stimulus in the fibres (data not shown).

### 3.1.10 Chloride manipulation in sensory axons using yellow light stimulation

In addition to the *Trpv1;ChR2* mouse line, a transgenic *Trpv1;eNpHR3.0* mouse line (see *Transgenic mouse lines* in Methods) was used to examine responses to GABA before and after yellow light stimulation of the chloride ion transporter halorhodopsin, labelled in *Trpv1* positive fibres (*Trpv1;eNpHR3.0*). Halorhodopsins are light-activated microbial opsins that pump chloride ions into the cell and respond maximally to light at approximately 580nm (see *Floxed reporter lines* in Methods). As has been explained, the action of GABA on peripheral afferents and their cell bodies leads to an efflux of chloride through the  $\text{GABA}_{\text{A}}$ R causing a depolarisation and inhibition, effectively stabilizing the membrane potential close to  $E_{\text{Cl}}$ . This is in contrast to its effects in other central neurons where  $\text{GABA}_{\text{A}}$ R activation causes an influx of chloride, hyperpolarisation and thereby, inhibition. In peripheral primary afferents, the depolarizing stimuli via  $\text{GABA}_{\text{A}}$ R activation induce primary afferent depolarisation (PAD), which is still an inhibitory mechanism of action, inhibiting at the level of the spinal cord. Occasionally, particularly in disease states,  $E_{\text{anion}}$  (the combined reversal potential for chloride and

bicarbonate) can shift, such that a depolarisation may reach action potential initiation threshold and therefore becomes excitatory and may lead to central sensitization and hypersensitivity (Prescott, 2015; Price et al., 2009). The ability to modulate intracellular chloride would allow control over this shift such that it does not become a hyperexcitable mechanism. Trpv1 is also known to co-localise with NKCC1 in approximately 50% of somatosensory neurons of the DRG and trigeminal ganglia (Price et al., 2009). This co-expression has been suggested as a gateway to allodynia and that the regulation of NKCC1 activity is coupled to TRPV1 activation (Deng et al., 2021), therefore it would be pertinent to assume that these neurons also maintain high intracellular chloride levels. Finding that functional GABA<sub>A</sub>R are present on TRPV1+ axons of primary afferents would thus perhaps yield strategies to access the modulation of spinal nociceptive inhibition. With this in mind, there might be an alternative approach to relieving pain, if GABA could stabilise an increase in chloride transporter activity to regulate intracellular chloride. The ability to modulate intracellular chloride would allow control over this shift such that it does not become a hyperexcitable mechanism.

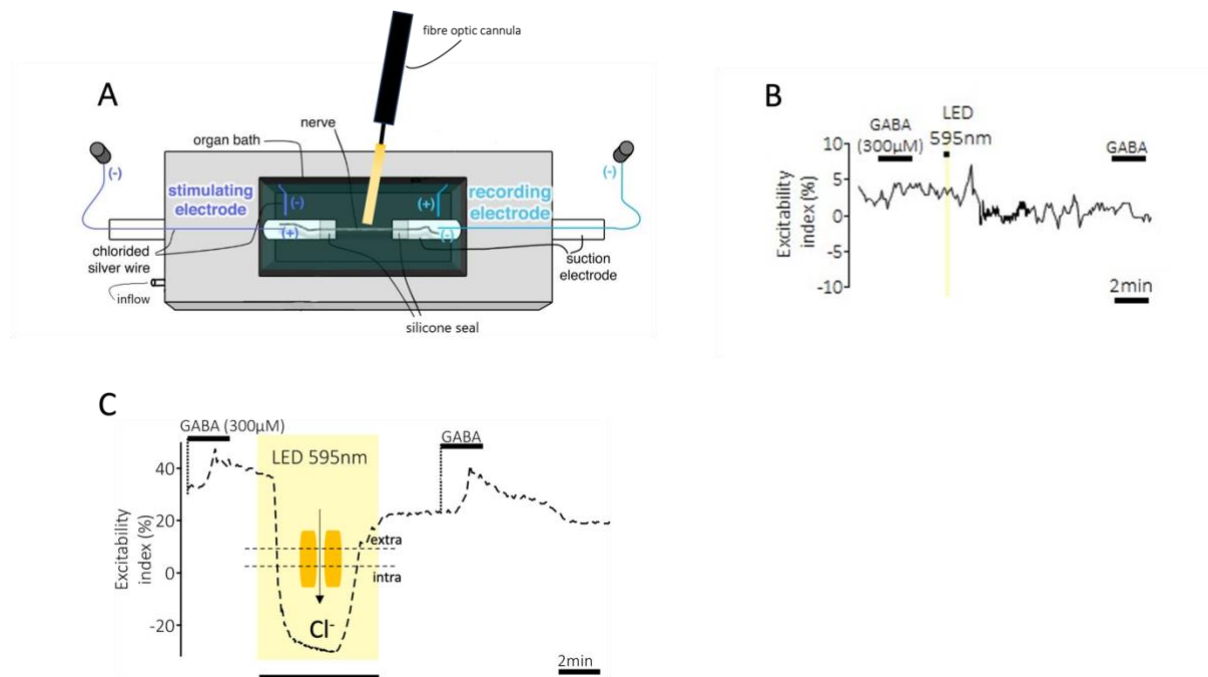


**Figure 24** Example of experimental approach to activation of Trpv1;eNpHR3.0 positive fibres in threshold tracking experiments A) A Schematic of the organ bath labelled with the stimulation and recording electrodes, where the nerve is placed in between the two silicone seals and the fibre optic cannula emitting yellow light at a wavelength of 595nm. B) An example trace of the experimental protocol; yellow shading depicts the yellow light exposure in between two GABA (300µM) applications C) The desired outcome of the protocol, with dashed lines depicting the expectation of an excitability trace in response to yellow light (yellow shading) in between two GABA applications, that should hyperpolarise the membrane by transporting chloride into the axon, as depicted by the membrane (dotted lines) and the ion channel (yellow rectangles).

It was thought, that an NKCC1-independent and thereby action potential and Na<sup>+</sup>/K<sup>+</sup>-ATPase pump-independent mechanism of re-loading chloride into the axon could also be used to test effects of chloride gradients in peripheral axons. Unfortunately, initial attempts to test chloride loading by activation of Trpv1;eNpHR3.0 positive axons were not fruitful (Fig. 24B), as there was no evidence of a hyperpolarisation as was hoped (this idea is depicted in Fig. 24C).

## 3.2 Chapter 2: Calcium imaging to evaluate GABA effects in DRG neurons

### 3.2.1 GABA evoked calcium transients in DRG neurons

To investigate the role of chloride in the regulation of excitability in individual primary sensory neurons, responses to GABA and further pharmacological and electrical interventions were monitored using calcium imaging with the intensity-based calcium dye, Fluo-8. Previous work has determined that a sub-population of DRG neurons responds to bath-applied GABA with an increase in intracellular calcium (Aptel et al., 2007; Schöbel et al., 2012). Schöbel et al. (2012) reported that approximately 70% of trigeminal ganglion neurons responded with a calcium transient to extracellular GABA (250 $\mu$ M), while Aptel et al. (2007) showed that GABA evoked calcium signals in medium-sized D-hair neurons. Calcium can serve as a second messenger in many physiological processes, including neurotransmitter release and synaptic plasticity (Catterall et al., 2013) and in some cases contribute to depolarisations leading to action potential generation (review by Catterall (2011)).

Here we confirm the observation that GABA can induce calcium transients in a sub-population of DRG neurons and does so in a concentration-dependent manner (10 $\mu$ M-200 $\mu$ M) with an EC<sub>50</sub> of 16.67 $\mu$ M (n=8, Fig. 25 A&B). Calcium responses to GABA (200 $\mu$ M) were evident in ca. 50% of dorsal root ganglion cells (subset of 664/1317). Cells responding to GABA (200 $\mu$ M) with a calcium transient had an average diameter of 24.0  $\pm$  6.3 $\mu$ m and ranged from 11.0 to 50.4 $\mu$ m. GABA-evoked calcium responses in DRG neurons exhibited a GABA<sub>A</sub> pharmacology (Fig. 25 C-H). The effects of GABA were blocked by the competitive antagonist bicuculline (50 $\mu$ M; one-way RM-ANOVA, F(2,92)=23.89, p<0.001, n=47; post-hoc t-test, GABA – GABA + Bic, t=6.36, p<0.001) and were also blocked by the non-competitive allosteric modulator picrotoxin (50 $\mu$ M; paired t-test, t(57)=8.32, p<0.001, n=58) (Fig. 25 E-H). Calcium responses in the same cells as those responding to GABA could also be evoked by the mushroom (*Amanita muscaria*) alkaloid muscimol (100 $\mu$ M, n=44) which is a potent and selective GABA<sub>A</sub> agonist. In contrast, application of the synthetic GABA derivative baclofen (100 $\mu$ M, n=11), which is a selective GABA<sub>B</sub> agonist, did not result in any detectable change in calcium levels (Fig. 25 C&D).

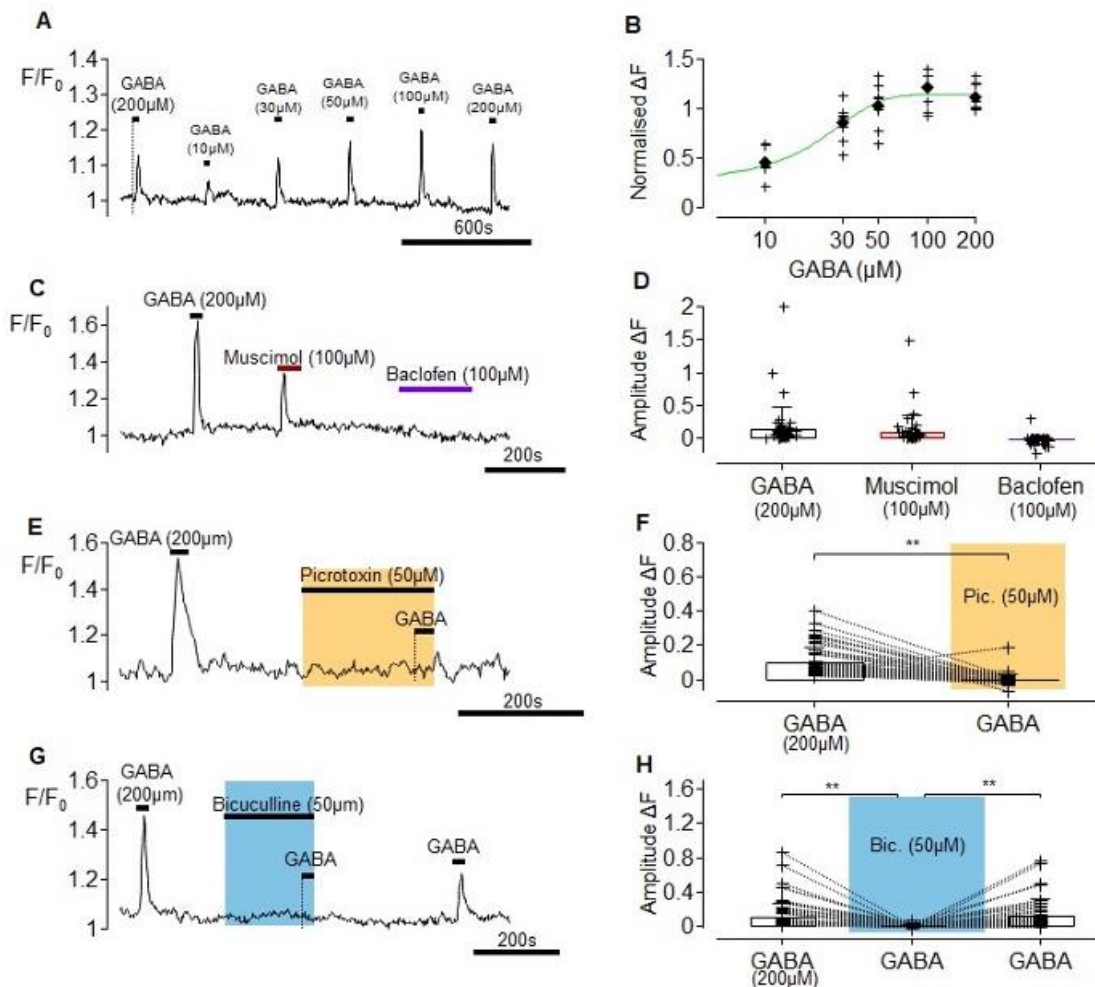


**Figure 25 GABA produced calcium transients in isolated dorsal root ganglion neurons with a GABA<sub>A</sub>-receptor pharmacology**  
 A) The amplitude of calcium transients in response to GABA are concentration-dependent B) Concentration-response curve of GABA evoked calcium responses (10-200 μM; EC<sub>50</sub>: 16.67 μM). C & D) Calcium responses were evoked by the GABA<sub>A</sub>R agonist muscimol (100 μM) but not by the GABA<sub>B</sub>R agonist baclofen (100 μM). E) Representative trace showing application of GABA in the presence of the non-competitive GABA<sub>A</sub>R antagonist picrotoxin (50 μM, orange shading). F) Picrotoxin reduced the amplitude of the GABA induced calcium transient (paired t-test,  $p < 0.001$ ). G) Representative trace for application of GABA during bicuculline (50 μM, blue shading). H) The GABA<sub>A</sub>R antagonist bicuculline blocked the calcium transient to GABA (RM one-way ANOVA,  $p < 0.001$ ).

### 3.2.2 Classification of GABA-responsive cells

To evaluate whether the GABA-sensitive neurons were nociceptors, their sensitivity to capsaicin (2 μM) was tested. Cells responding to capsaicin are presumed to be nociceptive. Approximately 37% (39/106) of DRG neurons responded to capsaicin with a calcium transient. Of this 106-cell subset, 39 cells responded to GABA (200 μM) and out of these, 22 also responded to capsaicin. Thus 56% percent of GABA responding DRG neurons were ostensibly nociceptors. The cells responding to both capsaicin and GABA were slightly smaller with a mean diameter of  $21.0 \mu\text{m} \pm 2.6 \mu\text{m}$  (range: 15.3 μm-25.2 μm).

In addition to capsaicin, TTX was used to provide a further characterization of possible nociceptors in the cultured cells. An initial test to establish efficacy for TTX was to examine its effect on electrically-evoked calcium responses. TTX (1 μM) significantly reduced the amplitude of calcium responses to electrical stimulation at 10 Hz (Fig. 26B) (RM-ANOVA,  $F(2, 148) = 14.88$ ,

$p < 0.001$ ,  $n = 75$ , Bonferroni corrected post-hoc t-test,  $t = 4.84$ ,  $p < 0.001$ ). Interestingly, not all calcium responses to electrical stimulation were completely blocked by TTX (Fig. 26A, upper trace; Fig. 26B). This suggests that calcium responses to electrical stimulation can be mediated in part or wholly, by TTX-resistant (TTX-r) or sensitive (TTX-s) NaV's (Bossu and Feltz, 1984; Pinto et al., 2008)

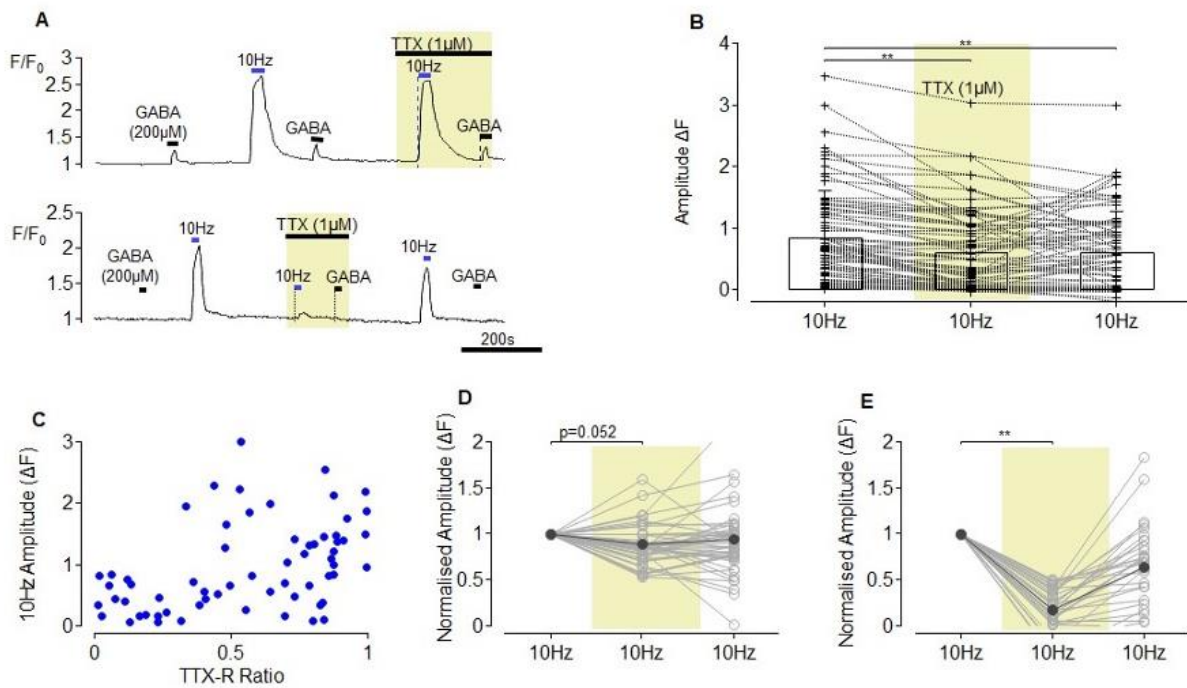


**Figure 26 Calcium responses to electrical stimulation can be split into TTX-r and TTX-s**

A) TTX-r electrical responses are more likely to show a GABA response (upper trace) while TTX-s responses are less GABA responsive (lower trace) B) TTX ( $1\mu\text{M}$ ) significantly reduced the calcium transient in response to 10Hz stimulation (RM-ANOVA,  $p < 0.001$ ) C) The amplitude of calcium responses to electrical stimulation tended to be larger in cells that were more TTX-r.) D) TTX-r ( $> 0.5$  nominal split) electrical responses are not blocked by TTX (Bonferroni corrected post-hoc t-test,  $p = 0.052$ ), while cells which are more TTX-s ( $< 0.5$ ) are significantly reduced by TTX blockade (post-hoc t-test,  $p < 0.001$ ). Yellow shading indicates application of TTX ( $1\mu\text{M}$ ).

To visualize the contribution of TTX-s and TTX-r channels to electrically-evoked calcium signals, an index of TTX sensitivity was developed by simply taking the ratio of the calcium response to stimulation during TTX to that prior to TTX. This TTX sensitivity index will be zero for DRG neurons in which electrical responses are completely blocked by TTX and 1 for cells in which electrically-evoked calcium responses are unaffected by TTX. Figure 26C shows the relationship between the amplitude of the electrical response and the TTX sensitivity index and reveals that those cells that are less sensitive to TTX (1, x-axis) are more likely to respond with a larger calcium response to electrical stimulation (y-axis). Assigning a nominal threshold of 0.5, cells with values above 0.5 were considered TTX-r and those with values below 0.5 were deemed TTX-s. Simple linear regression was used to test whether the size of the 10Hz calcium response (0-2) could predict the TTX-sensitivity (0-1) ( $Y = 0.84 * X + 0.35$ ) and revealed a significant model ( $R^2 = 0.23$ ,  $F(1,55) = 14$ ,  $p < 0.001$ ).

Furthermore, as expected, within the TTX-r population (Fig. 26D,  $n = 43$ ) there was no significant reduction in the electrically-evoked calcium response with TTX ( $1.18 \pm 0.77$  to  $0.98 \pm 0.62$ ; RM-

ANOVA,  $F(2,84)=4.73$ ,  $p=0.011$ ; Bonferroni corrected post-hoc t-test 10Hz – 10Hz+TTX,  $t=2.42$ ,  $p=0.052$ ) (Fig. 26D). In TTX-s cells, TTX ( $1\mu\text{M}$ ) significantly reduced the amplitude of electrically-evoked calcium responses from  $0.43 \pm 0.47$  to  $0.07 \pm 0.18$  (Fig. 26E) (RM-ANOVA,  $F(2,62)=25.03$ ,  $p<0.001$ , Bonferroni corrected post-hoc t-test,  $t=6.61$ ,  $p<0.001$ ,  $n=32$ ).

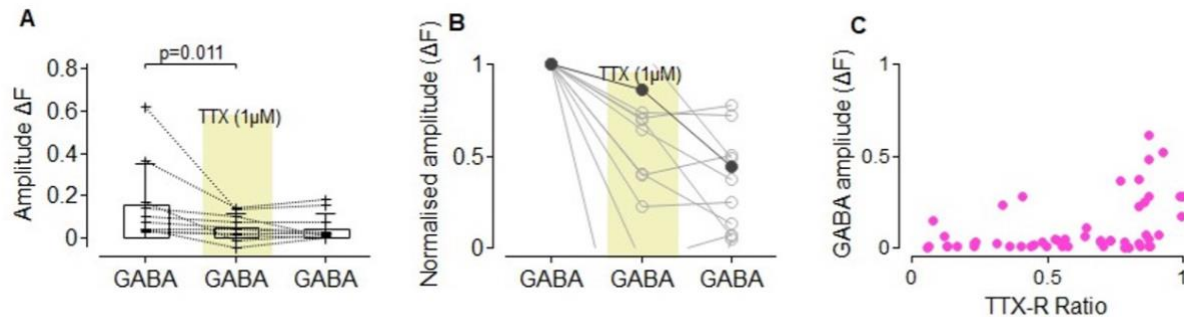


**Figure 27 Effect of TTX on GABA-evoked calcium responses**

A) TTX ( $1\mu\text{M}$ , indicated by yellow shading) reduced the amplitude of calcium responses to GABA [ $200\mu\text{M}$ ] (post hoc Wilcoxon,  $p=0.011$ ) B) The normalised responses from A reveal the decrement in GABA ( $200\mu\text{M}$ ) during TTX ( $1\mu\text{M}$ ) C) The amplitude of calcium responses to GABA tended to be larger in cells that with a higher TTX sensitivity index, i.e. higher TTX-r component.

Of most interest was the effect of TTX on the amplitude of GABA-evoked calcium responses. Patch clamp recordings from DRG neurons show that depolarizing responses to GABA do not elicit action potentials (Reichling et al., 1994), although this may be possible in immature neurons (Khazipov et al., 2004). Using TTX to block TTX-sensitive sodium channels, may therefore indicate the involvement of TTX-sensitive channels in the amplification of GABA-mediated mild prolonged depolarisations. Pooling TTX-s and TTX-r cells, in those cells that were GABA-responsive ( $n=10$ ), the GABA-evoked calcium response amplitude was reduced from  $0.16 \pm 0.19$  to  $0.05 \pm 0.06$  by TTX ( $1\mu\text{M}$ ) (Friedman test:  $\chi^2(3)=12.20$ ,  $p=0.001$ , post-hoc Wilcoxon with Dunn's correction,  $Z=2.907$ ,  $p=0.011$ ) (Fig. 27A & normalised responses in B). This effect was considered dependent upon the contribution of TTX-s channels to the GABA-evoked response. The amplitude of the calcium responses to GABA ( $200\mu\text{M}$ ) was larger in DRG neurons with low TTX sensitivity (i.e. high TTX sensitivity index, Fig. 27C). Calculating a simple linear regression here also revealed a significant deviation from 0 in the slope ( $Y=0.23*X-0.030$ ,  $R^2=0.13$ ,  $F(1, 61)=9.2$ ,  $p=0.004$ ). Thus similar to capsaicin, the TTX-sensitivity could in part determine, the size of the GABA response.

### 3.2.3 Extracellular calcium influx mediates the GABA transient

The increase in intracellular calcium in response to GABA as monitored using calcium imaging can principally derive from two sources, specifically release from intracellular stores (store-operated calcium entry, SOCE) or from the extracellular solution via influx through membrane delimited channels (eg. voltage-gated calcium channels; (Berridge et al., 2003)). To establish the source of the calcium transient, we applied GABA in an extracellular solution containing nominally  $0\text{mM}$   $[\text{Ca}^{2+}]_e$ . In the absence of extracellular calcium, it was not possible to evoke a calcium transient in response to GABA ( $200\mu\text{M}$ ) (RM-ANOVA,  $F(2,66)=10.33$ ,  $p<0.001$ ,  $n=34$ ) (Fig. 28 A&B). The absence of a calcium transient in response to GABA during removal of

extracellular calcium (post-hoc Bonferroni corrected t-test,  $t=4.40$ ,  $p<0.001$ ) was reversed upon re-establishment of extracellular calcium at 2mM ( $t=3.17$ ,  $p=0.007$ ) as shown in Fig. 28C. It is of course, possible that the removal of extracellular calcium may interfere with the binding of GABA at the receptor, however to date, there is principally evidence for the interaction of intracellular changes in calcium concentrations interfering with GABA<sub>A</sub>R desensitization (Mozzrymas and Cherubini, 1998).

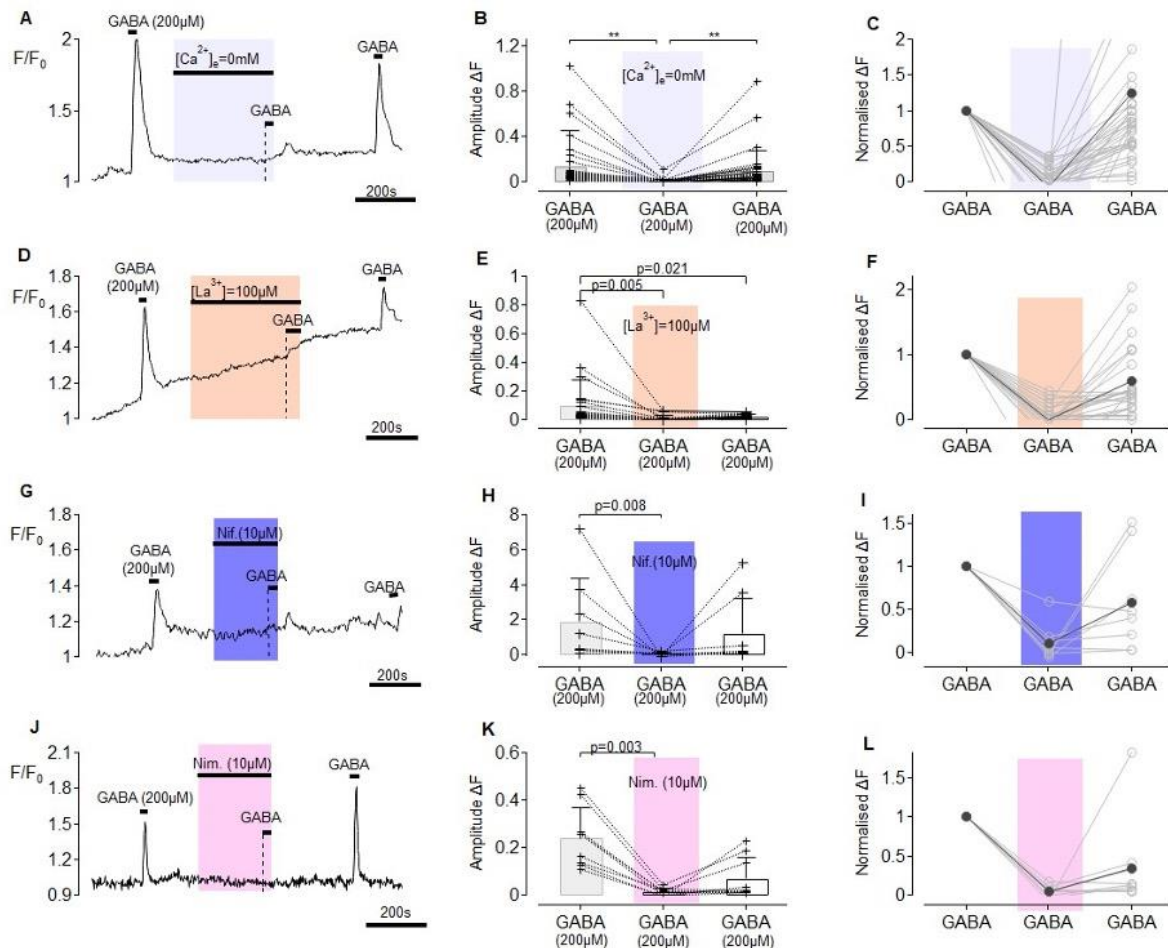


**Figure 28 Extracellular calcium influx mediates GABA induced calcium transients**

A) Representative trace of calcium transient to GABA (200 $\mu$ M) before during and after removal of calcium from the extracellular solution B) Calcium transients were abolished by removal of extracellular calcium (light purple shading) from the perfusing solution (RM-ANOVA,  $p<0.001$ ). C) GABA responses normalised to the amplitude of the first GABA application reveal return upon washout. D) Representative trace of cellular responses to GABA before during and after  $La^{3+}$  (100 $\mu$ M, peach shading) E)  $La^{3+}$  blocked calcium influx in response to GABA application (post-hoc Bonferroni corrected t-test,  $t=3.31$ ,  $p=0.005$ ). F) GABA responses normalised to the amplitude of the first show that responses return upon washout. G) Representative response to GABA (200 $\mu$ M) before during and after Nifedipine (10 $\mu$ M, blue). H) Nifedipine blocks the response to GABA by calcium influx (Friedman,  $p<0.001$ , post-hoc Wilcoxon,  $p=0.003$ ). I) GABA responses normalised to the first GABA. J) Representative response to GABA (200 $\mu$ M) before, during and after Nimodipine (10 $\mu$ M, pink). K) Nimodipine block of GABA-induced calcium transients (Friedman,  $p=0.010$ , post-hoc Wilcoxon,  $p=0.008$ ). L) Normalised responses from K.

Based on the fact that depolarisation of the membrane occurs in response to GABA application, it was interpreted that voltage-gated calcium channels, rather than SOCE, is involved in calcium signaling. Store-operated calcium influx requires a significantly more hyperpolarized membrane potential, at which voltage gated channels are usually inactivated, to conduct calcium (see Figure 3, *Introduction*) (Prakriya and Lewis, 2015). Subsequently, it was

investigated which voltage-gated calcium channels (VGCCs) contributed to calcium entry in response to GABA. Pharmacological tools were used to determine which VGCCs contributed to GABA-evoked calcium transients. The trivalent rare earth metal lanthanum ( $\text{La}^{3+}$ ) was utilized as a broad spectrum voltage-gated calcium channel antagonist (Reichling and Macdermott, 1991). Lanthanum ( $100\mu\text{M}$ ) blocked the calcium influx in response to GABA ( $200\mu\text{M}$ ) (RM-ANOVA:  $F(2,46)=6.39$ ,  $p=0.004$ ,  $n=24$ ) (Fig. 28D-F). The significant reduction in the amplitude of GABA-evoked calcium responses ( $t=3.31$ ,  $p=0.005$ ) was reversed upon washout, with GABA responses increasing ( $t=2.82$ ,  $p=0.021$ , Fig. 28E) back to an average of 59% of their original size as indicated by the normalised data in Figure 28F. The complete block by lanthanum would indicate that VGCC's are the principal calcium channel type responsible for GABA-mediated calcium transients.

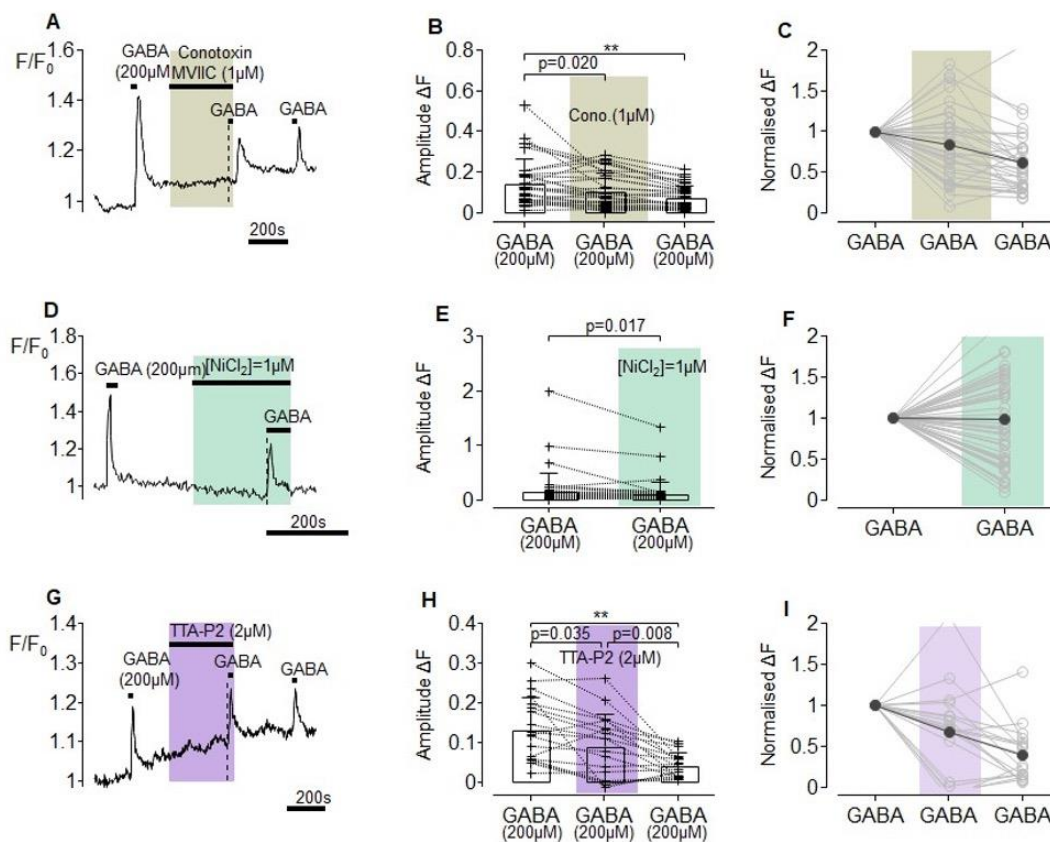


**Figure 29 Voltage-gated calcium channels responsible for calcium influx in response to GABA application**

A) Representative trace of N-type calcium channel block with  $\omega$ -Conotoxin MVIIC ( $1\mu\text{M}$ , brown). B)  $\omega$ -Conotoxin MVIIC reduced the calcium influx to GABA (RM-ANOVA,  $p<0.001$ , post-hoc t-test,  $p=0.020$ ). C) Normalisation to the first response shows that there is further reduction from GABA 1- 3 (post-hoc t-test,  $p<0.001$ ) D) T-type calcium channel block with Nickel ( $\text{NiCl}_2$ , green). E)  $\text{NiCl}_2$  ( $1\mu\text{M}$ ) reduced the GABA-induced calcium influx (paired t-test,  $p=0.017$ ). F) Normalisation shows no real deviation from the first response. G) The specific T-type channel blocker TTA-P2 ( $2\mu\text{M}$ , purple) in combination with GABA ( $200\mu\text{M}$ ). H) TTA-P2 had a significant effect of the GABA transient (RM-ANOVA,  $p<0.001$ , post-hoc t-test,  $p=0.035$ ), which was persistent after washout (I, post-hoc t-test, GABA 1-3  $p<0.001$ , GABA 2-3,  $p=0.008$ ).

There are predominantly two families of voltage-dependent calcium channels, as explained in the introduction; high voltage-activated (HVA) and low-voltage activated (LVA) calcium channels. HVA calcium channels include L-, P/Q-, R- and N-type channels, while T-type channels are LVA (Catterall, 2011). In a second series of experiments, the dihydropyridines (DHP) nimodipine and nifedipine were used to block high-voltage activated L-type calcium channels. GABA-induced calcium transients were blocked completely by both DHP-blockers. Nifedipine

(10 $\mu$ M) decreased GABA-evoked (200 $\mu$ M) calcium responses (n=8) from  $1.92 \pm 2.47$  to  $0.01 \pm 0.11$  (Friedman test:  $\chi^2(3)=9.00$ ,  $p=0.010$ , post-hoc Wilcoxon,  $Z=3.00$ ,  $p=0.008$ ) (Fig. 28 G-I). Similarly, nimodipine (10 $\mu$ M) reduced GABA-evoked (200 $\mu$ M) calcium responses (n=9) from  $0.24 \pm 0.13$  to  $0.01 \pm 0.02$  (Friedman test:  $\chi^2(3)= 11.56$ ,  $p<0.001$ , post-hoc Wilcoxon,  $Z=3.30$ ,  $p=0.003$ ) (Fig. 28 J-L).

The role of N-type voltage-gated calcium channels was examined using the peptide  $\omega$ -Conotoxin MVIIC isolated from conesnail venom (Kerr and Yoshikami, 1984).  $\omega$ -Conotoxin MVIIC (1 $\mu$ M) affected GABA-evoked (200 $\mu$ M) calcium transients (RM-ANOVA,  $F(2,62)=13.88$ ,  $p<0.001$ , n=32) (Fig. 29 A&B), reducing them from  $0.15 \pm 0.12$  to  $0.11 \pm 0.09$  (post-hoc Bonferroni corrected paired t-test,  $t=2.806$ ,  $p=0.020$ ). The reduction in GABA-evoked calcium responses by  $\omega$ -Conotoxin MVIIC was not fully reversed upon washout (post-hoc Bonferroni-corrected paired t-test,  $t=5.265$ ,  $p<0.001$ ) as shown in the normalised responses (Fig. 29C).

Finally, the role of T-type calcium channels in mediating GABA-evoked calcium responses was examined. Aptel et al. (2007) showed, using pharmacological techniques and global knock-out, that the low voltage activated T-type channel CaV3.2 was responsible for depolarizing responses to GABA and subsequent calcium influx in medium-sized D-hair neurons. To examine the role of T-type calcium channels in mediating GABA evoked calcium responses amongst all DRG neurons, the divalent cation nickel (NiCl<sub>2</sub>) and the synthetic compound TTA-P2 (Kraus et al., 2010) were used as blockers. In the presence of NiCl<sub>2</sub> (1 $\mu$ M), GABA-evoked calcium responses were reduced in amplitude from  $0.16 \pm 0.32$  to  $0.11 \pm 0.22$  (paired t-test,  $t(46)=2.48$ ,  $p=0.017$ , n= 47), but not blocked (Fig. 29 D-F). Similarly, GABA-evoked calcium responses were reduced from  $0.13 \pm 0.08$  to  $0.09 \pm 0.08$  by TTA-P2 (2 $\mu$ M; RM-ANOVA,  $F(2,36)=17.49$ ,  $p<0.001$ , n=19) (Fig. 29 G-I) and the reduction in GABA response amplitude during TTA-P2 (post-hoc Bonferroni corrected paired t-test,  $t=2.658$ ,  $p=0.035$ ) did not fully reverse upon washout (TTA-P2 - GABA wash:  $t=3.247$ ,  $p=0.008$ , GABA control – GABA wash,  $t=5.905$ ,  $p<0.001$ ) as shown in the plot of normalised GABA responses (Fig. 29I). According to the above findings, calcium responses to GABA were mediated by an influx of extracellular calcium (Fig. 28 A-C) and L-type HVA calcium channels were predominantly involved in the calcium influx in response to GABA (Figures 28 & 29).

## 3.2.4 Calcium responses to repeated GABA application

To examine the possibility that repeated application of GABA may itself affect the amplitude of subsequent GABA responses, calcium responses to repetitive GABA were tested in the absence of any additional interventions (Figure 30). Consecutive application of GABA (200 $\mu$ M) to DRG neurons for 30 seconds at ten minute intervals resulted in calcium response amplitudes of comparable size, without significant decrement (RM-ANOVA,  $F(2,40)=0.245$ ,  $p=0.784$ ,  $n=21$ ) (Fig. 30 A-C).

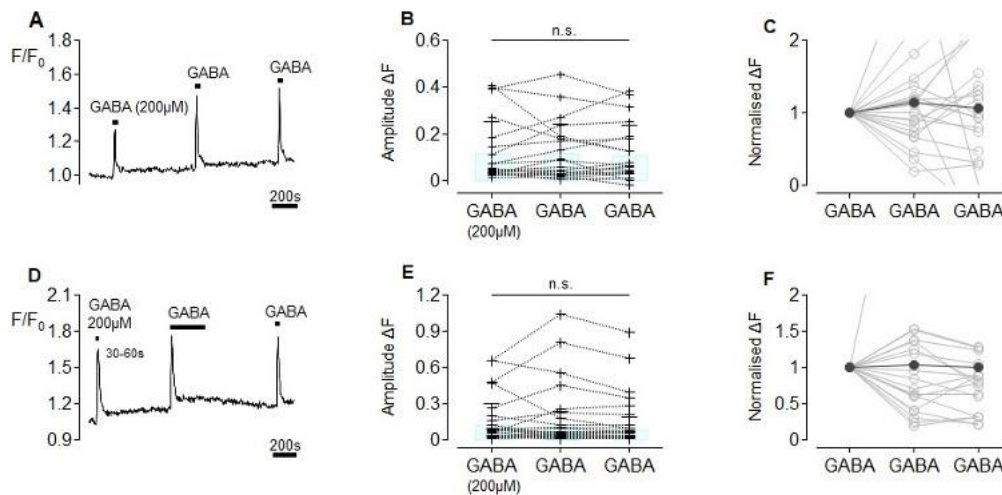


**Figure 30 Calcium responses to repeat GABA application**

A) Representative trace showing responses to repetitive GABA (200 $\mu$ M) application for 30s at 10 minute intervals B) No change in amplitude of calcium responses to repeat GABA at 10 minute intervals (RM-one way ANOVA,  $p=0.784$ ) C) Data as in B, normalised to the first GABA response. D) To test the effect of duration of GABA application, a longer exposure to GABA (300s) was used, with the first application at 30 or 60 seconds. E) There is no change in the responses to GABA at 30 vs 60s, nor with a longer application of 300s, (RM-one way ANOVA,  $p=0.192$ ). F) Data in E normalised to first GABA response for each respective cell.

In a second protocol, the time of GABA application was varied to test whether this affected the response to subsequent GABA application. Previous reports using voltage-clamped DRG neurons indicate that the chloride gradient can shift by up to 15mV during 5 minute GABA application (Akaike et al., 1987). The protocol used here comprised, an initial 30 or 60 second application of GABA (200 $\mu$ M), followed by a 300 second (5 minute) application and then a third GABA application, 30 seconds in duration (representative trace, Fig. 30D). The peak amplitude of the GABA response over the three applications showed no significant change (RM ANOVA,  $F(2, 50)= 0.607$ ,  $p=0.192$ ,  $n=26$ ) (Fig. 30 D-F).

A consequence of varying the application time of the second GABA was a shortening of the time interval between the end of the second GABA application and the beginning of the third GABA application, which was reduced to 5 minutes. Even at this shorter interval there was no significant decrement in the amplitude of the subsequent GABA response (Fig. 30 E&F; GABA 2- GABA 3,  $0.17 \pm 0.26$  to  $0.14 \pm 0.22$ ). Thus, prolonged application of GABA for 300s did not affect the amplitude of subsequent calcium transients to GABA tested at a 300s (5 minute) interval.

## 3.2.5 Effect of prolonged firing on calcium responses to GABA

A functional link between action potential firing rate and chloride loading has previously been shown in CA1 pyramidal neurons (Brumback and Staley, 2008) and also in peripheral C-fibre axons (Bonalume et al., 2021). Activity-dependent chloride loading posits that NKCC1 chloride transport is coupled to action potential firing such that NKCC1 activity increases intracellular chloride in proportion to firing rate. Carr et al. (2010) and Bonalume et al. (2021) show that an increase in frequency of electrical stimulation leads to a larger increase in excitability index during GABA application to peripheral C-fibre axons in human and in mouse sural nerve, respectively.

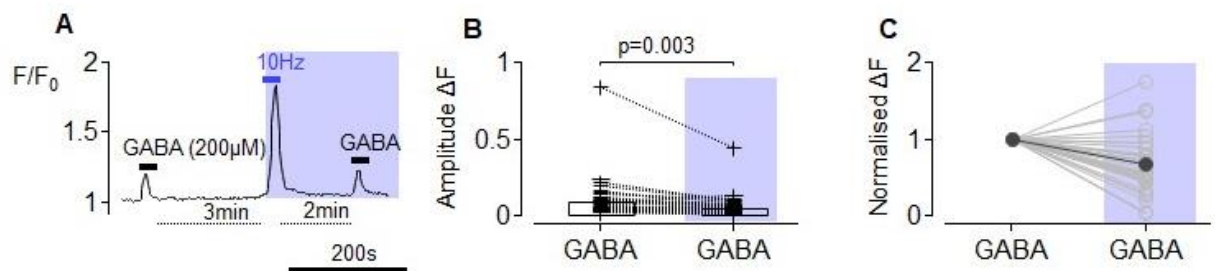


**Figure 31 An intervening bout of action potential activity reduces the calcium response amplitude to GABA**

A) Representative trace of a GABA (200 $\mu$ M) stimulus followed by a 10Hz electrical stimulation and a subsequent GABA application B) There is a reduction in the amplitude of the calcium transient in response to GABA when intervened by a depolarising action potential inducing stimulus (paired *t*-test,  $p=0.003$ ). C) A slight reduction from the normalisation to 1 is evident. Purple shading indicates the GABA application took place post-10Hz stimulus.

Having established that calcium responses to repeat GABA are consistent in amplitude even at 5 minute intervals, the effect of an intervening bout of electrical stimulation on GABA-induced calcium response amplitudes was tested. Initially, a 2 minute interval between the end of a bout of 10Hz electrical stimulation and the next GABA (200 $\mu$ M) application showed that contrary to expectation, the amplitude of the GABA response was reduced from  $0.11 \pm 0.14$  to  $0.06 \pm 0.08$  (paired *t*-test,  $t(32)=3.24$ ,  $p=0.003$ ,  $n=33$ ) (Fig 31 A-C).

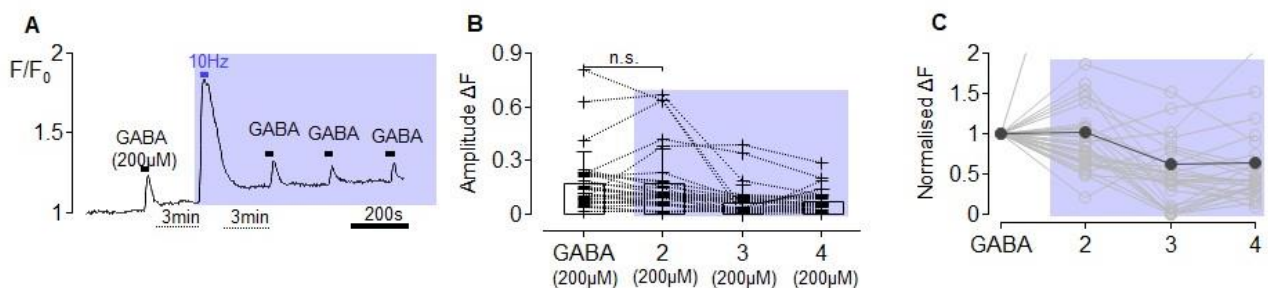


**Figure 32 A longer recovery between electrical stimulus and GABA response shows no evidence of action potential dependent increase**

A) Representative trace of the experimental protocol, with purple shading indicating the 10Hz stimulation and subsequent GABA responses. B) Pooled data of  $n=29$  cells used in the analysis (post-hoc *t*-test GABA 1- GABA 2,  $t=0.07$ , *n.s.*). GABA responses after 10Hz stimulation. C) Normalised data show no change between the first GABA and the second post-electrical stimulation. Purple shading indicates the GABA responses after 10Hz stimulation.

Allowing cells 3 minutes to recover after the electrical stimulation, revealed there was no change in the calcium response amplitude to GABA) (RM-ANOVA  $F(3,84)=9.53$ ,  $p<0.001$ ,  $n=29$ ; post-hoc Bonferroni corrected t-test,  $t=0.07$ , n.s.) after stimulation (Fig. 32 A-C).

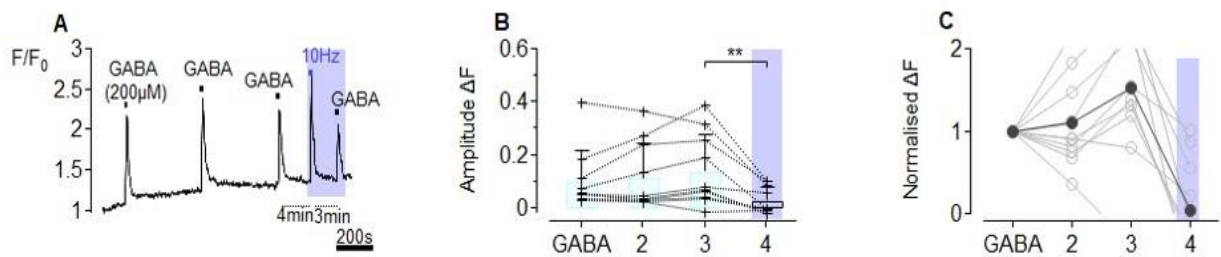


**Figure 33 Repetitive GABA applications at ten minute intervals, followed by a burst of high frequency firing reveals a reduction in amplitude of subsequent calcium transient in response to GABA**

A) Representative trace of GABA at ten minute intervals, followed by a stimulation of 10Hz (1ms) rectangular pulses and another GABA. B) Pooled data depicting the paired responses of cells to each stimulus. There was a reduction in the GABA response following 10Hz stimulus (Wilcoxon,  $p=0.004$ ). C) Normalised to the first GABA response, the cells also show a reduction following 10Hz stimulus. Purple shading represents GABA after electrical stimulation.

Nonetheless, a further test of GABA ( $200\mu\text{M}$ ) also with an interval of 3 minutes between electrical stimulation (7 minutes between consecutive GABA applications) and the following GABA response (representative trace in Fig. 33A,  $n=10$ ) shows a large reduction from  $0.14 \pm 0.14$  to  $0.02 \pm 0.05$  (Friedman's test:  $\chi^2(4)=14.88$   $p=0.002$ , post-hoc Wilcoxon with Dunn's correction,  $Z=3.811$ ,  $p<0.001$ ) (Fig. 33 B&C). Attempting to disentangle whether the interval after electrical stimulation affected the subsequent GABA response, all responses from GABA applications after electrical stimulation were pooled. Overall, there was a significant reduction between the GABA ( $200\mu\text{M}$ ) applications intervened by an electrical stimulus from  $0.14 \pm 0.16$  to  $0.10 \pm 0.14$  (paired t-test,  $t(70)=3.28$ ,  $p=0.002$ ,  $n=71$ ). This would indicate that irrespective of the time after an intense electrical stimulus, which is accompanied by a large calcium influx, there is a negative effect on the subsequent GABA response amplitude.

### 3.2.6 Effect of reduced extracellular chloride on GABA-evoked calcium response amplitude

Perforated patch recordings from DRG neurons indicate that the amplitudes of depolarizing responses to GABA increase in proportion to the transmembrane chloride gradient (Reichling et al., 1994). Having established that calcium responses to GABA in DRG neurons are mediated by extracellular calcium influx through L-type VGCC's, the effect of manipulation of the chloride gradient on GABA response amplitude was investigated. To alter the transmembrane chloride

gradient, extracellular chloride was reduced by replacement with equimolar amounts of gluconate salts.

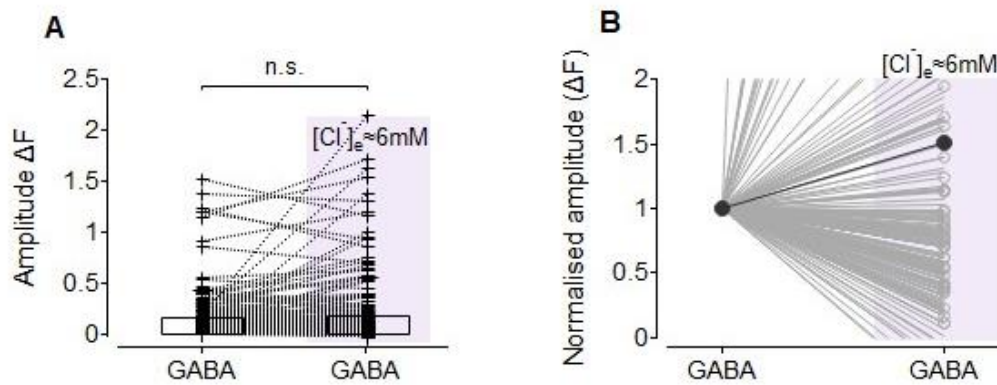


**Figure 34 No significant change in response size from normal GABA to GABA in low chloride**

A) Pooled data from protocols in Figures 35, 36 and 37 show no significant change in response size from the first GABA application to the first application in reduced chloride solution. B) Normalised data shows a wide array of responses, with an increased average from GABA 1 to GABA 2, indicated by the dark grey markers. Light pink shading indicates reduced extracellular chloride application.

An initial test of GABA after reduction of extracellular chloride from 145mM to 6mM resulted in no change in the response to GABA (GABA 1,  $0.18 \pm 0.26$ , to GABA 2 low chloride,  $0.21 \pm 0.4$ , paired t-test,  $t(170)=1.62$ ,  $p=0.107$ ,  $n=171$ ) (pooled data from Figures 35, 36 & 37 in Figure 34). One would assume that increasing the driving force for chloride outflux would increase the membrane potential difference, resulting in an increased depolarisation and a modestly increased calcium transient. Although there was no significant difference (Figure 34) for the entire GABA-responsive population in the experiments from Figures 35, 36 & 37, an increase in transient size was seen in many DRG neurons (evident in normalised data Fig. 36 C&F, Fig. 37 C&I) and is interpreted as reflecting an increase in the magnitude of the chloride current during activation of GABA<sub>A</sub>. Following the long exposure to GABA there was a prolonged reduction in responses (RM-ANOVA ( $F(7,336)=17.65$ ,  $p<0.001$ , GABA 3 – GABA 8 post-hoc Bonferroni corrected t-test,  $t=0.69$ ,  $p=0.977$ ,  $n=49$ ) (Fig 35 A-C).

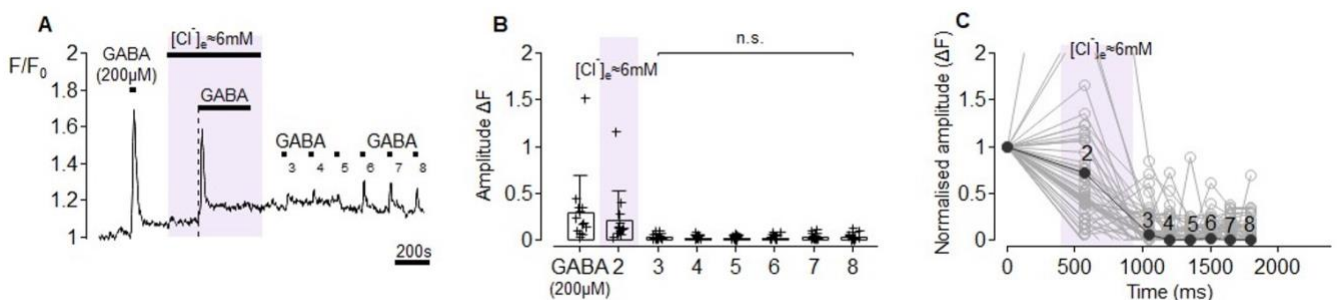


**Figure 35 Replacing chloride in the extracellular solution reduced the GABA-induced calcium transient significantly**

A) Representative trace showing GABA-induced calcium responses. B) There was a significant overall effect of reducing the chloride (RM-one way ANOVA,  $p<0.001$ ) and no recovery following reintroduction of chloride to the perfusing solution (post-hoc paired t-test GABA 3 – GABA 8, n.s). C) Normalisation to the first response shows a persistently low amplitude response to GABA from 1000s. Light pink shading indicates reduced extracellular chloride application.

To further test the concept of chloride depletion, an initial long GABA exposure was combined with several subsequent shorter GABA applications (30 seconds at two minute intervals). Consistent with the interpretation of chloride depletion, a progressive reduction and eventual abolition of calcium responses to GABA is evident in Figure 36 (Fig. 36B, post-hoc Bonferroni corrected t-test, GABA 3 - GABA 5,  $t(266)=0.38$ , n.s.,  $n=39$ ; Fig. 36E, post-hoc t-test GABA 3 - GABA 5,  $t(310)=0.29$ , n.s.,  $n=32$ ). This robust and reproducible effect is interpreted as resulting from depletion of chloride from DRG neuronal somata cumulatively with each GABA application.

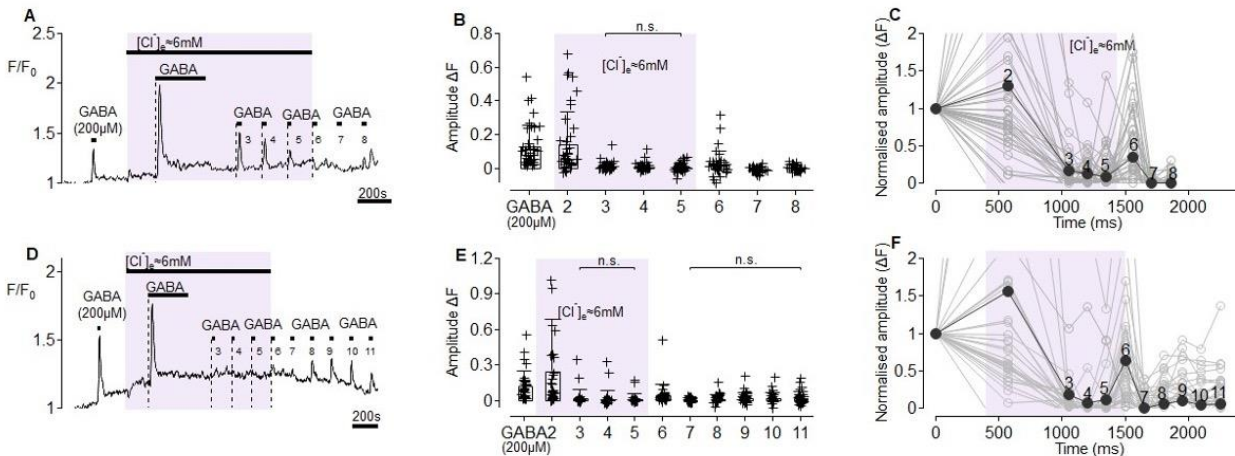


**Figure 36 Testing the depletion of the chloride gradient in a reduced extracellular chloride solution**

reveals a significant reduction of the calcium transient in response to GABA stimulus by approx. 1000 s. A, D) Representative traces of calcium response to GABA application. B) Applying GABA once for 300s followed by several 30s applications reveals no further reduction from GABA 3-5 (paired t-test, n.s.). C) Normalisation to the first response shows an increase of response amplitude, this returns to 0 indicating no lasting re-establishment of the gradient. E) Pooled data also shows that there was no further reduction in applying shorter GABA applications after one long (300s, GABA 3-5, paired t-test, n.s.) and no recovery of the transient (GABA 7-11, paired t-test, n.s.); also evident in the normalised data (F) revealing again persistently low calcium responses to GABA, despite brief increase after normal solution was washed back in. Light pink shading indicates timings of low chloride solution.

Having demonstrated depletion of intracellular chloride through repeated GABA<sub>A</sub>-R activation, the question of whether DRG neurons could restore their transmembrane chloride gradient was examined and if so, over what time course. After extended exposure to low extracellular chloride, re-establishment of the extracellular chloride concentration at 145mM resulted in an increase in GABA-evoked calcium response amplitude (Fig. 36 C&F, Fig. 37F) to GABA application immediately after reestablishing extracellular chloride. However, this recovery in GABA response amplitude was not sustained and the overall time course of recovery of the GABA-evoked calcium response was both slow and modest with no appreciable recovery even after 900 seconds (15 minutes) in most cells (Fig. 36 E&F, Fig 36F: GABA 7 – GABA 11, Bonferroni corrected paired t-test,  $t(310)=0.48$ , n.s.).

In the absence of a sustained recovery of GABA-evoked calcium responses a bout of electrical stimulation was used in an attempt to facilitate chloride reloading. An initial attempt to address this question failed as shown in Figure 37 A-C, because the GABA application began during the large calcium increase evoked by electrical stimulation.

Therefore, the electrical stimulation was executed in nominally 0mM  $[Ca^{2+}]_e$ , to abrogate the calcium increase (Fig. 37D). However, electrical stimulation did not potentiate the subsequent calcium response to GABA (Fig. 37 E&F) (GABA 6 – GABA 7, Bonferroni corrected t-test,  $t=0.13$ , n.s.,  $n=20$ ).

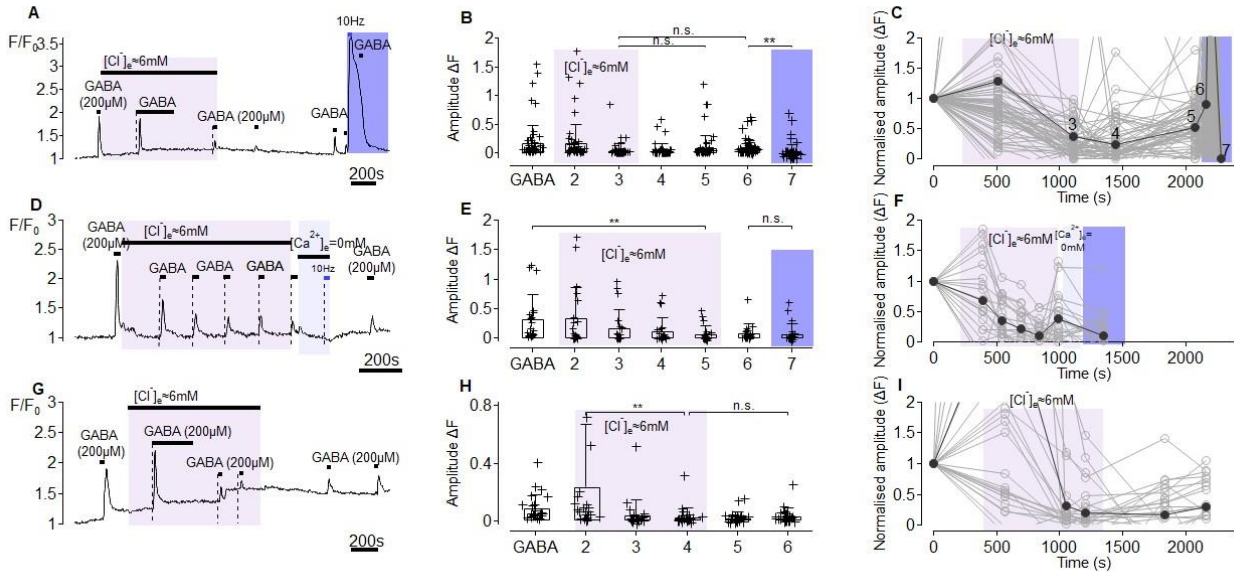


**Figure 37 Recovery of the chloride-depleted GABA transients**

A, D, G) Representative trace of experimental protocols. B) Pooled data of experimental protocol in A depicting a reduction in the GABA-induced calcium transient in response to application in low chloride extracellular solution (RM-one way ANOVA,  $p<0.001$ ) but no recovery when chloride was washed back in (post-hoc t-tests, GABA 3-5, GABA 3-6) and a reduction in response after electrical stimulation (GABA 6-7). C) The normalised data from that depicted in B, revealing the increase in GABA 6 is a piggy-back off of the electrically-induced calcium influx. E) pooled data from cells following depletion and application of a calcium-free electrical stimulus designed to eliminate the calcium influx thereby revealing a possible activity-dependent mechanism (post-hoc t-tests reveal the significant reduction in GABA induced transient, GABA 1 – 5,  $p<0.001$  and no significant difference between GABA 6 pre-10Hz and GABA 7 post-10Hz). F) Normalised data of pooled responses shown in E. H) Pooled data showing a control experiment without intervention at similar timings and the expected reduction following low chloride treatment (post-hoc Bonferroni corrected t-test,  $p<0.001$ ) I) Normalised data of pooled responses shown in H. Light pink shading indicates reduced extracellular chloride, light purple shading indicates  $Ca^{2+}$ -free solution and purple shadings indicate responses after electrical stimulation

In keeping with experiments depicted in Figures 35 & 36, in a control experiment without electrical stimulation as shown in Figure 37G, the reduction of GABA response amplitudes seen with manipulation of extracellular chloride concentration was expected (GABA 2,  $0.23 \pm 0.44$  to GABA 4,  $0.02 \pm 0.07$ ) (post-hoc Bonferroni corrected paired t-test,  $t(110)=4.09$ ,  $p<0.001$ ,  $n=23$ ). In this case, there was an assumption of recovery by waiting a similar amount of time, in the absence of electrical intervention. Nonetheless, there was no significant change in amplitude from GABA 4 ( $0.02 \pm 0.07$ ) to GABA 6 ( $0.03 \pm 0.05$ ; Bonferroni-corrected post-hoc t-test,  $t(110)=0.08$ , n.s.) (Fig 37 G-I).

## 3.2.7 Bumetanide inhibits NKCC1-associated chloride loading in DRG somata

To test whether bumetanide, an NKCC1 antagonist, could mimic the effects of low extracellular chloride solution on the reduction of the transmembrane chloride gradient, the loop diuretic was applied together with GABA. It is possible that by creating a synthetic extracellular, although the osmolarity of solutions was controlled for, prolonged exposure to abnormal environments could cause cell volume changes which could impact other aspects of cell signaling (Hochman et al., 1999). Therefore, this was considered a good independent alternative. NKCC1 utilizes the inward sodium gradient to transport two chloride, one sodium and one potassium ion into the cell per cycle. Following 6 minutes incubation with bumetanide (50 $\mu$ M), the calcium response to GABA (200 $\mu$ M) was unchanged (RM-ANOVA,  $F(2, 96)=9.46$   $p<0.001$ ,  $n=49$ , Bonferroni corrected post-hoc t-test, GABA 1 - GABA 2,  $t=1.94$ ,  $p=0.166$ ) (Fig. 38 A&B).

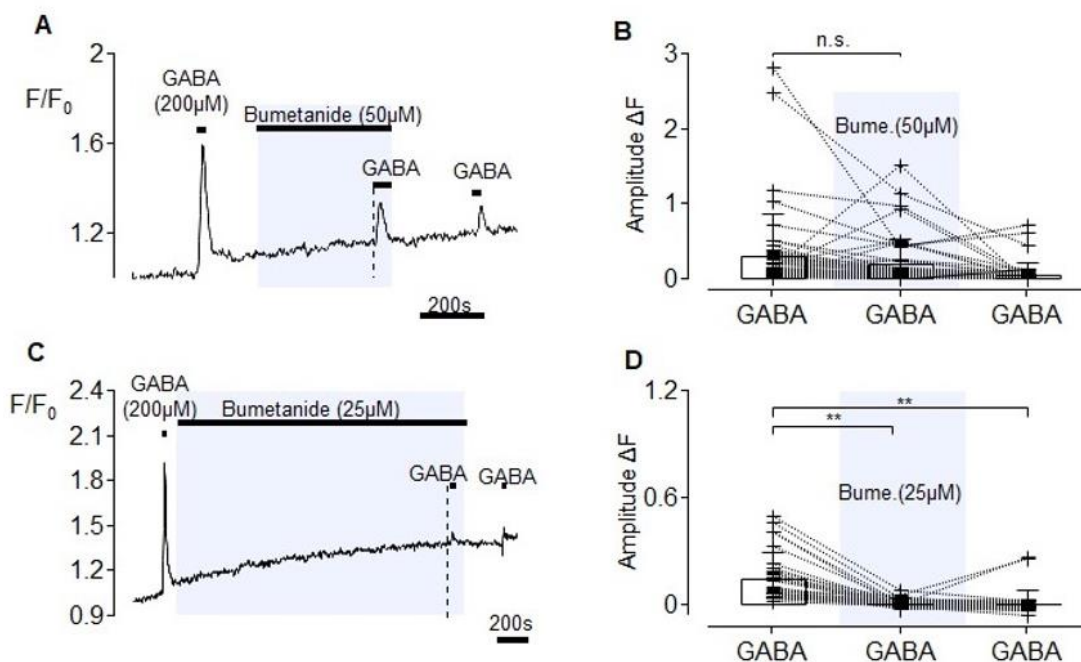


**Figure 38 GABA-evoked calcium transients are reduced by bumetanide after long exposure**

A) Representative trace of protocol with incubation of Bumetanide (50 $\mu$ M, pale blue shading) for 6 minutes, prior to co-application with GABA (200 $\mu$ M) B) GABA response amplitude is not significantly influenced by a short incubation with bumetanide followed by co-application of both substances (post-hoc t-test, n.s.) C) Representative trace of protocol showing a 30 minute incubation of bumetanide (25 $\mu$ M) prior to co-application with GABA (200 $\mu$ M) D) Bumetanide incubation significantly reduces the GABA-evoked calcium transient (RM-ANOVA,  $p<0.001$ , Bonferroni corrected post-hoc t-test,  $p<0.001$ ), which remains low after washout.

According to the experiments using axonal threshold tracking, Bumetanide may need longer exposure to take effect, therefore the incubation time with bumetanide (25 $\mu$ M) was extended to 30 minutes before application of GABA (200 $\mu$ M). As shown in the example trace Fig. 38C, there was a significant reduction in the amplitude of the GABA-evoked calcium transient ( $0.15 \pm 0.14$  to  $0.01 \pm 0.02$ , Bonferroni corrected post-hoc t-test,  $t(56)=5.96$ ,  $p<0.001$ ) and this reduction was not reversed upon washout, with little recovery of the GABA calcium response (GABA 2 – GABA 3; Bonferroni corrected post-hoc t-test,  $t=0.10$ , n.s.,  $n=29$ ) (Fig. 38 C&D).

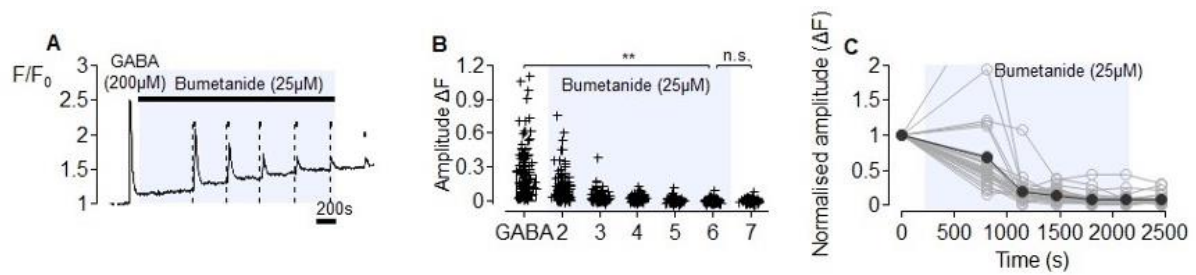


**Figure 39 NKCC1 blockade with bumetanide progressively reduces the GABA-evoked calcium transients**

A) Representative trace indicating the experimental protocol of repetitive GABA (200µM) application under bumetanide (25µM, pale blue shading) exposure B) The incubation of bumetanide whilst repetitively applying GABA reduces the calcium transient to a state of depletion (RM-ANOVA,  $p < 0.001$ , Bonferroni corrected post-hoc t-test,  $p < 0.001$ ) without evidence of recovery. C) Normalised pooled data in B.

Bumetanide was also used to examine the effect of intracellular chloride depletion. This strategy was similar to that used by (Bonalume et al., 2021) using axonal threshold tracking and comprised repeat GABA (200µM) application during continued exposure to bumetanide (25µM, Fig 39A). In the absence of bumetanide, i.e. under control conditions, repeat GABA elicited robust and reproducible calcium transients of similar amplitude at five minute intervals (Fig. 30 D-F). In the presence of bumetanide, the amplitude of calcium responses to successive GABA applications at five minute intervals was progressively reduced in amplitude from GABA 1 – GABA 7 (Fig 39B) as follows:  $0.38 \pm 0.29$ ,  $0.22 \pm 0.18$ ,  $0.07 \pm 0.08$ ,  $0.04 \pm 0.03$ ,  $0.02 \pm 0.02$ ,  $0.02 \pm 0.02$ ,  $0.02 \pm 0.02$  (RM-ANOVA,  $F(6,162)=39.20$ ,  $p < 0.001$ , Bonferroni corrected post-hoc t-test,  $t=11.45$ ,  $p < 0.001$ ,  $n=28$ ). Although bumetanide is primarily an NKCC1 antagonist it can also act as a GABA<sub>A</sub> antagonist (Sung et al., 2000), however, this provides evidence indicate that blockade of NKCC1 prevents replenishment of intracellular chloride efflux associated with each GABA application. An additional observation was the progressive increase in baseline calcium that paralleled, in time course the progressive decrement in GABA evoked calcium responses (Fig. 39A). While the reduction in GABA-evoked calcium responses likely reflects a reduction in the transmembrane chloride gradient, it is difficult to ascribe a singular mechanism to the increase in baseline calcium.

4 DISCUSSION

## 4.1 Axonal threshold tracking in C-fibre axons

### 4.1.1 Unusual role of GABA in modulating nociceptor excitability

GABA and glycine are the two main inhibitory neurotransmitters in the CNS mediating fast inhibitory transmission. In general, inhibitory neurotransmitters are expected to be analgesic owing to their hyperpolarising and shunting actions that reduce neuronal excitability. Indeed, application of inhibitory neurotransmitters or their synthetic receptor agonists has analgesic effects (Carlton et al., 1999; Garcia-Nicas et al., 2006), while antagonising these in the spinal cord can exacerbate hyperalgesia (Lee and Lim, 2010; Yamamoto and Yaksh, 1993). Particularly in the spinal cord, GABA-mediated inhibitory transmission is well-established in the processing of nociceptive information. This concept is also at the heart of the Gate Control Theory proposed by Melzack and Wall (1965), stating that inhibitory interneurons in the spinal dorsal horn (SDH) gate nociceptive information coming from the periphery. When the gate is open, painful stimuli are conveyed, while non-painful signals close the gate. They posit small diameter fibres (C- and A-delta fibres) synapse on and excite nociceptive projection neurons, which carry their information further to the brain, while also synapsing on and inhibiting inhibitory interneurons (see Figure 1, *Introduction*). Low threshold large diameter fibres (A $\beta$ ) on the other hand, activate these inhibitory interneurons whereas under normal conditions their synapses on nociceptive projection neurons are subthreshold. It should be mentioned, that the Gate Control Theory was based on limited data and the research since has elucidated that some of the propositions are outdated (Woolf, 2022).

In primary afferent neurons, the intracellular chloride concentration is kept high resulting in an  $E_{Cl}$  above resting membrane potential, due to a low expression of KCC2 and high expression of NKCC1, which transports chloride back into the cell. This high intracellular chloride concentration explains GABA-mediated depolarizing currents in normal primary afferents. Interestingly, such depolarizing currents will actually reduce excitability of presynaptic endings of nociceptors via sodium channel inactivation and thereby mediate presynaptic inhibition (Eccles, 1961). Indeed, a reversal of the chloride gradient in spinal cord neurons can switch a normal GABA-mediated inhibition to the opposite excitatory effect which has been hypothesized as an important mechanism to explain hyperexcitability in chronic pain (Price et al., 2009; Wu and Wang, 2023). Therefore, the key element for controlling presynaptic inhibition is the maintenance of a high intracellular chloride concentration in primary afferent nociceptors.

Nevertheless, GABA-mediated chloride currents can have opposite effects on nociceptor excitability along the axon, in particular for activity-dependent changes. In general, nociceptor excitability decreases upon repetitive discharge based on hyperpolarisation, increase in intracellular sodium or inactivation of sodium channels (De Col et al., 2008; Zhang et al., 2017). However, as GABA-mediated chloride currents are facilitated by hyperpolarisation, they are optimally positioned to limit activity-dependent reduction of excitability.

Therefore, it was of particular interest to study the role of GABA-mediated chloride currents in limiting activity-dependent inhibition in peripheral primary afferents. Traditionally, mechanisms inducing hyperexcitability are in the forefront of concepts for chronic pain, such

as gain of function mutations of voltage-gated sodium channels (Alsaloum et al., 2021;Dib-Hajj et al., 2005).This work focused on axonal GABA effects that might provide evidence for a complementary concept of chronic pain, namely reduced activity-dependent inhibition via regulation of the axonal chloride gradient.

#### 4.1.2 Pharmacological characterization of GABA mediated chloride currents

In this study, the threshold tracking technique was used to assess the functional role of GABA-mediated chloride currents on excitability of axons within the sural nerve, which are primarily skin afferents. The excitability index was used to indirectly determine a change in the membrane potential as has been done previously (Bonalume et al., 2021;Carr et al., 2010;Moalem-Taylor et al., 2007). It was found that GABA induced an increase in electrical excitability in C-fibre axons in a concentration-dependent manner. An increase in the peak of the C-fibre action potential, and a decrease in the latency, reflecting an increase in axonal conduction velocity, would suggest that GABA induced a depolarisation of the membrane (Figure 11), consistent with the high intracellular chloride concentration maintained in peripheral afferents, and the chloride efflux associated with opening of GABA receptors. The receptor activation was blocked by bicuculline and picrotoxin and replicated by muscimol, thereby suggesting that the currents were mediated by GABA<sub>A</sub>R. The GABA<sub>B</sub>R agonist, baclofen, did not affect the excitability of the C-fibre axons (Figure 12).

#### 4.1.3 Activity-dependent modulation of GABA responses

The excitability increase induced by GABA was increased by intermittent bouts of high frequency electrical stimulation (Figure 16), confirming previous data (Bonalume et al., 2021) and also corroborating the unusual role of GABA in limiting activity-dependent axonal hypo-excitability. The increase in excitability by GABA is interpreted as hyperexcitability and we suggested, in line with previous interpretations (Bonalume et al., 2021), that increased activity of NKCC1 reloading the intra-axonal chloride concentration during high frequency firing may be responsible. The relationship between action potential firing and NKCC1 activity has previously been suggested in CA1 neurons (Brumback and Staley, 2008) and in axons (Bonalume et al., 2021). The exact mechanism, by which neuronal activity could increase NKCC1 activity is unclear, but phosphorylation of NKCC1 might contribute (Pieraut et al., 2007).

In a series of experiments to investigate the role of increased neuronal activity on NKCC1-mediated chloride transport, bumetanide was employed to block NKCC1 and repetitive GABA probing was used to assess resulting excitability changes by depolarizing chloride currents. Our data indicate that NKCC1 is indeed responsible for re-establishing the intra-axonal chloride concentration, as repetitive probing with GABA in combination with NKCC1 block completely depleted the chloride gradient (Figure 21). However, we also showed that repetitive GABA application at shorter intervals leads to a strong GABA<sub>A</sub>R desensitisation (Figure 20). Thus, in our interpretation of reduced GABA responses, we need to consider both a reduced chloride gradient and increased receptor desensitization. When applying the intermittent high

frequency firing under an NKCC1 block, increases in subsequent GABA response were still apparent (Figures 19 & 22) speaking against a key role of this transporter.

The predominant effect of action potential activity on unmyelinated axons is a reduction in excitability and conduction velocity. This activity-dependent slowing (ADS) of conduction velocity is due to influx of sodium, inactivation of NaV channels and hyperpolarisation. ADS is particularly pronounced in nociceptive C-fibres (Gee et al., 1996; Schmidt et al., 1995; Serra et al., 1999; Weidner et al., 1999) and slowing profiles are often altered in injured states (De Col et al., 2008; Obreja et al., 2018; Shim et al., 2007; Werland et al., 2021)

As NKCC1 is electroneutral, hyperpolarisation alone is not expected to interfere with its activity. However, as it utilizes the sodium gradient to transport two chloride, one potassium and one sodium molecule into the axon, one could assume that an activity-dependent increase of intracellular sodium concentration would reduce its activity. However, trains of activity in neurons cause a long-lasting increase of sodium-potassium ATPase pump (Na<sup>+</sup>/K<sup>+</sup>-ATPase) activity in neurons (Brumback and Staley, 2008), thereby actually reducing the intracellular sodium concentration. Thus, the thermodynamic equilibrium for NKCC1 would be expected to be shifted to higher intracellular chloride concentrations when the transmembrane sodium gradient, and therefore driving force for NKCC1, is increased (Brumback and Staley, 2008). Fiumelli et al. (2005) showed that modulation of GABAergic transmission due to activity-dependent modification of the  $E_{Cl}$  contributes to the plasticity of neural circuits in the hippocampus and that with trains of action potentials, the  $Cl_i$  steadily increases. Perhaps, the action of NKCC1 to maintain the axonal intracellular chloride concentration during bouts of increased action potential firing could reduce activity-induced hyperpolarisation and thereby ADS and would stabilize the membrane excitability and limit activity-dependent reduction of excitability (Bonalume et al., 2021).

Interestingly, previous studies have shown that even one bout of increased firing can induce an increase in GABA modulated excitability index over tens of minutes after normalisation of electrical stimulation (Bonalume et al., 2021). Here we find that only subsequent to two bouts of 2.5 Hz, there is a significant increase in the GABA-induced excitability increase (Figure 16). The GABA applications themselves were separated by sufficiently long intervals to ensure stable responses and rule out potential receptor desensitization. The observed differences may be dependent on the actual number and frequency of action potentials, but may also depend on the timing, as discussed above, for long-lasting activation of the Na<sup>+</sup>/K<sup>+</sup>-ATPase. Most probably, also, the timing between the end of the increased firing and the start of the second GABA application will determine the effect on excitability; at shorter intervals, activity-dependent hyperpolarisation and increased Na<sup>+</sup>/K<sup>+</sup>-ATPase activity is expected to have a more pronounced effect and thus, a GABA-evoked depolarisation should be larger.

#### 4.1.4 Repetitive GABA responses

The transmembrane chloride gradient is intricately linked with excitability, in particular in muscle cells (Lueck et al., 2007) and neurons (Price et al., 2009), in which dysregulation of

intracellular chloride concentrations dramatically changes the balance between excitation and inhibition. For example, tissue injury may result in a depolarising shift of  $E_{\text{anion}}$  (Coull et al., 2003) which, in peripheral afferents, sensitizes action potential thresholds and leads to hyperexcitability of neurons upon activation of chloride channels (Kurki et al., 2023; Raimondo et al., 2017).

Here, the repetitive application of GABA at ten-minute intervals revealed reproducible increases in the excitability index reflecting a depolarizing effect (Figure 15). Upon shorter intervals a gradual decrease of this effect was observed (Figures 13 & 14). We hypothesised that this gradual decrease would be based on an imbalance between chloride outflow through  $\text{GABA}_{\text{A}}\text{R}$  and chloride inward transport through the NKCC1 transporter, resulting in a depletion of the chloride gradient. Previous studies demonstrate that NKCC1 inward chloride transport in axons requires about 5 minutes to re-establish the original gradient (Bonalume et al., 2021). In patch clamp experiments, GABA puffs have been shown to deplete intracellular chloride (Schmidt et al., 2018) and prolonged GABA application can reduce the  $E_{\text{Cl}}$  by about 10-15 mV (Akaike et al., 1987). We therefore posited that the frequent GABA application at short intervals in an axonal preparation would be even more effective to deplete intracellular chloride, as the surface area to volume ratio is far larger than in cell bodies.

We used blocking of NKCC1 by bumetanide to selectively investigate the role of this chloride transporter and facilitate the depletion of intracellular chloride. Potential confounding antagonistic effects of bumetanide on  $\text{GABA}_{\text{A}}\text{R}$  were excluded (Figure 18). The effect of NKCC1 antagonism has been previously investigated, however, less so in the context of axonal excitability (Andreasen and Nedergaard, 2017; Bonalume et al., 2021). We blocked NKCC1 to prevent re-establishing the chloride gradient, while using repetitive GABA to induce chloride currents to reduce the intra-axonal chloride concentration. This block was particularly important as such a depletion of  $\text{Cl}_i$  will increase the driving force for inward chloride transport via NKCC1 and therefore its activity, based on its thermodynamic regulation (Brumback and Staley, 2008).

We initially attributed the reduction in GABA responses at short intervals to depletion of intracellular chloride (GABA 3 & GABA 7, Figure 17), as explained above. However, we did not observe the expected fast decrease in GABA responses following blockade of NKCC1 with bumetanide, as GABA responses were fairly stable (Figure 17).

We hypothesized that perhaps the activity-induced modulation of NKCC1 would be affected with blockade of bumetanide and in fact, bumetanide may require a brief increase in firing to become more effective (Dzhala et al., 2010). However, the use of bouts of high frequency firing to increase the potential gradient difference did not yield a more pronounced effect. Unfortunately, the different number of stimulation periods within (and between) protocols (Figures 19 & 22) were potentially a limiting factor in improving conditions for a block of NKCC1. Nonetheless, despite this variation, we can conclude that one bout of increased stimulation at 1 Hz did not facilitate the blockade of NKCC1 by bumetanide. In fact, the GABA response after bumetanide was comparable to that after an effective charging intervention (GABA 2- GABA 4, Figure 19).

Importantly, we observed a reduction in the GABA responses upon repetition (GABA 6 – GABA 7, Figure 17) even without intervention of bumetanide. Therefore, the application of GABA at

intervals, which would produce a stable response (based on findings in Figure 15), was tested during bumetanide incubation (Figure 21). In this protocol, bumetanide induced a progressive reduction in GABA excitability responses indicating that the block of NKCC1-mediated inward chloride transport is essential to maintain a depolarizing GABA effect. This is in accordance with previous results that also reveal a reduction in amplitude of sustained GABA responses during bumetanide exposure (Bonalume et al., 2021) and corroborates the action of bumetanide on NKCC1 and not GABA<sub>A</sub>R antagonism (Bonalume et al., 2021; Sung et al., 2000).

Interestingly, when regarding the small volume structure of a C-fibre axon and the corresponding large surface area to volume ratio, the time required for bumetanide to block GABA responses was quite long (approx. 20 minutes, Figure 21). Taking this information into account we had to reconsider our interpretation of repetitive GABA stimulations at 2-minute intervals. Rather than an assumed depletion of the chloride gradient, desensitization of GABA<sub>A</sub>R in the early phase is probable. Thus, our results reflected a mechanistically combined effect of chloride depletion and GABA<sub>A</sub>R desensitization. We attempted to separate the two mechanisms by comparing time course of GABA induced excitability changes for different application durations and intervals. Interestingly, shorter intervals (1-2 min vs. varying 2-5 min) between the GABA stimulations were more effective to reduce the excitability change, compared to longer durations of the application period (2 min vs. 1 min.; Fig. 20 A&B).

The desensitization of the GABA<sub>A</sub>R complex strongly depends on the GABA concentration and duration, the application frequency and the receptor subunits compiling the pentameric ion channel (Sallard et al., 2021). There are 19 subunits known and usually the composition includes two alpha, two beta and one gamma subunit. It has been shown that the  $\beta 3$  subunit is required in nociceptors to constitute a functional GABA<sub>A</sub>R (Bonalume et al., 2021). Nonetheless, while some subunits are cell-specific (Ghit et al., 2021), there are still a myriad of possible combinations (Sieghart et al., 1999) and the exact subunit composition in C-fibre axons has not been established (Bonalume et al., 2021; Lorenzo et al., 2014). Additionally, since the subtypes may desensitize independently from one another (Gielen et al., 2020) their kinetics as a whole are expected to be complex. Furthermore, there are also fast and slow components of desensitization and of course the kinetics and extent of desensitization are critical for the efficacy of inhibitory synaptic events (Sallard et al., 2021), and may even contribute to inducing hyperexcitability due to loss of inhibition.

Albeit, our study did not clarify the exact determinants for GABA<sub>A</sub>R desensitization, the results have major implications for our main hypothesis that GABA counteracts an activity-dependent reduction of excitability in nociceptors. When considering the pronounced receptor desensitization, it appears obvious that under physiological conditions, an effect of GABA is expected to be transient. Clinically, a transient effect on the primary afferent neurons may not be suited to exert a tonic sensitizing effect in the context of chronic pain in which nociceptive activity is ongoing for months and years, unless the pathophysiology also includes modifications of the desensitization process. On the other hand, transient depolarising effects could be of major clinical relevance when they modulate the ability of axons to conduct high frequency discharge. For short bursts, peak frequencies of up to 180 Hz have been reported for human C-nociceptors (Weidner et al., 2002) and moderate changes of membrane potential in nociceptors can influence their ability to transmit action potentials at 30 Hz firing frequency

(within upper range for unmyelinated fibres) to the spinal cord (Du et al., 2014). Perhaps, these short bursts of activity could be related to intermittent shooting pain experienced in some pain disorders (Lenz et al., 1989), drastically influencing quality of life in these patients. Importantly, depending on the resting membrane potential, GABA-induced depolarizing and shunting effects can also lead to a reduction of excitability leading to an increased filter function in particular when the T-junction at the dorsal root ganglion is affected (Du et al., 2017).

#### 4.1.5 Limitations of electrically-induced CAP for excitability testing

Our initial experimental approach was based on the ability for action potential firing to increase activity of NKCC1 inward chloride transport and its block by bumetanide. However, rather than specifically activating NKCC1 activity in nociceptors, the action potential firing results in a complex modulation of neuronal excitability of all C-fibres in the nerve which complicates the interpretation. Electrical stimulation has been widely used as an alternative treatment approach in various neurological conditions (Matarazzo et al., 2023) and electrically evoked compound action potentials are useful in diagnosis and in determining the progression of peripheral nerve diseases like polyneuropathy (Djouhri, 2016). However, electrical stimulation techniques in humans to determine excitability, cover mainly myelinated fibres and will not yield information about single functional fibre classes.

A major advantage of optogenetic control of neural activity is that it allows the activation of specific fibre types of interest. We therefore used the optogenetic Trpv1;ChR2 line in first experiments as a tool to more specifically investigate the role of activity in TRPV1-positive nociceptors (Figure 23). We aimed for high frequency light pulses, to provoke action potentials in the nociceptors and check whether this would lead to an increase in subsequent GABA responses.

TRPV1 is known to co-localise with NKCC1 in approximately 50% of somatosensory neurons of the DRG and trigeminal ganglia (Price et al., 2006). This co-expression has been suggested to represent a gateway to allodynia; the release of endogenous TRPV1 agonists may activate TRPV1 on primary afferents that might further influence activity of the NKCC1 transporter thereby causing increase in chloride (Pitcher et al., 2007). Thus, modulating the activity specifically in these fibres would provide insights into the modulation of specific nociceptive afferents. Initially, it was simply tested whether blue light activation of Trpv1;ChR2 fibres was possible and whether there is a possibility to track ensuing compound action potentials using the threshold tracking technique. We were able to optogenetically evoke C-CAPs (Fig. 23B) and successfully track excitability using the QTRAC software in a single recording. Refining this approach would enable adjustment of the stimulus amplitude to maintain C-CAP amplitudes of 40% and allow assessment of changes in axonal excitability specifically in Trpv1-positive nociceptors.

A further advantage for optogenetic tools to evoke changes in membrane potential is the independent modulation of the chloride gradient via a light-activated chloride pump. In our study, we experienced the limitations linked to desensitization of GABA<sub>A</sub>R upon repetitive stimulation, when trying to modify the chloride gradient. Moreover, when applying trains of action potentials, the resulting hyperpolarisation and changes in intracellular sodium

concentration will produce a quite complex pattern of changes that might not be ideal to specifically investigate the effect of the chloride gradient. Using optogenetically activated chloride transport mechanisms would allow to assess changes in the chloride gradient independent of GABA<sub>A</sub>R, the NKCC1 transporter, and also independent of activity-dependent changes in membrane potential and intracellular sodium concentration. Here we attempted to use the Trpv1;eNpHR3.0 transgenic line to induce chloride loading by light activation (Figure 24). eNpHR3.0, when activated with yellow light, pumps chloride into the cell. This would have the same effect as activation of NKCC1, namely reducing activity-induced hyperpolarisation and stabilizing the membrane potential, limiting activity-dependent reduction of excitability. However, the main advantage of this approach is the selective change of the chloride gradient without the side effects that limited our earlier approaches. Unfortunately, initial experiments here did not show effects of light-activated chloride conductance, albeit the modulation of EGABA has been successful in dissociated neuronal preparations (Alfonsa et al., 2015; Raimondo et al., 2012). Thus more time will have to be invested to enable control of the chloride gradient via halorhodopsin in axonal preparations.

Despite their advantages optogenetic tools are also limited. Activation and inactivation kinetics for example, prevent true insight into the whole frequency response range (Malyshev et al., 2015). However, work is ongoing to improve the gating characteristics of some of the optogenetic actuators being used currently. For example, Gt\_CCR4, a light-gated cation channel, has shown promise for stable, reproducible light-induced neuronal excitability (Hososhima et al., 2020). Some groups have also used the combination of blue and yellow light-activated optogenetic currents in specific cell-subsets because blue light enables a quicker reactivation of yellow light channels (Zhang et al., 2007).

In contrast to these approaches, a relatively simple technique that could provide alternative advantages is calcium imaging. It allows a visualization of several cells at a time, improving output and leaves the membrane and intracellular milieu intact, in contrast to patch clamping methods. Additionally, it would be possible to combine a genetic approach with an electrical approach, for example the use of specific electrical stimuli to activate a subclass while simultaneously imaging with a genetically-encoded calcium indicator.

## 4.2 Calcium imaging to evaluate GABA effects in DRG neurons

The primary role of GABA receptors on primary afferent neurons in the spinal cord is presynaptic inhibition. Presynaptic inhibition, the consequence of PAD, constitutes the depolarising and inhibitory actions of GABA in the spinal dorsal horn, which reduces transmitter release in response to excitatory stimulation. This of course, contrasts with an apparent excitatory effect of GABA during sensitised and injured states where it has been shown to potentiate formalin-induced pain behaviour (Jang et al., 2017). Only recently has a fully functional GABAergic system been characterized in the dorsal root ganglia of the mouse, showing that GABA can be produced and released by DRG neurons and taken up by satellite glial cells. The authors suggest that the GABA release from somata of DRG neurons reduced pain behaviours *in vivo* by reducing the reliability of action potential conduction via the axonal T-junction in the DRG (Du et al., 2017). The functional consequences of the depolarizing effect of GABA directly at the T-junction are apparently similar to spinal presynaptic inhibition and thus, the authors suggest a gate control mechanism of pain within the local environment of peripheral afferent somata (Du et al., 2017; Fuller et al., 2023). The expression of the NKCC1 chloride transporter in primary afferent neurons maintains a high intracellular chloride concentration, in the absence of the KCC2 transporter to extrude chloride. Thus, upon GABA<sub>A</sub>R activation the ensuing efflux of chloride will depolarise these cells. Consequently, GABA<sub>A</sub>R activation in dorsal root ganglion neurons of the mouse will also stimulate calcium influx (Aptel et al., 2007; Reichling et al., 1994; Schöbel et al., 2012). Further intracellular chloride accumulation, such as in the case of injury, may lead to hyperexcitability of these cells (Coull et al., 2003; Pieraut et al., 2007). Following nerve injury, inhibition or decrease of GABA<sub>A</sub>R may lead to aberrant sensory processing (Meisner et al., 2010). Increasing evidence suggests a role for NKCC1 upregulation in sensitisation of spinal neurons also during inflammatory states (Funk et al., 2008; Pieraut et al., 2007). Thus, the regulation of intracellular chloride in primary afferent fibres and their cell bodies is intricately involved in the transmission of nociceptive signals and the investigation of the role of NKCC1 in the maintenance of neuronal excitability might provide an avenue to potential therapeutic interventions in chronic pain. In light of these results, it is important to address that the functional consequences of depolarisation in primary afferents may be increased or decreased excitability depending on the extent, location and context of this depolarisation.

### 4.2.1 Mechanisms of GABA-induced calcium transients

Using calcium imaging it was confirmed that GABA induces calcium transients in a concentration-dependent manner (Figure 25). The GABA<sub>A</sub>R mediates these responses, since bicuculline and picrotoxin block the calcium transient, while muscimol mimics it (Figure 25). The calcium responses result from an influx of extracellular calcium via voltage-gated calcium channels (Figures 28 & 29). Specifically, here we find that L-type VGCC's are responsible for the influx of calcium subsequent to GABA<sub>A</sub>R activation, in line with several previous studies on hypothalamic hamartoma cells (Kim et al., 2008), rat dorsal horn neurons and dorsal root

ganglia (Reichling et al., 1994;Zhao et al., 2016) and subventricular zone astrocyte-like cells (Young et al., 2010). L-type voltage gated calcium channels are high-voltage activated channels that open in response to a large membrane depolarisation.

In primary afferent neurons, the activation of GABA<sub>A</sub>R has also been shown to activate low voltage-activated T-type calcium channels (Aptel et al., 2007). T-type channels have been shown to influence pain states (Bourinet et al., 2005;Dogrul et al., 2003) and activate at membrane potentials close to the resting membrane potential of sensory neurons (Weiss and Zamponi, 2019) and therefore require only a small depolarisation to open (see Figure 3, *Introduction*).

The mechanism of GABA-induced depolarisation and inhibition is partially dependent on the reduction of the post-synaptic excitatory stimulus and glutamate release by shunting conductance (Banke and McBain, 2006;Fatt and Katz, 1953). In response to GABA, there is an increase in membrane conductivity reflecting the decrease in membrane resistance. According to Ohm's Law, this will decrease the voltage change in response to a depolarising current effectively stabilising the membrane potential. Furthermore, the slow depolarisation elicited by Cl<sup>-</sup> efflux following GABA<sub>A</sub>R activation inactivates sodium channels. Therefore, one may suggest that T-type calcium channels, active at more hyperpolarised potentials than HVA calcium channels (see Figure 3, *Introduction*) would be activated in response to the relatively slow change in membrane potential (Wilke et al., 2020). Interestingly, previous research has found that in fact both channels are responsible for the calcium increase in response to GABA<sub>A</sub>R activation in subventricular zone astrocyte-like cells (Young et al., 2010). In mechanoreceptive D-hair neurons, from a subset of cultured DRG neurons, Aptel et al. (2007) also find a current produced by HVA calcium channels, and suggest that while T-type currents are solely responsible for initiating a calcium influx in response to membrane depolarisation, HVA currents also contribute to the intracellular calcium increase in response to GABA. Therefore, it is possible that T-type calcium channels act as an initial carrier of depolarising calcium currents, but that the overall calcium influx is then potentiated and dominated by HVA activated L-type channels (Reichling et al., 1994). In the current study, the complete blockade of calcium influx in response to GABA with nimodipine or nifedipine and the merely partial reduction of influx in response to blockade with NiCl<sub>2</sub> may suit these findings. Further to this, the incomplete block by NiCl<sub>2</sub> suggests that the voltage-threshold for HVA calcium channels can also be reached, independent of T-type channels. On the other hand, it is possible that a store-operated calcium entry further increases the intracellular calcium in response to GABA<sub>A</sub> mediated activation of VGCC's (Young et al., 2010). However, this mechanism was not further investigated here.

#### 4.2.2 Cell-specific GABA responses

In our study, positive GABA responses often overlapped with capsaicin responses, indicating that sensitivity to GABA was higher in nociceptors. Additionally, capsaicin positive cells exhibited significantly larger GABA-induced calcium responses than those that detected in capsaicin insensitive cells. Corroborating the higher sensitivity of nociceptive neurons to GABA we found that cells resistant to TTX (high TTX-r index, Figure 26) also showed larger calcium

responses to GABA (Fig. 27C). The finding here that capsaicin and GABA sensitivity overlap in some cells is in line with previous findings (Jang et al., 2017). Of the cells responding to GABA (39/106), 22 cells also responded to capsaicin, indicating 56% were ostensibly nociceptors. Importantly, latest studies classifying primary afferent neurons based on single cell expression patterns indicate that a smaller proportion of mouse nociceptors are TRPV1-positive (Qi et al., 2023), in accordance with the traditional concept separating peptidergic TRPV1-positive from non-peptidergic TRPV1 negative nociceptors in the mouse, (Kupari and Ernfors, 2023; Usoskin et al., 2015), whereas in humans such a separation is not found and virtually all nociceptors are TRPV1-positive (Tavares-Ferreira et al., 2022). It should be mentioned, that the method of analysis used here might favour larger neurons (see below for further explanation), which may contain fewer nociceptive cells (Moraes et al., 2014) and thereby underestimate the nociceptive population.

Capsaicin is a TRPV1 agonist and the activation of TRPV1 causes depolarisation, action potential initiation and a calcium influx similar to GABA<sub>A</sub>R activation. TRPV1 activation stimulates release of a host of neuropeptides leading to sensitisation, as well as lowering its activation threshold, potentially facilitating the maintenance of inflammatory states (Caterina et al., 1997; Frias and Merighi, 2016). Interestingly, GABA<sub>B</sub>R have been found to be modulators of TRPV1 (Hanack et al., 2015). Overall, the co-localisation of GABA receptors and TRPV1 may facilitate a complex response of excitability changes in nociceptors under inflammatory conditions (Hanack et al., 2015).

We found a small but significant reduction in GABA responses with co-application of TTX (Fig 3). This is perhaps unexpected as in mature neurons, GABA does not initiate action potentials (Reichling et al., 1994). On the one hand this could be explained by methodological issues. In the protocol exhibited in Fig 26A, a brief high frequency electrical stimulus was given shortly before application of GABA. Such a stimulation may reduce the subsequent GABA-induced calcium transients. In TTX-s cells, this may not be apparent, because they are less likely to respond with large GABA transients anyway (Fig 26A lower trace, Fig 27C).

On the other hand, using TTX to block TTX-sensitive sodium channels during GABA<sub>A</sub>R activation, may indicate the involvement of TTX-sensitive channels in the amplification of GABA-mediated mild prolonged depolarisations. In particular, Nav1.7 is known to induce ramp currents upon slow and mild depolarisation and therefore amplifies them (Cummins et al., 1998). Nonetheless, lidocaine, an unspecific sodium channel blocker, has no effect on GABA-induced calcium transients (Jang et al., 2017), while here, the use of TTX reveals a reduction in the GABA-evoked calcium influx. Previous studies have eluded to a role for TTX-sensitive channels in contributing to the GABA-induced depolarisation (Panek et al., 2008). Panek et al. (2008) show that in spider VS-3 mechanosensory neurons, the GABA-induced depolarisation is smaller during blockade with TTX and that the sodium currents produced by a depolarisation are only partially inactivated by GABA-mediated inhibitory mechanisms. Nonetheless, while there may be a role for sodium channel activation in the depolarising GABA responses, their results also confirm that chloride is the main carrier. Using a Hodgkin-Huxley (Hodgkin and Huxley, 1952) type model, French et al. (2006) show that the GABA-induced depolarisations can be entirely accounted for with chloride conductance thereby corroborating that GABA-mediated chloride conductance has a key role in modulating neuronal excitability.

#### 4.2.3 Repetitive GABA application and chloride loading in naïve sensory somata

In our study, repetitive GABA application at ten-minute intervals in the absence of other interventions (Figure 30), produced robust calcium transients supporting previous reports (Reichling et al., 1994). Even at five-minute intervals, there was no change in the size of the GABA-evoked calcium transient (Figure 30). Reichling et al. (1994) posit that with shorter application intervals of less than 1 minute, there is a rundown of the amplitude of the calcium transient. Here, 3-minute intervals of GABA application showed a reduction in the GABA response amplitude (Figure 32). Presumably, this is due to depletion of the intracellular chloride concentration with GABA application. Ballanyi and Grafe (1985) show that in response to a depolarizing GABA stimulus, there is a decrease in the intracellular chloride in neuronal somata, while during a hyperpolarizing GABA stimulus there is an increase in intracellular chloride.

To test a possible activity-dependent upregulation of NKCC1 we used a bout of high frequency firing between two GABA applications (Figures 31-33). The coupling between action potential activity and upregulation of activity of NKCC1 has previously been shown in CA1 neurons (Brumback and Staley, 2008) and axons (Bonalume et al., 2021), and this mechanism may actually elucidate a role of GABA<sub>A</sub>R in the neuronal sensory soma or peripheral axons, that currently remains incompletely described. Normally, the hyperpolarisation associated with an increase in frequency of stimulation would modulate increase the difference between  $E_{Cl}$  and membrane potential, by increasing intracellular sodium and increasing the activity of the Na<sup>+</sup>/K<sup>+</sup>-ATPase for a longer time period, as needed to re-establish a normal gradient, thereby actually resulting in a reduced intracellular sodium concentration (Brumback and Staley, 2008), and increasing the driving force for chloride. Thus, lower intracellular sodium concentrations are expected to shift the thermodynamic equilibrium for NKCC1 towards higher intracellular chloride concentrations (Brumback and Staley, 2008).

Initial experiments revealed an overall negative effect of HFS on the subsequent GABA response (Figures 31 & 33). We hypothesized that this may have been due to the timing between GABA responses and the electrical stimulation. However, even with an increased time between the calcium transient evoked by HFS and a GABA application, there was still an obvious reduction (Figure 33). Perhaps, the kinetics of NKCC1 to re-establish an intracellular chloride concentration might be a limiting factor. In axons, the inward chloride transport via NKCC1 has been suggested to take approximately 5 minutes to restore the gradient after depletion (Bonalume et al., 2021), which might be in line with the results here (Figure 30), whereas in embryonic motoneurons (Gonzalez-Islas et al., 2009) and immature CA3 neurons (Kolbaev et al., 2020), inward chloride transport is rather slow and inefficient. As we are unaware of starting chloride gradients, our observations are merely indirect measures of the potential changes in chloride gradients and therefore it is difficult to determine what influence the kinetic of NKCC1 has and over what time course. In contrast, chloride imaging would glean insight into chloride flux evoked by a HFS. However, the probes are often complicated to use and bicarbonate flux, occurring as a result of GABA<sub>A</sub>R activation alongside Cl<sup>-</sup> flux, limits the use of many of them, as they are often strongly pH-dependent.

Therefore, we decided to alter the extracellular chloride concentration, thereby manipulating the transmembrane chloride gradient and perhaps simplifying observations of changes.

#### 4.2.4 Modulation of chloride gradients

By reducing the extracellular chloride concentration in the standard imaging solution we aimed to increase the chloride gradient that might boost GABA-induced chloride currents and subsequently necessitates increased NKCC1 activity to restore the physiological equilibrium. Indeed, in some cases a lower chloride concentration in the extracellular solution increased the first subsequent GABA-evoked calcium transient (Figures 34, 35 & 36). In addition, repetitively applied GABA under low extracellular chloride concentrations massively reduced the calcium responses to a minimum by approx. 15 min (Figures 36 & 37) suggesting a depletion of the intracellular chloride.

From such a depleted state we examined the time course of restoring the original gradient. Normalising the extracellular chloride concentration did not result in a sustained increase in GABA-evoked calcium response amplitude and the overall time course of recovery of the GABA-evoked calcium response was both slow and modest with no appreciable recovery even after 15 minutes in most cells (Figures 36 & 37). This was interesting, as the initial response in normalising extracellular chloride showed some increase in GABA responses. However, we cannot exclude that the intracellular chloride concentration was depleted to such an extent, that upon normalising the extracellular chloride concentration, the chloride gradient might have been reversed resulting in chloride influx, rather than efflux upon GABA<sub>A</sub>R activation. Moreover, the lack of an appreciable recovery may also result from repetitive probing of GABA, which may contribute to a persistently reduced chloride gradient. In fact, in a control experiment without repetitive probing of GABA (Fig. 37 G-I) there was a trend towards increase in GABA response, however this is not significant.

We had expected that increasing the chloride gradient would boost GABA-induced chloride currents and would facilitate intracellular chloride depletion thereby the amplifying effects of action potential firing may have become apparent. Still, even in the presence of a presumably reduced chloride gradient, a period of HFS did not incur a change in subsequent GABA responses. In fact, an initial attempt to address this question failed (Figure 37 A-C). This may be based on methodological problems, as the GABA application began during the large calcium increase evoked by electrical stimulation thereby not showing the GABA-induced calcium increase.

It should be mentioned, that the analysis method of the cells used here required them to return to the baseline prior to a previous intervention to be included in the analysis of amplitude. This prevented inclusion of cells that did not recover in time, therefore making the amplitude analyses more stringent. It is of course possible, that these cells are specifically larger neurons, and perhaps these can normalise intracellular calcium concentrations faster than smaller neurons. However, analyzing only those cells that returned to the baseline prior to a subsequent intervention upon cessation of electrical stimulation, may skew the data to show only those cells. Even so, this apparently did not influence the significant reduction.

Based on our results in axonal threshold tracking, we cannot rule out that receptor desensitization might have contributed to the prolonged reduction of calcium responses to GABA<sub>A</sub>R activation, potentially driven by high calcium concentrations during electrical stimulation. Indeed, reduced GABA<sub>A</sub> currents by higher intracellular calcium concentrations have been reported in cerebellar granule cells (Martina et al., 1994). In hippocampal cells an increased intracellular calcium concentration accelerates a rundown of GABA-mediated chloride currents (Chen et al., 1990; Mozrzymas and Cherubini, 1998) and in dorsal root ganglia from bullfrog, intracellular calcium decreases the affinity of the GABA receptor to its agonist (Inoue et al., 1986). On the other hand, Reichling et al. (1994) show that the attenuation of GABA responses upon applications at short intervals was not due to the increase in intracellular calcium. Rather than targeting GABA<sub>A</sub>R, calcium channels themselves can also be inhibited in a calcium-dependent fashion. HVA calcium channels have an intrinsic mechanism to limit their pore opening, specifically to prevent a calcium influx that could become toxic (Cens et al., 2006). Such an effect could also contribute to our observation of reduced calcium influx in response to GABA applications subsequent to HFS, considering the calcium increase induced by the electrical activity. To circumvent potential calcium effects, we removed calcium from the extracellular solution during the bout of HFS (Figure 37 D-F). However, the subsequent GABA-induced calcium response was still reduced. Thus, increased intracellular calcium during the stimulation alone cannot explain the still-reduced GABA response post-HFS.

An alternative explanation for the incomplete recovery of the chloride gradient after depletion could be linked to the expression density of NKCC1 in DRG neurons. If this were low, the effective re-establishment of a chloride gradient might take longer, particularly after an extreme intracellular depletion as performed in our experiments. Previous studies have found that NKCC1 mRNA is present in all small-diameter DRG and TG that are TRPV1-positive (Price et al., 2006). However, there are also reports about considerable heterogeneity in NKCC1 expression which is independent of neuronal cell size (Gilbert et al., 2007). While there is an overlap in NKCC1 and TRPV1 expression (Price et al., 2006), the functional relevance remains unclear and also neuronal cell body to surface area ratio is an important factor. Even though it has been posited that non-peptidergic IB4-positive neurons have larger chloride fluxes (Mao et al., 2012) absolute levels and potential differences of NKCC1 expression between functional classes of afferents remains unclear.

In an independent attempt to modify the neuronal chloride gradient, we used a pharmacologic blocker of NKCC1. Bumetanide, a clinically used loop diuretic and specific NKCC1 antagonist (Russell, 2000), was applied for a prolonged period and responses to repetitive GABA stimulations were assessed. We did not find a direct inhibitory effect of bumetanide on the GABA<sub>A</sub>R (Figure 38), but there was a gradual reduction of the GABA responses (Figure 39) suggesting a successful depletion of the chloride gradient with repetitive GABA<sub>A</sub> currents in combination with a block of NKCC1. This result is in accordance with previous results from other groups (Bonalume et al., 2021; Jang et al., 2017) and also corroborated by the axonal tracking experiments in Chapter 2. Further to this, the slow recovery of the chloride gradient after these experiments might corroborate the notion that NKCC1 expression density may be too low in the neuronal somata to ensure fast intracellular chloride re-establishment.

#### 4.2.5 Comparison of excitability parameters assessed by CAP recordings and calcium imaging

The nature of the assessed response differs considerably between CAP recordings and calcium imaging, i.e. direct recordings of action potentials in axons vs. indirect assessment of depolarisation leading to increased intracellular calcium concentrations in calcium live cell imaging. In CAP recordings activation thresholds and amplitudes are well defined and are directly related to axonal excitability. The repeatability is excellent and contributions of A- vs. C-fibres are easily separated by conduction velocity. Moreover, the conditions reflect more closely the physiological setting. On the other hand, CAP recordings do not allow analysis of single axons and do not differentiate between functional C-fibre classes. Electrical stimulation techniques in humans to determine excitability, cover mainly myelinated fibres and do not yield information about single functional fibre classes. If used for conditions of neuropathy for example, it is not possible to determine which populations of C-fibres are causing a reduction in a C-fibre CAP, therefore this would only be useful in conditions where populations are uniformly affected (Bostock et al., 1998). In terms of single neuron approaches, time-consuming microneurography has been used in humans in vivo, but the main approach to investigate spontaneous activity and changes in excitability are DRG neurons that serve as model systems in rodents, but also in humans (North et al., 2022; Tian et al., 2023). Nonetheless, in the absence of an additional marker system, electrical stimulation in neurons to test patterns of spontaneous discharge or excitability changes in reaction to changes in membrane potentials will also not differentiate between classes of C-fibres and thus, it will stimulate non-nociceptive afferent C-fibres and efferent sympathetic fibres in peripheral nerves.

In unmyelinated axons, direct intracellular measurement with patch clamp is difficult due to the small diameter (Vasylyev and Waxman, 2012). In contrast, live cell calcium imaging allows the study of responses of single characterized neurons without disturbing the integrity of the membrane and altering intracellular ion concentrations, as for example in patch clamp, and thus, nociceptor classes can be separated. Direct and sensitizing effects of mediators can be examined when a calcium influx is triggered, in real time (see Table 8). Importantly, neither method quantifies changes in membrane potential or spontaneous action potentials.

Advanced genetically-encoded calcium indicators (GECI) may be of value to improve the sensitivity and selectivity for the testing of specific functional groups of afferent neurons. Nonetheless, the calcium imaging method still relies on an indirect indicator of excitability of a cell via the influx of calcium in response to a depolarisation. Therefore, it is perhaps prudent to use a combination of electrical and optogenetic techniques in single cell recordings, to gain further insight into excitability of single fibre types while attempting to circumvent the temporal and spatial limitations of each individual stimulation paradigm.

CAP recordings		DRG neuronal calcium imaging	
Advantages	Disadvantages	Advantages	Disadvantages
Exact electrical thresholds and conduction velocity for APs	No information about a single axon	Responses in single neurons	Differentiation between AP and subthreshold depolarisation unclear
Separation between A- and C-fibres possible	Differentiation between C-fibre classes not easy/dispersion in CAP	Nociceptor populations can be separated by distinct chemical/electrical approaches	No simple differentiation between A- and C-fibres
Repeatability excellent	Temporal resolution limited by time to determine threshold and only responses above AP threshold are tested	Calcium signals in real time	
Only action potentials contribute to a CAP	Ambiguity of number of axons contributing to a CAP	Ratiometric dyes allow calculations of specific intracellular calcium concentrations	Several mechanisms determining intracellular calcium increases
	Indirect readout of chemical effects for sensitization on the electrical excitability	Direct readout of sensitizing chemical effects producing calcium signals	Neurotoxic effects of calcium
Ex vivo conditions resemble physiological conditions	Damage to the nerve while removing the sheath can unbeknownst impact signal		Preparation can damage the membrane and other cell signaling
	Low throughput	High throughput	
	No direct assessment of membrane potential		No direct assessment of membrane potential

*Table 8 Comparison of analysis methods used in this study*

A complementary method may be the use of voltage-sensitive dyes. This is suited to imaging many neurons with single neuron specificity (Preuss and Stein, 2013). Although this method requires a much higher throughput, it presents more temporal specificity as it measures direct membrane potential changes and therefore the key event determining neuronal excitability.

Overall, our study provides insights into the complexity of chloride regulation via the GABA<sub>A</sub>R in primary somatosensory neurons and their peripheral axons and reveals that the inward chloride transport is mediated by NKCC1, is to an extent activity-dependent and could provide insight into counter-mechanisms for an activity-dependent reduction of excitability in nociceptors. However, the use of a method that quantifies changes in membrane potential or spontaneous action potentials might be more useful in determining exactly how this may be translated to clinically-relevant mediums.

#### 4.2.6 Conclusions

Here, it was of particular interest to study the role of GABA-mediated chloride currents in limiting activity-dependent inhibition in peripheral primary afferents. Traditionally, mechanisms inducing hyperexcitability are in the forefront of concepts for chronic pain. This work focused on axonal and somal GABA effects which were hypothesized to provide evidence for a complementary concept of chronic pain, namely reduced activity-dependent inhibition via regulation of the chloride gradient. Our study provides insights into the complexity of chloride regulation via the GABA<sub>A</sub>R and resulting excitability changes in primary somatosensory neurons and their peripheral axons.

We find that GABA-induced excitability changes can be dynamically regulated by activity, however these effects may be obscured by parallel GABA<sub>A</sub> receptor desensitization. We also provide evidence that GABA<sub>A</sub>R activation and NKCC1-mediated inward chloride transport can counteract activity-dependent reduction of excitability in nociceptors.

Despite not clarifying the exact determinants for GABA<sub>A</sub>R-mediated effects, our results have major implications for our main hypothesis that GABA counteracts an activity-dependent reduction of excitability in nociceptors. We verify a transient effect on primary afferent neurons that may be of clinical relevance for brief bursts in nociceptors underlying the experience of short-lasting intermittent pain. However, our results speak against a role of GABA<sub>A</sub>R in exerting tonic sensitizing effects in the context of chronic pain, in which nociceptive activity is persistent for months and even years.

## 5 SUMMARY

GABA and glycine are the two main inhibitory neurotransmitters in the central nervous system mediating fast inhibitory transmission. In general, inhibitory neurotransmitters are expected to be analgesic owing to their hyperpolarising and shunting actions that reduce neuronal excitability. The expression of the NKCC1 chloride transporter in primary afferent neurons maintains a high intracellular chloride concentration, in the absence of the KCC2 transporter to extrude chloride. Thus, upon GABA<sub>A</sub>R activation the ensuing efflux of chloride will depolarise these cells. Indeed, GABA<sub>A</sub>R activation in dorsal root ganglion neurons of the mouse stimulate calcium influx. Interestingly, primary afferent depolarisation will still reduce excitability of presynaptic endings of nociceptors via presynaptic inhibition. Importantly, GABA-mediated chloride currents can have opposite effects on nociceptor excitability along the axon, in particular for activity-dependent changes. In general, nociceptor excitability decreases upon repetitive discharge that initiates a negative feedback loop via hyperpolarisation, increase in intracellular sodium and inactivation of sodium channels. On the other hand, GABA-mediated chloride currents are facilitated by hyperpolarisation and thus, they are optimally positioned to limit activity-dependent reduction of excitability. Thus, GABA<sub>A</sub>R activation and modulation of the chloride gradient can maintain neuronal excitability despite ongoing activity.

Therefore, it was of particular interest to study the role of GABA-mediated chloride currents in limiting activity-dependent inhibition in peripheral primary afferents. Traditionally, mechanisms inducing hyperexcitability are in the forefront of concepts for chronic pain. This work focused on axonal and somal GABA effects which were hypothesized to provide evidence for a complementary concept of chronic pain, namely reduced activity-dependent inhibition via regulation of the chloride gradient.

In this study, the threshold tracking technique was used to assess the functional role of GABA<sub>A</sub>R-mediated chloride currents on excitability of axons within the sural nerve, which are primarily skin afferents. The excitability index was used to indirectly determine a change in the membrane potential. We find that GABA-induced excitability changes can be dynamically regulated by activity, however these effects may be obscured by parallel GABA<sub>A</sub> receptor desensitization.

Additionally, this study employed the calcium imaging technique to determine excitability changes by GABA application in the DRG of mice. We find an L-type voltage-gated calcium channel-mediated influx of calcium in response to GABA, indicating a depolarizing action of GABA in the DRG in line with previous studies. This calcium signal is further dependent on the existence of a chloride gradient, which we manipulated by reduction of the extracellular chloride concentration. The use of high frequency stimulation, in contrast to axonal threshold tracking experiments, did not yield evidence of an activity-dependent increase in NKCC1 inward chloride transport in the cell somata, but rather reduced the subsequent GABA-mediated calcium signal. The expected activity-dependent increase in NKCC1 activity was not even evident after depletion of intracellular chloride via a reduced extracellular chloride concentration and a repetitive GABA<sub>A</sub>R activation. Based on our results in axonal threshold

tracking, we cannot rule out that receptor desensitization might have contributed to the prolonged reduction of calcium responses to GABA<sub>A</sub>R activation. Additional explanations include excessive intracellular calcium increases due to the electrical stimulation protocols and low expression density of NKCC1 in DRG neurons, that would prolong effective re-establishment of an original chloride gradient.

Our study provides insights into the complexity of chloride regulation via the GABA<sub>A</sub>R and resulting excitability changes in primary somatosensory neurons and their peripheral axons.

We provide evidence that GABA<sub>A</sub>R activation and NKCC1-mediated inward chloride transport can counteract activity-dependent reduction of excitability in nociceptors.

New methods such as voltage-sensitive dyes that allow direct quantification of membrane potential changes and action potentials may further clarify the role of GABA<sub>A</sub>R activation on nociceptor excitability and potential clinical implications.

Despite not clarifying the exact determinants for GABA<sub>A</sub>R-mediated effects, our results have major implications for our main hypothesis that GABA counteracts an activity-dependent reduction of excitability in nociceptors. We verify a transient effect on primary afferent neurons that may be of clinical relevance for brief bursts in nociceptors underlying the experience of short-lasting intermittent pain. However, our results speak against a role of GABA<sub>A</sub>R in exerting tonic sensitizing effects in the context of chronic pain, in which nociceptive activity is persistent for months and even years.

## 6 REFERENCES

- Akaike, N., Inomata, N., and Tokutomi, N. (1987). Contribution of chloride shifts to the fade of gamma-aminobutyric acid-gated currents in frog dorsal root ganglion cells. *J Physiol* 391, 219-234. <https://doi.org/10.1113/jphysiol.1987.sp016735>
- Alfonsa, H., Merricks, E.M., Codadu, N.K., Cunningham, M.O., Deisseroth, K., Racca, C., and Trevelyan, A.J. (2015). The contribution of raised intraneuronal chloride to epileptic network activity. *J Neurosci* 35, 7715-7726. <https://doi.org/10.1523/JNEUROSCI.4105-14.2015>
- Alsalamoun, M., Labau, J.I.R., Sosniak, D., Zhao, P., Almomani, R., Gerrits, M., Hoeijmakers, J.G.J., Lauria, G., Faber, C.G., Waxman, S.G., and Dib-Hajj, S. (2021). A novel gain-of-function sodium channel beta2 subunit mutation in idiopathic small fiber neuropathy. *J Neurophysiol* 126, 827-839. <https://doi.org/10.1152/jn.00184.2021>
- Alvarez-Leefmans, F.J., and Delpire, E. (2009). Physiology and pathology of chloride transporters and channels in the nervous system : from molecules to diseases, 1st ed edn (Amsterdam ; Boston: Elsevier/Academic Press).
- Alvarez-Leefmans, F.J., Gamino, S.M., Giraldez, F., and Nogueron, I. (1988). Intracellular chloride regulation in amphibian dorsal root ganglion neurones studied with ion-selective microelectrodes. *J Physiol* 406, 225-246. <https://doi.org/10.1113/jphysiol.1988.sp017378>
- Amoiridis, G., Schols, L., Ameridis, N., and Przuntek, H. (1997). Motor fibers in the sural nerve of humans. *Neurology* 49, 1725-1728. <https://doi.org/10.1212/wnl.49.6.1725>
- Andreasen, M., and Nedergaard, S. (2017). Furosemide depresses the presynaptic fiber volley and modifies frequency-dependent axonal excitability in rat hippocampus. *J Neurophysiol* 117, 1512-1523. <https://doi.org/10.1152/jn.00704.2016>
- Aptel, H., Hilaire, C., Pieraut, S., Boukhaddaoui, H., Mallie, S., Valmier, J., and Scamps, F. (2007). The Cav3.2/alpha1H T-type Ca<sup>2+</sup> current is a molecular determinant of excitatory effects of GABA in adult sensory neurons. *Mol Cell Neurosci* 36, 293-303. <https://doi.org/10.1016/j.mcn.2007.07.009>
- Arjun McKinney, A., Petrova, R., and Panagiotakos, G. (2022). Calcium and activity-dependent signaling in the developing cerebral cortex. *Development* 149. <https://doi.org/10.1242/dev.198853>
- Baev, A.Y., Vinokurov, A.Y., Novikova, I.N., Dremin, V.V., Potapova, E.V., and Abramov, A.Y. (2022). Interaction of Mitochondrial Calcium and ROS in Neurodegeneration. *Cells* 11. <https://doi.org/10.3390/cells11040706>
- Ballanyi, K., and Grafe, P. (1985). An intracellular analysis of gamma-aminobutyric-acid-associated ion movements in rat sympathetic neurones. *J Physiol* 365, 41-58. <https://doi.org/10.1113/jphysiol.1985.sp015758>

- Banke, T.G., and McBain, C.J. (2006). GABAergic input onto CA3 hippocampal interneurons remains shunting throughout development. *J Neurosci* 26, 11720-11725. <https://doi.org/10.1523/JNEUROSCI.2887-06.2006>
- Bannai, H., Levi, S., Schweizer, C., Inoue, T., Launey, T., Racine, V., Sibarita, J.B., Mikoshiba, K., and Triller, A. (2009). Activity-dependent tuning of inhibitory neurotransmission based on GABAAR diffusion dynamics. *Neuron* 62, 670-682. <https://doi.org/10.1016/j.neuron.2009.04.023>
- Basbaum, A.I., Bautista, D.M., Scherrer, G., and Julius, D. (2009). Cellular and molecular mechanisms of pain. *Cell* 139, 267-284. <https://doi.org/10.1016/j.cell.2009.09.028>
- Baylor, D.A., and Nicholls, J.G. (1969). After-effects of nerve impulses on signalling in the central nervous system of the leech. *J Physiol* 203, 571-589. <https://doi.org/10.1113/jphysiol.1969.sp008880>
- Beaudry, H., Daou, I., Ase, A.R., Ribeiro-da-Silva, A., and Seguela, P. (2017). Distinct behavioral responses evoked by selective optogenetic stimulation of the major TRPV1+ and MrgD+ subsets of C-fibers. *Pain* 158, 2329-2339. <https://doi.org/10.1097/j.pain.0000000000001016>
- Ben-Ari, Y. (2002). Excitatory actions of gaba during development: the nature of the nurture. *Nat Rev Neurosci* 3, 728-739. <https://doi.org/10.1038/nrn920>
- Ben-Ari, Y. (2007). GABA excites and sculpts immature neurons well before delivery: modulation by GABA of the development of ventricular progenitor cells. *Epilepsy Curr* 7, 167-169. <https://doi.org/10.1111/j.1535-7511.2007.00214.x>
- Benarroch, E.E. (2011). Na<sup>+</sup>, K<sup>+</sup>-ATPase: functions in the nervous system and involvement in neurologic disease. *Neurology* 76, 287-293. <https://doi.org/10.1212/WNL.0b013e3182074c2f>
- Berridge, M.J., Bootman, M.D., and Roderick, H.L. (2003). Calcium signalling: dynamics, homeostasis and remodelling. *Nat Rev Mol Cell Biol* 4, 517-529. <https://doi.org/10.1038/nrm1155>
- Blair, N.T., and Bean, B.P. (2002). Roles of tetrodotoxin (TTX)-sensitive Na<sup>+</sup> current, TTX-resistant Na<sup>+</sup> current, and Ca<sup>2+</sup> current in the action potentials of nociceptive sensory neurons. *J Neurosci* 22, 10277-10290. <https://doi.org/10.1523/JNEUROSCI.22-23-10277.2002>
- Bonalume, V., Caffino, L., Castelnovo, L.F., Faroni, A., Liu, S., Hu, J., Milanese, M., Bonanno, G., Sohns, K., Hoffmann, T., *et al.* (2021). Axonal GABA(A) stabilizes excitability in unmyelinated sensory axons secondary to NKCC1 activity. *J Physiol* 599, 4065-4084. <https://doi.org/10.1113/JP279664>
- Bossu, J.L., and Feltz, A. (1984). Patch-Clamp Study of the Tetrodotoxin-Resistant Sodium Current in Group C Sensory Neurons. *Neurosci Lett* 51, 241-246. [https://doi.org/10.1016/0304-3940\(84\)90558-5](https://doi.org/10.1016/0304-3940(84)90558-5)
- Bostock, H., Campero, M., Serra, J., and Ochoa, J. (2003). Velocity recovery cycles of C fibres innervating human skin. *J Physiol* 553, 649-663. <https://doi.org/10.1113/jphysiol.2003.046342>

- Bostock, H., Cikurel, K., and Burke, D. (1998). Threshold tracking techniques in the study of human peripheral nerve. *Muscle Nerve* 21, 137-158. [https://doi.org/10.1002/\(sici\)1097-4598\(199802\)21:2<137::aid-mus1>3.0.co;2-c](https://doi.org/10.1002/(sici)1097-4598(199802)21:2<137::aid-mus1>3.0.co;2-c)
- Bourinet, E., Alloui, A., Monteil, A., Barrere, C., Couette, B., Poirot, O., Pages, A., McRory, J., Snutch, T.P., Eschalier, A., and Nargeot, J. (2005). Silencing of the Cav3.2 T-type calcium channel gene in sensory neurons demonstrates its major role in nociception. *EMBO J* 24, 315-324. <https://doi.org/10.1038/sj.emboj.7600515>
- Bowery, N.G., and Smart, T.G. (2006). GABA and glycine as neurotransmitters: a brief history. *British Journal of Pharmacology* 147, S109-S119. <https://doi.org/10.1038/sj.bjp.0706443>
- Brandt, M.R., Beyer, C.E., and Stahl, S.M. (2012). TRPV1 Antagonists and Chronic Pain: Beyond Thermal Perception. *Pharmaceuticals (Basel)* 5, 114-132. <https://doi.org/10.3390/ph5020114>
- Brini, M., Cali, T., Ottolini, D., and Carafoli, E. (2014). Neuronal calcium signaling: function and dysfunction. *Cell Mol Life Sci* 71, 2787-2814. <https://doi.org/10.1007/s00018-013-1550-7>
- Brumback, A.C., and Staley, K.J. (2008). Thermodynamic regulation of NKCC1-mediated Cl<sup>-</sup> cotransport underlies plasticity of GABA(A) signaling in neonatal neurons. *J Neurosci* 28, 1301-1312. <https://doi.org/10.1523/JNEUROSCI.3378-07.2008>
- Cameron, M., Kekesi, O., Morley, J.W., Tapson, J., Breen, P.P., van Schaik, A., and Buskila, Y. (2016). Calcium Imaging of AM Dyes Following Prolonged Incubation in Acute Neuronal Tissue. *PLoS One* 11, e0155468. <https://doi.org/10.1371/journal.pone.0155468>
- Carlton, S.M., Zhou, S., and Coggeshall, R.E. (1999). Peripheral GABA(A) receptors: evidence for peripheral primary afferent depolarization. *Neuroscience* 93, 713-722. [https://doi.org/10.1016/s0306-4522\(99\)00101-3](https://doi.org/10.1016/s0306-4522(99)00101-3)
- Carr, R.W., Sittl, R., Fleckenstein, J., and Grafe, P. (2010). GABA increases electrical excitability in a subset of human unmyelinated peripheral axons. *PLoS One* 5, e8780. <https://doi.org/10.1371/journal.pone.0008780>
- Caterina, M.J., and Julius, D. (2001). The vanilloid receptor: a molecular gateway to the pain pathway. *Annu Rev Neurosci* 24, 487-517. <https://doi.org/10.1146/annurev.neuro.24.1.487>
- Caterina, M.J., Schumacher, M.A., Tominaga, M., Rosen, T.A., Levine, J.D., and Julius, D. (1997). The capsaicin receptor: a heat-activated ion channel in the pain pathway. *Nature* 389, 816-824. <https://doi.org/10.1038/39807>
- Catterall, W.A. (2011). Voltage-gated calcium channels. *Cold Spring Harb Perspect Biol* 3, a003947. <https://doi.org/10.1101/cshperspect.a003947>
- Catterall, W.A., Leal, K., and Nanou, E. (2013). Calcium Channels and Short-term Synaptic Plasticity. *J Biol Chem* 288, 10742-10749. <https://doi.org/10.1074/jbc.R112.411645>
- Cens, T., Rousset, M., Leyris, J.P., Fesquet, P., and Charnet, P. (2006). Voltage- and calcium-dependent inactivation in high voltage-gated Ca(2+) channels. *Prog Biophys Mol Biol* 90, 104-117. <https://doi.org/10.1016/j.pbiomolbio.2005.05.013>

- Chen, J.T., Guo, D., Campanelli, D., Frattini, F., Mayer, F., Zhou, L., Kuner, R., Heppenstall, P.A., Knipper, M., and Hu, J. (2014). Presynaptic GABAergic inhibition regulated by BDNF contributes to neuropathic pain induction. *Nat Commun* 5, 5331. <https://doi.org/10.1038/ncomms6331>
- Chen, Q.X., Stelzer, A., Kay, A.R., and Wong, R.K. (1990). GABAA receptor function is regulated by phosphorylation in acutely dissociated guinea-pig hippocampal neurones. *J Physiol* 420, 207-221. <https://doi.org/10.1113/jphysiol.1990.sp017908>
- Choe, W., Messinger, R.B., Leach, E., Eckle, V.S., Obradovic, A., Salajegheh, R., Jevtovic-Todorovic, V., and Todorovic, S.M. (2011). TTA-P2 is a potent and selective blocker of T-type calcium channels in rat sensory neurons and a novel antinociceptive agent. *Mol Pharmacol* 80, 900-910. <https://doi.org/10.1124/mol.111.073205>
- Chuang, L.Y., Cheng, Y.H., and Yang, C.H. (2013). Specific primer design for the polymerase chain reaction. *Biotechnol Lett* 35, 1541-1549. <https://doi.org/10.1007/s10529-013-1249-8>
- Cifelli, P., Palma, E., Roseti, C., Verlengia, G., and Simonato, M. (2013). Changes in the sensitivity of GABAA current rundown to drug treatments in a model of temporal lobe epilepsy. *Front Cell Neurosci* 7, 108. <https://doi.org/10.3389/fncel.2013.00108>
- Connolly, C.N., and Wafford, K.A. (2004). The Cys-loop superfamily of ligand-gated ion channels: the impact of receptor structure on function. *Biochem Soc Trans* 32, 529-534. <https://doi.org/10.1042/BST0320529>
- Conti, F., Minelli, A., and Melone, M. (2004). GABA transporters in the mammalian cerebral cortex: localization, development and pathological implications. *Brain Res Brain Res Rev* 45, 196-212. <https://doi.org/10.1016/j.brainresrev.2004.03.003>
- Coull, J.A., Boudreau, D., Bachand, K., Prescott, S.A., Nault, F., Sik, A., De Koninck, P., and De Koninck, Y. (2003). Trans-synaptic shift in anion gradient in spinal lamina I neurons as a mechanism of neuropathic pain. *Nature* 424, 938-942. <https://doi.org/10.1038/nature01868>
- Cummins, T.R., Howe, J.R., and Waxman, S.G. (1998). Slow closed-state inactivation: a novel mechanism underlying ramp currents in cells expressing the hNE/PN1 sodium channel. *J Neurosci* 18, 9607-9619. <https://doi.org/10.1523/JNEUROSCI.18-23-09607.1998>
- De Col, R., Messlinger, K., and Carr, R.W. (2008). Conduction velocity is regulated by sodium channel inactivation in unmyelinated axons innervating the rat cranial meninges. *J Physiol* 586, 1089-1103. <https://doi.org/10.1113/jphysiol.2007.145383>
- De Col, R., Messlinger, K., and Carr, R.W. (2012). Repetitive activity slows axonal conduction velocity and concomitantly increases mechanical activation threshold in single axons of the rat cranial dura. *J Physiol* 590, 725-736. <https://doi.org/10.1113/jphysiol.2011.220624>
- Deisseroth, K., and Hegemann, P. (2017). The form and function of channelrhodopsin. *Science* 357. <https://doi.org/10.1126/science.aan5544>
- Delgado-Lezama, R., Bravo-Hernandez, M., Franco-Enzastiga, U., De la Luz-Cuellar, Y.E., Alvarado-Cervantes, N.S., Raya-Tafolla, G., Martinez-Zaldivar, L.A., Vargas-Parada, A., Rodriguez-Palma, E.J., Vidal-Cantu, G.C., *et al.* (2021). The role of spinal cord extrasynaptic

- alpha(5) GABA(A) receptors in chronic pain. *Physiol Rep* 9, e14984. <https://doi.org/10.14814/phy2.14984>
- Deng, S.Y., Tang, X.C., Chang, Y.C., Xu, Z.Z., Chen, Q.Y., Cao, N., Kong, L.J., Wang, Y., Ma, K.T., Li, L., and Si, J.Q. (2021). Improving NKCC1 Function Increases the Excitability of DRG Neurons Exacerbating Pain Induced After TRPV1 Activation of Primary Sensory Neurons. *Front Cell Neurosci* 15, 665596. <https://doi.org/10.3389/fncel.2021.665596>
- Dib-Hajj, S.D., Rush, A.M., Cummins, T.R., Hisama, F.M., Novella, S., Tyrrell, L., Marshall, L., and Waxman, S.G. (2005). Gain-of-function mutation in Nav1.7 in familial erythromelalgia induces bursting of sensory neurons. *Brain* 128, 1847-1854. <https://doi.org/10.1093/brain/awh514>
- Dickie, A.C., McCormick, B., Lukito, V., Wilson, K.L., and Torsney, C. (2017). Inflammatory Pain Reduces C Fiber Activity-Dependent Slowing in a Sex-Dependent Manner, Amplifying Nociceptive Input to the Spinal Cord. *J Neurosci* 37, 6488-6502. <https://doi.org/10.1523/JNEUROSCI.3816-16.2017>
- Djoughri, L. (2016). Electrophysiological evidence for the existence of a rare population of C-fiber low threshold mechanoreceptive (C-LTM) neurons in glabrous skin of the rat hindpaw. *Neurosci Lett* 613, 25-29. <https://doi.org/10.1016/j.neulet.2015.12.040>
- Dogrul, A., Gardell, L.R., Ossipov, M.H., Tulunay, F.C., Lai, J., and Porreca, F. (2003). Reversal of experimental neuropathic pain by T-type calcium channel blockers. *Pain* 105, 159-168. [https://doi.org/10.1016/s0304-3959\(03\)00177-5](https://doi.org/10.1016/s0304-3959(03)00177-5)
- Doyon, N., Vinay, L., Prescott, S.A., and De Koninck, Y. (2016). Chloride Regulation: A Dynamic Equilibrium Crucial for Synaptic Inhibition. *Neuron* 89, 1157-1172. <https://doi.org/10.1016/j.neuron.2016.02.030>
- Du, X., Hao, H., Gigout, S., Huang, D., Yang, Y., Li, L., Wang, C., Sundt, D., Jaffe, D.B., Zhang, H., and Gamper, N. (2014). Control of somatic membrane potential in nociceptive neurons and its implications for peripheral nociceptive transmission. *Pain* 155, 2306-2322. <https://doi.org/10.1016/j.pain.2014.08.025>
- Du, X., Hao, H., Yang, Y., Huang, S., Wang, C., Gigout, S., Ramli, R., Li, X., Jaworska, E., Edwards, I., *et al.* (2017). Local GABAergic signaling within sensory ganglia controls peripheral nociceptive transmission. *J Clin Invest* 127, 1741-1756. <https://doi.org/10.1172/JCI86812>
- Dwivedi, D., and Bhalla, U.S. (2021). Physiology and Therapeutic Potential of SK, H, and M Medium AfterHyperPolarization Ion Channels. *Front Mol Neurosci* 14, 658435. <https://doi.org/10.3389/fnmol.2021.658435>
- Dzhala, V.I., Kuchibhotla, K.V., Glykys, J.C., Kahle, K.T., Swiercz, W.B., Feng, G., Kuner, T., Augustine, G.J., Bacskai, B.J., and Staley, K.J. (2010). Progressive NKCC1-dependent neuronal chloride accumulation during neonatal seizures. *J Neurosci* 30, 11745-11761. <https://doi.org/10.1523/JNEUROSCI.1769-10.2010>
- Eccles, J.C. (1961). The mechanism of synaptic transmission. *Ergeb Physiol* 51, 299-430.

- Erlanger, J., and Gasser, H.S. (1924). The compound nature of the action current of nerve as disclosed by the cathode ray oscillograph. *American Journal of Physiology-Legacy Content* 70, 624-666.
- Espinosa-Juarez, J.V., Chiquete, E., Estanol, B., and Aceves, J.J. (2023). Optogenetic and Chemogenic Control of Pain Signaling: Molecular Markers. *Int J Mol Sci* 24. <https://doi.org/10.3390/ijms241210220>
- Farrant, M., and Nusser, Z. (2005). Variations on an inhibitory theme: phasic and tonic activation of GABA(A) receptors. *Nat Rev Neurosci* 6, 215-229. <https://doi.org/10.1038/nrn1625>
- Fatt, P., and Katz, B. (1953). The electrical properties of crustacean muscle fibres. *J Physiol* 120, 171-204. <https://doi.org/10.1113/jphysiol.1953.sp004884>
- Fiumelli, H., Cancedda, L., and Poo, M.M. (2005). Modulation of GABAergic transmission by activity via postsynaptic Ca<sup>2+</sup>-dependent regulation of KCC2 function. *Neuron* 48, 773-786. <https://doi.org/10.1016/j.neuron.2005.10.025>
- French, A.S., Panek, I., and Torkkeli, P.H. (2006). Shunting versus inactivation: simulation of GABAergic inhibition in spider mechanoreceptors suggests that either is sufficient. *Neurosci Res* 55, 189-196. <https://doi.org/10.1016/j.neures.2006.03.002>
- Frias, B., and Merighi, A. (2016). Capsaicin, Nociception and Pain. *Molecules* 21. <https://doi.org/10.3390/molecules21060797>
- Fuller, A.M., Luiz, A., Tian, N., Arcangeletti, M., Iseppon, F., Sexton, J.E., Millet, Q., Caxaria, S., Ketabi, N., Celik, P., *et al.* (2023). Gate control of sensory neurotransmission in peripheral ganglia by proprioceptive sensory neurons. *Brain* 146, 4033-4039. <https://doi.org/10.1093/brain/awad182>
- Funk, K., Woitecki, A., Franjic-Wurtz, C., Gensch, T., Mohrlen, F., and Frings, S. (2008). Modulation of chloride homeostasis by inflammatory mediators in dorsal root ganglion neurons. *Mol Pain* 4, 32. <https://doi.org/10.1186/1744-8069-4-32>
- Garcia-Nicas, E., Laird, J.M., and Cervero, F. (2006). GABAA-Receptor blockade reverses the injury-induced sensitization of nociceptor-specific (NS) neurons in the spinal dorsal horn of the rat. *J Neurophysiol* 96, 661-670. <https://doi.org/10.1152/jn.00377.2006>
- Gee, M.D., Lynn, B., and Cotswell, B. (1996). Activity-dependent slowing of conduction velocity provides a method for identifying different functional classes of C-fibre in the rat saphenous nerve. *Neuroscience* 73, 667-675. [https://doi.org/10.1016/0306-4522\(96\)00070-x](https://doi.org/10.1016/0306-4522(96)00070-x)
- Ghit, A., Assal, D., Al-Shami, A.S., and Hussein, D.E.E. (2021). GABA(A) receptors: structure, function, pharmacology, and related disorders. *J Genet Eng Biotechnol* 19, 123. <https://doi.org/10.1186/s43141-021-00224-0>
- Gielen, M., Barilone, N., and Corringier, P.J. (2020). The desensitization pathway of GABA(A) receptors, one subunit at a time. *Nat Commun* 11, 5369. <https://doi.org/10.1038/s41467-020-19218-6>

- Gilbert, D., Franjic-Wurtz, C., Funk, K., Gensch, T., Frings, S., and Mohrlen, F. (2007). Differential maturation of chloride homeostasis in primary afferent neurons of the somatosensory system. *Int J Dev Neurosci* 25, 479-489. <https://doi.org/10.1016/j.ijdevneu.2007.08.001>
- Gold, M.S., and Gebhart, G.F. (2010). Nociceptor sensitization in pain pathogenesis. *Nat Med* 16, 1248-1257. <https://doi.org/10.1038/nm.2235>
- Gonzalez-Islas, C., Chub, N., and Wenner, P. (2009). NKCC1 and AE3 appear to accumulate chloride in embryonic motoneurons. *J Neurophysiol* 101, 507-518. <https://doi.org/10.1152/jn.90986.2008>
- Gradinaru, V., Zhang, F., Ramakrishnan, C., Mattis, J., Prakash, R., Diester, I., Goshen, I., Thompson, K.R., and Deisseroth, K. (2010). Molecular and cellular approaches for diversifying and extending optogenetics. *Cell* 141, 154-165. <https://doi.org/10.1016/j.cell.2010.02.037>
- Guo, A., Vulchanova, L., Wang, J., Li, X., and Elde, R. (1999). Immunocytochemical localization of the vanilloid receptor 1 (VR1): relationship to neuropeptides, the P2X3 purinoceptor and IB4 binding sites. *Eur J Neurosci* 11, 946-958. <https://doi.org/10.1046/j.1460-9568.1999.00503.x>
- Gwak, Y.S., and Hulsebosch, C.E. (2011). Neuronal hyperexcitability: a substrate for central neuropathic pain after spinal cord injury. *Curr Pain Headache Rep* 15, 215-222. <https://doi.org/10.1007/s11916-011-0186-2>
- Han, X., and Boyden, E.S. (2007). Multiple-color optical activation, silencing, and desynchronization of neural activity, with single-spike temporal resolution. *PLoS One* 2, e299. <https://doi.org/10.1371/journal.pone.0000299>
- Hanack, C., Moroni, M., Lima, W.C., Wende, H., Kirchner, M., Adelfinger, L., Schrenk-Siemens, K., Tappe-Theodor, A., Wetzel, C., Kuich, P.H., *et al.* (2015). GABA blocks pathological but not acute TRPV1 pain signals. *Cell* 160, 759-770. <https://doi.org/10.1016/j.cell.2015.01.022>
- Hochman, D.W., D'Ambrosio, R., Janigro, D., and Schwartzkroin, P.A. (1999). Extracellular chloride and the maintenance of spontaneous epileptiform activity in rat hippocampal slices. *J Neurophysiol* 81, 49-59. <https://doi.org/10.1152/jn.1999.81.1.49>
- Hodgkin, A.L., and Huxley, A.F. (1952). Currents carried by sodium and potassium ions through the membrane of the giant axon of Loligo. *J Physiol* 116, 449-472. <https://doi.org/10.1113/jphysiol.1952.sp004717>
- Hodgkin, A.L., and Huxley, A.F. (1952). A quantitative description of membrane current and its application to conduction and excitation in nerve. *J Physiol* 117, 500-544. <https://doi.org/10.1113/jphysiol.1952.sp004764>
- Hopper, A.J., Beswick-Jones, H., and Brown, A.M. (2023). Resilience of compound action potential peaks to high-frequency firing in the mouse optic nerve. *Physiol Rep* 11, e15606. <https://doi.org/10.14814/phy2.15606>
- Hososhima, S., Shigemura, S., Kandori, H., and Tsunoda, S.P. (2020). Novel optogenetics tool: Gt\_CCR4, a light-gated cation channel with high reactivity to weak light. *Biophys Rev* 12, 453-459. <https://doi.org/10.1007/s12551-020-00676-7>

- Ilfeld, B.M., Preciado, J., and Trescot, A.M. (2016). Novel cryoneurolysis device for the treatment of sensory and motor peripheral nerves. *Expert Rev Med Devices* 13, 713-725. <https://doi.org/10.1080/17434440.2016.1204229>
- Immke, D.C., and Gavva, N.R. (2006). The TRPV1 receptor and nociception. *Semin Cell Dev Biol* 17, 582-591. <https://doi.org/10.1016/j.semcdb.2006.09.004>
- Inoue, M., Oomura, Y., Yakushiji, T., and Akaike, N. (1986). Intracellular calcium ions decrease the affinity of the GABA receptor. *Nature* 324, 156-158. <https://doi.org/10.1038/324156a0>
- Jang, I.J., Davies, A.J., Akimoto, N., Back, S.K., Lee, P.R., Na, H.S., Furue, H., Jung, S.J., Kim, Y.H., and Oh, S.B. (2017). Acute inflammation reveals GABA(A) receptor-mediated nociception in mouse dorsal root ganglion neurons via PGE(2) receptor 4 signaling. *Physiol Rep* 5. <https://doi.org/10.14814/phy2.13178>
- Kanaka, C., Ohno, K., Okabe, A., Kuriyama, K., Itoh, T., Fukuda, A., and Sato, K. (2001). The differential expression patterns of messenger RNAs encoding K-Cl cotransporters (KCC1,2) and Na-K-2Cl cotransporter (NKCC1) in the rat nervous system. *Neuroscience* 104, 933-946. [https://doi.org/10.1016/s0306-4522\(01\)00149-x](https://doi.org/10.1016/s0306-4522(01)00149-x)
- Kandel, E.R., Koester, J., Mack, S., and Siegelbaum, S. (2021). *Principles of neural science*, Sixth edition edn.
- Kerr, L.M., and Yoshikami, D. (1984). A venom peptide with a novel presynaptic blocking action. *Nature* 308, 282-284. <https://doi.org/10.1038/308282a0>
- Khazipov, R., Khalilov, I., Tyzio, R., Morozova, E., Ben-Ari, Y., and Holmes, G.L. (2004). Developmental changes in GABAergic actions and seizure susceptibility in the rat hippocampus. *Eur J Neurosci* 19, 590-600. <https://doi.org/10.1111/j.0953-816x.2003.03152.x>
- Kim, D.Y., Fenoglio, K.A., Simeone, T.A., Coons, S.W., Wu, J., Chang, Y., Kerrigan, J.F., and Rho, J.M. (2008). GABAA receptor-mediated activation of L-type calcium channels induces neuronal excitation in surgically resected human hypothalamic hamartomas. *Epilepsia* 49, 861-871. <https://doi.org/10.1111/j.1528-1167.2007.01455.x>
- Kolbaev, S.N., Mohapatra, N., Chen, R., Lombardi, A., Staiger, J.F., Luhmann, H.J., Jedlicka, P., and Kilb, W. (2020). NKCC-1 mediated Cl(-) uptake in immature CA3 pyramidal neurons is sufficient to compensate phasic GABAergic inputs. *Sci Rep* 10, 18399. <https://doi.org/10.1038/s41598-020-75382-1>
- Koopmeiners, A.S., Mueller, S., Kramer, J., and Hogan, Q.H. (2013). Effect of electrical field stimulation on dorsal root ganglion neuronal function. *Neuromodulation* 16, 304-311; discussion 310-301. <https://doi.org/10.1111/ner.12028>
- Kraus, R.L., Li, Y., Gregan, Y., Gotter, A.L., Uebele, V.N., Fox, S.V., Doran, S.M., Barrow, J.C., Yang, Z.Q., Reger, T.S., *et al.* (2010). In vitro characterization of T-type calcium channel antagonist TTA-A2 and in vivo effects on arousal in mice. *J Pharmacol Exp Ther* 335, 409-417. <https://doi.org/10.1124/jpet.110.171058>

- Kueh, D., Barnett, W.H., Cymbalyuk, G.S., and Calabrese, R.L. (2016). Na(+)/K(+) pump interacts with the h-current to control bursting activity in central pattern generator neurons of leeches. *Elife* 5. <https://doi.org/10.7554/eLife.19322>
- Kupari, J., and Ernfors, P. (2023). Molecular taxonomy of nociceptors and pruriceptors. *Pain* 164, 1245-1257. <https://doi.org/10.1097/j.pain.0000000000002831>
- Kurki, S.N., Srinivasan, R., Laine, J., Virtanen, M.A., Ala-Kurikka, T., Voipio, J., and Kaila, K. (2023). Acute neuroinflammation leads to disruption of neuronal chloride regulation and consequent hyperexcitability in the dentate gyrus. *Cell Rep* 42, 113379. <https://doi.org/10.1016/j.celrep.2023.113379>
- Latremoliere, A., and Woolf, C.J. (2009). Central sensitization: a generator of pain hypersensitivity by central neural plasticity. *J Pain* 10, 895-926. <https://doi.org/10.1016/j.jpain.2009.06.012>
- Lee, I.O., and Lim, E.S. (2010). Intracisternal or intrathecal glycine, taurine, or muscimol inhibit bicuculline-induced allodynia and thermal hyperalgesia in mice. *Acta Pharmacol Sin* 31, 907-914. <https://doi.org/10.1038/aps.2010.82>
- Lenz, F.A., Kwan, H.C., Dostrovsky, J.O., and Tasker, R.R. (1989). Characteristics of the bursting pattern of action potentials that occurs in the thalamus of patients with central pain. *Brain Res* 496, 357-360. [https://doi.org/10.1016/0006-8993\(89\)91088-3](https://doi.org/10.1016/0006-8993(89)91088-3)
- Lorenzo, L.E., Godin, A.G., Wang, F., St-Louis, M., Carbonetto, S., Wiseman, P.W., Ribeiro-da-Silva, A., and De Koninck, Y. (2014). Gephyrin clusters are absent from small diameter primary afferent terminals despite the presence of GABA(A) receptors. *J Neurosci* 34, 8300-8317. <https://doi.org/10.1523/JNEUROSCI.0159-14.2014>
- Lueck, J.D., Mankodi, A., Swanson, M.S., Thornton, C.A., and Dirksen, R.T. (2007). Muscle chloride channel dysfunction in two mouse models of myotonic dystrophy. *J Gen Physiol* 129, 79-94. <https://doi.org/10.1085/jgp.200609635>
- Madisen, L., Mao, T.Y., Koch, H., Zhuo, J.M., Berenyi, A., Fujisawa, S., Hsu, Y.W.A., Garcia, A.J., Gu, X., Zanella, S., *et al.* (2012). A toolbox of Cre-dependent optogenetic transgenic mice for light-induced activation and silencing. *Nat Neurosci* 15, 793-802. <https://doi.org/10.1038/nn.3078>
- Malyshev, A., Goz, R., LoTurco, J.J., and Volgushev, M. (2015). Advantages and limitations of the use of optogenetic approach in studying fast-scale spike encoding. *PLoS One* 10, e0122286. <https://doi.org/10.1371/journal.pone.0122286>
- Mao, S., Garzon-Muvdi, T., Di Fulvio, M., Chen, Y., Delpire, E., Alvarez, F.J., and Alvarez-Leefmans, F.J. (2012). Molecular and functional expression of cation-chloride cotransporters in dorsal root ganglion neurons during postnatal maturation. *J Neurophysiol* 108, 834-852. <https://doi.org/10.1152/jn.00970.2011>
- Martina, M., Kilic, G., and Cherubini, E. (1994). The effect of intracellular Ca<sup>2+</sup> on GABA-activated currents in cerebellar granule cells in culture. *J Membr Biol* 142, 209-216. <https://doi.org/10.1007/BF00234942>

- Matarazzo, J.V., Ajay, E.A., Payne, S.C., Trang, E.P., Thompson, A.C., Marroquin, J.B., Wise, A.K., Fallon, J.B., and Richardson, R.T. (2023). Combined optogenetic and electrical stimulation of the sciatic nerve for selective control of sensory fibers. *Front Neurosci* 17, 1190662. <https://doi.org/10.3389/fnins.2023.1190662>
- Mazo, I., Rivera-Arconada, I., and Roza, C. (2013). Axotomy-induced changes in activity-dependent slowing in peripheral nerve fibres: role of hyperpolarization-activated/HCN channel current. *Eur J Pain* 17, 1281-1290. <https://doi.org/10.1002/j.1532-2149.2013.00302.x>
- Meisner, J.G., Marsh, A.D., and Marsh, D.R. (2010). Loss of GABAergic interneurons in laminae I-III of the spinal cord dorsal horn contributes to reduced GABAergic tone and neuropathic pain after spinal cord injury. *J Neurotrauma* 27, 729-737. <https://doi.org/10.1089/neu.2009.1166>
- Melzack, R., and Wall, P.D. (1965). Pain mechanisms: a new theory. *Science* 150, 971-979. <https://doi.org/10.1126/science.150.3699.971>
- Moalem-Taylor, G., Lang, P.M., Tracey, D.J., and Grafe, P. (2007). Post-spike excitability indicates changes in membrane potential of isolated C-fibers. *Muscle Nerve* 36, 172-182. <https://doi.org/10.1002/mus.20793>
- Moraes, E.R., Kushmerick, C., and Naves, L.A. (2014). Characteristics of dorsal root ganglia neurons sensitive to Substance P. *Mol Pain* 10, 73. <https://doi.org/10.1186/1744-8069-10-73>
- Mozrzymas, J.W., and Cherubini, E. (1998). Changes in intracellular calcium concentration affect desensitization of GABAA receptors in acutely dissociated P2-P6 rat hippocampal neurons. *J Neurophysiol* 79, 1321-1328. <https://doi.org/10.1152/jn.1998.79.3.1321>
- Nagel, G., Szellas, T., Huhn, W., Kateriya, S., Adeishvili, N., Berthold, P., Ollig, D., Hegemann, P., and Bamberg, E. (2003). Channelrhodopsin-2, a directly light-gated cation-selective membrane channel. *Proc Natl Acad Sci U S A* 100, 13940-13945. <https://doi.org/10.1073/pnas.1936192100>
- Nimmrich, V., and Gross, G. (2012). P/Q-type calcium channel modulators. *Br J Pharmacol* 167, 741-759. <https://doi.org/10.1111/j.1476-5381.2012.02069.x>
- North, R.Y., Odem, M.A., Li, Y., Tatsui, C.E., Cassidy, R.M., Dougherty, P.M., and Walters, E.T. (2022). Electrophysiological Alterations Driving Pain-Associated Spontaneous Activity in Human Sensory Neuron Somata Parallel Alterations Described in Spontaneously Active Rodent Nociceptors. *J Pain* 23, 1343-1357. <https://doi.org/10.1016/j.jpain.2022.02.009>
- O'Neill, N., and Sylantyev, S. (2019). The Functional Role of Spontaneously Opening GABA(A) Receptors in Neural Transmission. *Front Mol Neurosci* 12, 72. <https://doi.org/10.3389/fnmol.2019.00072>
- Obreja, O., Rukwied, R., Nagler, L., Schmidt, M., Schmelz, M., and Namer, B. (2018). Nerve growth factor locally sensitizes nociceptors in human skin. *Pain* 159, 416-426. <https://doi.org/10.1097/j.pain.0000000000001108>
- Olivera, B.M., Miljanich, G.P., Ramachandran, J., and Adams, M.E. (1994). Calcium channel diversity and neurotransmitter release: the omega-conotoxins and omega-agatoxins. *Annu Rev Biochem* 63, 823-867. <https://doi.org/10.1146/annurev.bi.63.070194.004135>

- Olsen, R.W., and Sieghart, W. (2008). International Union of Pharmacology. LXX. Subtypes of gamma-aminobutyric acid(A) receptors: classification on the basis of subunit composition, pharmacology, and function. Update. *Pharmacol Rev* 60, 243-260. <https://doi.org/10.1124/pr.108.00505>
- Ordelman, S.C., Kornet, L., Cornelussen, R., Buschman, H.P., and Veltink, P.H. (2010). An indirect component in the evoked compound action potential of the vagal nerve. *J Neural Eng* 7, 066001. <https://doi.org/10.1088/1741-2560/7/6/066001>
- Palma, E., Roseti, C., Maiolino, F., Fucile, S., Martinello, K., Mazzuferi, M., Aronica, E., Manfredi, M., Esposito, V., Cantore, G., *et al.* (2007). GABA(A)-current rundown of temporal lobe epilepsy is associated with repetitive activation of GABA(A) "phasic" receptors. *Proc Natl Acad Sci U S A* 104, 20944-20948. <https://doi.org/10.1073/pnas.0710522105>
- Panek, I., Hoger, U., French, A.S., and Torkkeli, P.H. (2008). Contributions of voltage- and Ca<sup>2+</sup>-activated conductances to GABA-induced depolarization in spider mechanosensory neurons. *J Neurophysiol* 99, 1596-1606. <https://doi.org/10.1152/jn.01267.2007>
- Payne, J.A., Rivera, C., Voipio, J., and Kaila, K. (2003). Cation-chloride co-transporters in neuronal communication, development and trauma. *Trends Neurosci* 26, 199-206. [https://doi.org/10.1016/S0166-2236\(03\)00068-7](https://doi.org/10.1016/S0166-2236(03)00068-7)
- Pieraut, S., Laurent-Matha, V., Sar, C., Hubert, T., Mechaly, I., Hilaire, C., Mersel, M., Delpire, E., Valmier, J., and Scamps, F. (2007). NKCC1 phosphorylation stimulates neurite growth of injured adult sensory neurons. *J Neurosci* 27, 6751-6759. <https://doi.org/10.1523/JNEUROSCI.1337-07.2007>
- Pinto, V., Derkach, V.A., and Safronov, B.V. (2008). Role of TTX-sensitive and TTX-resistant sodium channels in A $\delta$  and C-fiber conduction and synaptic transmission. *J Neurophysiol* 99, 617-628. <https://doi.org/10.1152/jn.00944.2007>
- Pitcher, M.H., Price, T.J., Entrena, J.M., and Cervero, F. (2007). Spinal NKCC1 blockade inhibits TRPV1-dependent referred allodynia. *Mol Pain* 3, 17. <https://doi.org/10.1186/1744-8069-3-17>
- Prakriya, M., and Lewis, R.S. (2015). Store-Operated Calcium Channels. *Physiol Rev* 95, 1383-1436. <https://doi.org/10.1152/physrev.00020.2014>
- Prescott, S.A. (2015). Synaptic inhibition and disinhibition in the spinal dorsal horn. *Prog Mol Biol Transl Sci* 131, 359-383. <https://doi.org/10.1016/bs.pmbts.2014.11.008>
- Prescott, S.A., Sejnowski, T.J., and De Koninck, Y. (2006). Reduction of anion reversal potential subverts the inhibitory control of firing rate in spinal lamina I neurons: towards a biophysical basis for neuropathic pain. *Mol Pain* 2, 32. <https://doi.org/10.1186/1744-8069-2-32>
- Pressey, J.C., de Saint-Rome, M., Raveendran, V.A., and Woodin, M.A. (2023). Chloride transporters controlling neuronal excitability. *Physiol Rev* 103, 1095-1135. <https://doi.org/10.1152/physrev.00025.2021>
- Preuss, S., and Stein, W. (2013). Comparison of two voltage-sensitive dyes and their suitability for long-term imaging of neuronal activity. *PLoS One* 8, e75678. <https://doi.org/10.1371/journal.pone.0075678>

- Price, T.J., Cervero, F., Gold, M.S., Hammond, D.L., and Prescott, S.A. (2009). Chloride regulation in the pain pathway. *Brain Research Reviews* 60, 149-170. <https://doi.org/10.1016/j.brainresrev.2008.12.015>
- Price, T.J., Cervero, F., Gold, M.S., Hammond, D.L., and Prescott, S.A. (2009). Chloride regulation in the pain pathway. *Brain Res Rev* 60, 149-170. [https://doi.org/S0165-0173\(08\)00154-9](https://doi.org/S0165-0173(08)00154-9) [pii];10.1016/j.brainresrev.2008.12.015 [doi]
- Price, T.J., Hargreaves, K.M., and Cervero, F. (2006). Protein expression and mRNA cellular distribution of the NKCC1 cotransporter in the dorsal root and trigeminal ganglia of the rat. *Brain Res* 1112, 146-158. <https://doi.org/10.1016/j.brainres.2006.07.012>
- Qi, L., Iskols, M., Shi, D., Reddy, P., Walker, C., Lezgiyeva, K., Voisin, T., Pawlak, M., Kuchroo, V.K., Chiu, I., *et al.* (2023). A DRG genetic toolkit reveals molecular, morphological, and functional diversity of somatosensory neuron subtypes. *bioRxiv*. <https://doi.org/10.1101/2023.04.22.537932>
- Raimondo, J.V., Kay, L., Ellender, T.J., and Akerman, C.J. (2012). Optogenetic silencing strategies differ in their effects on inhibitory synaptic transmission. *Nat Neurosci* 15, 1102-1104. <https://doi.org/10.1038/nn.3143>
- Raimondo, J.V., Richards, B.A., and Woodin, M.A. (2017). Neuronal chloride and excitability - the big impact of small changes. *Curr Opin Neurobiol* 43, 35-42. <https://doi.org/10.1016/j.conb.2016.11.012>
- Raja, S.N., Carr, D.B., Cohen, M., Finnerup, N.B., Flor, H., Gibson, S., Keefe, F.J., Mogil, J.S., Ringkamp, M., Sluka, K.A., *et al.* (2020). The revised International Association for the Study of Pain definition of pain: concepts, challenges, and compromises. *Pain* 161, 1976-1982. <https://doi.org/10.1097/j.pain.0000000000001939>
- Rane, S.G., Holz, G.G.t., and Dunlap, K. (1987). Dihydropyridine inhibition of neuronal calcium current and substance P release. *Pflugers Arch* 409, 361-366. <https://doi.org/10.1007/BF00583789>
- Rang, H.P., and Ritchie, J.M. (1968). On the electrogenic sodium pump in mammalian non-myelinated nerve fibres and its activation by various external cations. *J Physiol* 196, 183-221. <https://doi.org/10.1113/jphysiol.1968.sp008502>
- Reichling, D.B., Kyrozi, A., Wang, J., and MacDermott, A.B. (1994). Mechanisms of GABA and glycine depolarization-induced calcium transients in rat dorsal horn neurons. *J Physiol* 476, 411-421. <https://doi.org/10.1113/jphysiol.1994.sp020142>
- Reichling, D.B., and Macdermott, A.B. (1991). Lanthanum actions on excitatory amino acid-gated currents and voltage-gated calcium currents in rat dorsal horn neurons. *The Journal of Physiology* 441, 199-218. <https://doi.org/10.1113/jphysiol.1991.sp018746>
- Restrepo, D. (2005). The ins and outs of intracellular chloride in olfactory receptor neurons. *Neuron* 45, 481-482. <https://doi.org/10.1016/j.neuron.2005.02.002>
- Roberts, E., and Frankel, S. (1950). gamma-Aminobutyric acid in brain: its formation from glutamic acid. *J Biol Chem* 187, 55-63.

- Rocha-Gonzalez, H.I., Mao, S., and Alvarez-Leefmans, F.J. (2008). Na<sup>+</sup>,K<sup>+</sup>,2Cl<sup>-</sup> cotransport and intracellular chloride regulation in rat primary sensory neurons: thermodynamic and kinetic aspects. *J Neurophysiol* 100, 169-184. <https://doi.org/10.1152/jn.01007.2007>
- Rowley, N.M., Madsen, K.K., Schousboe, A., and Steve White, H. (2012). Glutamate and GABA synthesis, release, transport and metabolism as targets for seizure control. *Neurochem Int* 61, 546-558. <https://doi.org/10.1016/j.neuint.2012.02.013>
- Rukwied, R., Weinkauf, B., Main, M., Obreja, O., and Schmelz, M. (2013). Inflammation meets sensitization--an explanation for spontaneous nociceptor activity? *Pain* 154, 2707-2714. <https://doi.org/10.1016/j.pain.2013.07.054>
- Russell, J.M. (2000). Sodium-potassium-chloride cotransport. *Physiol Rev* 80, 211-276. <https://doi.org/10.1152/physrev.2000.80.1.211>
- Sallard, E., Letourneur, D., and Legendre, P. (2021). Electrophysiology of ionotropic GABA receptors. *Cell Mol Life Sci* 78, 5341-5370. <https://doi.org/10.1007/s00018-021-03846-2>
- Sandrini, G., Friberg, L., Coppola, G., Janig, W., Jensen, R., Kruit, M., Rossi, P., Russell, D., Sanchez del Rio, M., Sand, T., *et al.* (2011). Neurophysiological tests and neuroimaging procedures in non-acute headache (2nd edition). *Eur J Neurol* 18, 373-381. <https://doi.org/10.1111/j.1468-1331.2010.03212.x>
- Schindelin, J., Arganda-Carreras, I., Frise, E., Kaynig, V., Longair, M., Pietzsch, T., Preibisch, S., Rueden, C., Saalfeld, S., Schmid, B., *et al.* (2012). Fiji: an open-source platform for biological-image analysis. *Nat Methods* 9, 676-682. <https://doi.org/10.1038/nmeth.2019>
- Schmalbruch, H. (1986). Fiber composition of the rat sciatic nerve. *Anat Rec* 215, 71-81. <https://doi.org/10.1002/ar.1092150111>
- Schmidt, R., Schmelz, M., Forster, C., Ringkamp, M., Torebjork, E., and Handwerker, H. (1995). Novel classes of responsive and unresponsive C nociceptors in human skin. *J Neurosci* 15, 333-341. <https://doi.org/10.1523/JNEUROSCI.15-01-00333.1995>
- Schmidt, T., Ghaffarian, N., Philippot, C., Seifert, G., Steinhauser, C., Pape, H.C., and Blaesse, P. (2018). Differential regulation of chloride homeostasis and GABAergic transmission in the thalamus. *Sci Rep* 8, 13929. <https://doi.org/10.1038/s41598-018-31762-2>
- Schneider, T., Neumaier, F., Hescheler, J., and Alpdogan, S. (2020). Cav2.3 R-type calcium channels: from its discovery to pathogenic de novo CACNA1E variants: a historical perspective. *Pflugers Arch* 472, 811-816. <https://doi.org/10.1007/s00424-020-02395-0>
- Schöbel, N., Radtke, D., Lübbert, M., Gisselmann, G., Lehmann, R., Cichy, A., Schreiner, B.S.P., Altmüller, J., Spector, A.C., Spehr, J., *et al.* (2012). Trigeminal Ganglion Neurons of Mice Show Intracellular Chloride Accumulation and Chloride-Dependent Amplification of Capsaicin-Induced Responses. *Plos One* 7. <https://doi.org/ARTN> e48005  
10.1371/journal.pone.0048005
- Schobert, B., and Lanyi, J.K. (1982). Halorhodopsin Is a Light-Driven Chloride Pump. *J Biol Chem* 257, 306-313.

- Schulte, J.T., Wierenga, C.J., and Bruining, H. (2018). Chloride transporters and GABA polarity in developmental, neurological and psychiatric conditions. *Neurosci Biobehav Rev* 90, 260-271. <https://doi.org/10.1016/j.neubiorev.2018.05.001>
- Sen, A.K., and Post, R.L. (1964). Stoichiometry and Localization of Adenosine Triphosphate-Dependent Sodium and Potassium Transport in the Erythrocyte. *J Biol Chem* 239, 345-352.
- Serra, J., Campero, M., Ochoa, J., and Bostock, H. (1999). Activity-dependent slowing of conduction differentiates functional subtypes of C fibres innervating human skin. *J Physiol* 515 (Pt 3), 799-811. <https://doi.org/10.1111/j.1469-7793.1999.799ab.x>
- Sharma, N., Flaherty, K., Lezgiyeva, K., Wagner, D.E., Klein, A.M., and Ginty, D.D. (2020). The emergence of transcriptional identity in somatosensory neurons. *Nature* 577, 392-398. <https://doi.org/10.1038/s41586-019-1900-1>
- Sharples, S.A., Parker, J., Vargas, A., Milla-Cruz, J.J., Lognon, A.P., Cheng, N., Young, L., Shonak, A., Cymbalyuk, G.S., and Whelan, P.J. (2021). Contributions of h- and Na(+)/K(+) Pump Currents to the Generation of Episodic and Continuous Rhythmic Activities. *Front Cell Neurosci* 15, 715427. <https://doi.org/10.3389/fncel.2021.715427>
- Shim, B., Ringkamp, M., Lambrinos, G.L., Hartke, T.V., Griffin, J.W., and Meyer, R.A. (2007). Activity-dependent slowing of conduction velocity in uninjured L4 C fibers increases after an L5 spinal nerve injury in the rat. *Pain* 128, 40-51. <https://doi.org/10.1016/j.pain.2006.08.023>
- Sieghart, W., Fuchs, K., Tretter, V., Ebert, V., Jechlinger, M., Hoyer, H., and Adamiker, D. (1999). Structure and subunit composition of GABA(A) receptors. *Neurochem Int* 34, 379-385. [https://doi.org/10.1016/s0197-0186\(99\)00045-5](https://doi.org/10.1016/s0197-0186(99)00045-5)
- Simms, B.A., and Zamponi, G.W. (2014). Neuronal voltage-gated calcium channels: structure, function, and dysfunction. *Neuron* 82, 24-45. <https://doi.org/10.1016/j.neuron.2014.03.016>
- Smith, G., Sweeney, S.T., O'Kane, C.J., and Prokop, A. (2023). How neurons maintain their axons long-term: an integrated view of axon biology and pathology. *Front Neurosci* 17, 1236815. <https://doi.org/10.3389/fnins.2023.1236815>
- Spira, M.E., and Hai, A. (2013). Multi-electrode array technologies for neuroscience and cardiology. *Nat Nanotechnol* 8, 83-94. <https://doi.org/10.1038/nnano.2012.265>
- Staley, K.J., and Proctor, W.R. (1999). Modulation of mammalian dendritic GABA(A) receptor function by the kinetics of Cl<sup>-</sup> and HCO<sub>3</sub><sup>-</sup> transport. *J Physiol* 519 Pt 3, 693-712. <https://doi.org/10.1111/j.1469-7793.1999.0693n.x>
- Sung, K.W., Kirby, M., McDonald, M.P., Lovinger, D.M., and Delpire, E. (2000). Abnormal GABAA receptor-mediated currents in dorsal root ganglion neurons isolated from Na-K-2Cl cotransporter null mice. *J Neurosci* 20, 7531-7538. <https://doi.org/10.1523/JNEUROSCI.20-20-07531.2000>
- Tavares-Ferreira, D., Shiers, S., Ray, P.R., Wangzhou, A., Jeevakumar, V., Sankaranarayanan, I., Cervantes, A.M., Reese, J.C., Chamesian, A., Copits, B.A., *et al.* (2022). Spatial transcriptomics of dorsal root ganglia identifies molecular signatures of human nociceptors. *Sci Transl Med* 14, eabj8186. <https://doi.org/10.1126/scitranslmed.abj8186>

- Terunuma, M. (2018). Diversity of structure and function of GABA(B) receptors: a complexity of GABA(B)-mediated signaling. *Proc Jpn Acad Ser B Phys Biol Sci* *94*, 390-411. <https://doi.org/10.2183/pjab.94.026>
- Thalhammer, J.G., Raymond, S.A., Popitz-Bergez, F.A., and Strichartz, G.R. (1994). Modality-dependent modulation of conduction by impulse activity in functionally characterized single cutaneous afferents in the rat. *Somatosens Mot Res* *11*, 243-257. <https://doi.org/10.3109/08990229409051392>
- Tian, J., Bavencoffe, A.G., Zhu, M.X., and Walters, E.T. (2023). Readiness of nociceptor cell bodies to generate spontaneous activity results from background activity of diverse ion channels and high input resistance. *Pain*. <https://doi.org/10.1097/j.pain.0000000000003091>
- Tigerholm, J., Petersson, M.E., Obreja, O., Lampert, A., Carr, R., Schmelz, M., and Fransen, E. (2014). Modeling activity-dependent changes of axonal spike conduction in primary afferent C-nociceptors. *J Neurophysiol* *111*, 1721-1735. <https://doi.org/10.1152/jn.00777.2012>
- Usoskin, D., Furlan, A., Islam, S., Abdo, H., Lonnerberg, P., Lou, D., Hjerling-Leffler, J., Haeggstrom, J., Kharchenko, O., Kharchenko, P.V., *et al.* (2015). Unbiased classification of sensory neuron types by large-scale single-cell RNA sequencing. *Nat Neurosci* *18*, 145-153. <https://doi.org/10.1038/nn.3881>
- Vasylyev, D.V., and Waxman, S.G. (2012). Membrane Properties and Electrogenesis in the Distal Axons of Small Dorsal Root Ganglion Neurons in vitro. *J Neurophysiol* *108*, 729-740.
- Weidner, C., Schmelz, M., Schmidt, R., Hammarberg, B., Orstavik, K., Hilliges, M., Torebjörk, H.E., and Handwerker, H.O. (2002). Neural signal processing: the underestimated contribution of peripheral human C-fibers. *JNeurosci* *22*, 6704-6712.
- Weidner, C., Schmelz, M., Schmidt, R., Hansson, B., Handwerker, H.O., and Torebjörk, H.E. (1999). Functional attributes discriminating mechano-insensitive and mechano-responsive C nociceptors in human skin. *J Neurosci* *19*, 10184-10190.
- Weiss, N., and Zamponi, G.W. (2019). T-type calcium channels: From molecule to therapeutic opportunities. *Int J Biochem Cell Biol* *108*, 34-39. <https://doi.org/10.1016/j.biocel.2019.01.008>
- Werland, F., Hirth, M., Rukwied, R., Ringkamp, M., Turnquist, B., Jorum, E., Namer, B., Schmelz, M., and Obreja, O. (2021). Maximum axonal following frequency separates classes of cutaneous unmyelinated nociceptors in the pig. *J Physiol* *599*, 1595-1610. <https://doi.org/10.1113/JP280269>
- Wilke, B.U., Kummer, K.K., Leitner, M.G., and Kress, M. (2020). Chloride - The Underrated Ion in Nociceptors. *Front Neurosci* *14*, 287. <https://doi.org/10.3389/fnins.2020.00287>
- Woolf, C.J. (2022). Pain modulation in the spinal cord. *Front Pain Res (Lausanne)* *3*, 984042. <https://doi.org/10.3389/fpain.2022.984042>
- Wormuth, C., Lundt, A., Henseler, C., Muller, R., Broich, K., Papazoglou, A., and Weiergraber, M. (2016). Review: Ca(v)2.3 R-type Voltage-Gated Ca(2+) Channels - Functional Implications in Convulsive and Non-convulsive Seizure Activity. *Open Neurol J* *10*, 99-126. <https://doi.org/10.2174/1874205X01610010099>

- Wu, F.S., Gibbs, T.T., and Farb, D.H. (1993). Dual activation of GABAA and glycine receptors by beta-alanine: inverse modulation by progesterone and 5 alpha-pregnan-3 alpha-ol-20-one. *Eur J Pharmacol* 246, 239-246. [https://doi.org/10.1016/0922-4106\(93\)90037-a](https://doi.org/10.1016/0922-4106(93)90037-a)
- Wu, Y., and Wang, F. (2023). Inhibition of NKCC1 in spinal dorsal horn and dorsal root ganglion results in alleviation of neuropathic pain in rats with spinal cord contusion. *Mol Pain* 19, 17448069231159855. <https://doi.org/10.1177/17448069231159855>
- Wu, Y., and Wang, F.Y. (2023). Inhibition of NKCC1 in spinal dorsal horn and dorsal root ganglion results in alleviation of neuropathic pain in rats with spinal cord contusion. *Molecular Pain* 19. <https://doi.org/Artn> 17448069231159855  
10.1177/17448069231159855
- Yamada, J., Okabe, A., Toyoda, H., Kilb, W., Luhmann, H.J., and Fukuda, A. (2004). Cl<sup>-</sup> uptake promoting depolarizing GABA actions in immature rat neocortical neurones is mediated by NKCC1. *J Physiol* 557, 829-841. <https://doi.org/10.1113/jphysiol.2004.062471>
- Yamamoto, T., and Yaksh, T.L. (1993). Effects of intrathecal strychnine and bicuculline on nerve compression-induced thermal hyperalgesia and selective antagonism by MK-801. *Pain* 54, 79-84. [https://doi.org/10.1016/0304-3959\(93\)90102-U](https://doi.org/10.1016/0304-3959(93)90102-U)
- Yawo, H., Asano, T., Sakai, S., and Ishizuka, T. (2013). Optogenetic manipulation of neural and non-neural functions. *Dev Growth Differ* 55, 474-490. <https://doi.org/10.1111/dgd.12053>
- Young, S.Z., Platel, J.C., Nielsen, J.V., Jensen, N.A., and Bordey, A. (2010). GABA(A) Increases Calcium in Subventricular Zone Astrocyte-Like Cells Through L- and T-Type Voltage-Gated Calcium Channels. *Front Cell Neurosci* 4, 8. <https://doi.org/10.3389/fncel.2010.00008>
- Zamani, A., Sakuragi, S., Ishizuka, T., and Yawo, H. (2017). Kinetic characteristics of chimeric channelrhodopsins implicate the molecular identity involved in desensitization. *Biophys Physicobiol* 14, 13-22. [https://doi.org/10.2142/biophysico.14.0\\_13](https://doi.org/10.2142/biophysico.14.0_13)
- Zhang, F., Wang, L.P., Brauner, M., Liewald, J.F., Kay, K., Watzke, N., Wood, P.G., Bamberg, E., Nagel, G., Gottschalk, A., and Deisseroth, K. (2007). Multimodal fast optical interrogation of neural circuitry. *Nature* 446, 633-639. <https://doi.org/10.1038/nature05744>
- Zhang, X.L., Lee, K.Y., Priest, B.T., Belfer, I., and Gold, M.S. (2015). Inflammatory mediator-induced modulation of GABAA currents in human sensory neurons. *Neuroscience* 310, 401-409. <https://doi.org/10.1016/j.neuroscience.2015.09.048>
- Zhang, Y., Bucher, D., and Nadim, F. (2017). Ionic mechanisms underlying history-dependence of conduction delay in an unmyelinated axon. *Elife* 6. <https://doi.org/10.7554/eLife.25382>
- Zhao, L., Li, L.I., Ma, K.T., Wang, Y., Li, J., Shi, W.Y., Zhu, H.E., Zhang, Z.S., and Si, J.Q. (2016). NSAIDs modulate GABA-activated currents via Ca(2+)-activated Cl(-) channels in rat dorsal root ganglion neurons. *Exp Ther Med* 11, 1755-1761. <https://doi.org/10.3892/etm.2016.3158>
- Zhu, Y., Zhang, X.L., and Gold, M.S. (2014). Activity-dependent hyperpolarization of EGABA is absent in cutaneous DRG neurons from inflamed rats. *Neuroscience* 256, 1-9. <https://doi.org/10.1016/j.neuroscience.2013.10.004>

## 7 CURICULUM VITAE

### Personal information

Surname und Name: Sohns, Kyra  
Date of Birth: 23/12/1995  
Birthplace: Ludwigsburg, Germany

### SCHOOL CAREER

2004-2008 Licensed Victuallers' School, Ascot, England  
2008-2014 International School of Stuttgart, Germany  
30/05/2014 International Baccalaureate (IB) and German Abitur equivalent

### UNIVERSITY CAREER

2014-2017 BSc Psychology, Clinical and Cognitive Neuroscience Royal Holloway University of London  
01/07/2017 Degree Grade: Upper Second Class Honours  
2018-2019 MSc Clinical Neuroscience, King's College London  
01/10/2019 Degree Grade: Pass with Merit  
09/2020 – 03/2024 PhD Candidate in Department of Experimental Pain Research, Medical Faculty Mannheim of the University of Heidelberg

## 8 ACKNOWLEDGEMENTS

There are so many people I have to thank, this might be a really long list.

Firstly, my biggest thanks go to my supervisor Dr. Richard Carr. Thank you for always saying it would be okay, but always being realistic. Thank you for your support and your honesty and pushing me to do things I thought I couldn't. Thank you for everything you taught me showing me I could be a real scientist, but most importantly, thank you for your mentorship and kindness. I knew that I could do the hard thing, because of the skills you provided me with during this journey.

My sincerest thanks also to my supervisor Dr. Martin Schmelz. I couldn't have finished this without you. Thank you for taking over, being pragmatic, helpful and understanding. Thank you for putting the finishing touches on this piece of work. Your enjoyment in what you do is an inspiration and I hope to have that in my future career.

Thank you also Dr. Jürgen Solinski, for your help and sometimes just asking if I want to talk about it. I truly admire your ability to juggle everything and be efficient and generous in the process.

Thank you Ilona for your words of wisdom, your positivity, your encouragement. Thank you Anja for your help, goodwill and thoughtfulness.

Thank you to all the members of the AG Schmelz for your help, kindness and creating a safe environment - to make mistakes, ask questions and also celebrate wins. I got really lucky with you guys.

This wouldn't be a proper acknowledgment without saying thank you to my parents. Thank you for giving me this opportunity and enabling me to follow my dreams. Your belief in me has helped me grow as a person and I will be forever grateful. And while you think I am grown up, I will never not need you.

To Klaire, my sister, maid of honour, best friend and my soul-sibling. Thank you for letting me speak without judgement, for your advice to stay true to myself and for reminding me I am good enough, but I myself must also believe it.

Thank you also to friends and extended family I haven't mentioned by name. Thank you for standing by my side even if I was sometimes absent and in my own head. You know who you are. I am honoured and grateful to have had all of you in this journey with me. My heart is full of thanks.

Hendrik, I am not sure I can express how much your support on this journey has meant to me. You were the cure for my lack of confidence, my rock, my biggest cheerleader and were always there with guiding words and a hug. You made me laugh when I didn't think it possible, you indulged my sometimes crazy thought processes and you believed in me. It is a privilege to know you and to experience your energy.